Novel players in COPD and their molecular implication in the disease immunopathology

Dissertation

zum Erwerb des Doctor of Philosophy (Ph.D.)

an der Medizinischen Fakultät der

Ludwig-Maximilians-Universität München.

Helmholtz Zentrum München.

submitted by

Carolina Ballester López

from

Madrid, Spain

on

19th of June 2019

Supervisors: PD Dr. Claudia Staab-Weijnitz

Dr. Ali Önder Yildirim

Second expert: PD Dr. Ursula Zimber-Strobl

Dean: Prof. Dr. med. dent. Reinhard Hickel

Date of oral defense: 16th of October 2019

El fracaso es el condimento que le da al éxito su sabor.

TABLE OF CONTENTS

1. ABBREVIATIONS

AAT	Alpha-anti trypsin
BMDM	Bone marrow derived macrophages
CCL2	Chemokine (C-C motif) ligand 2
COPD	Chronic obstructive pulmonary disease
CRP	C-reactive protein
CS	Cigarette smoke
CT	Computed tomography
CTGF	Connective tissue growth factor
CXCL1	Chemokine (C-X-C motif) ligand 1
CXCL8	Chemokine (C-X-C motif) ligand 8
DNER	Delta And Notch-Like Epidermal Growth Factor-Related Receptor
DSL	Delta / Serrate / Lag-2
EMP	endothelial microparticles
GM-CSF	Granulocyte-macrophage colony-stimulating factor
GOLD	Global initiative for obstructive Lung Disease
GSEA	Gen set enrichment analysis
GWAS	Genome-wide association study
HIV	Human immunodeficiency viruses
ICS	Inhaled corticosteroids
IFNγ	Interferon γ
IL-10	Interleukin 10
IL-13	Interleukin 13
IL-1β	Interleukin 1β
IL-4	Interleukin 4
IL-6	Interleukin 6
IL-8	Interleukin 8
IRF	Interferon regulatory factor
LABA	Long acting β adrenergic receptor (B_2) agonists

LAMA	Long acting muscarinic antagonists
LPS	Lipopolysaccharide
NF-κB	Nuclear factor kappa-light-chain-enhancer of activated B cells
NICD1	Notch1 intracellular domain
NK	Natural killers
PALD1	Paladin
ROS	Reactive oxygen species
SNP	Single nucleotide polymorphisms
SOCS	Suppressor of cytokine signaling
STAT	Signal transducer and activator of transcription
TGFβ	Transforming growth factor β
TLR	Toll like receptor
TNFα	Tumor necrosis factor α
VEGF	Vascular endothelial growth factor
WCC	White cell count
WHO	World health organization
WT	Wild type

2. PUBLICATION LIST

Paper 1: The Notch ligand DNER regulates macrophage IFNγ release in chronic obstructive pulmonary diseases.
Ballester-Lopez C, Conlon TM, Ertüz Z, Greiffo FR, Irmler M, Verleden SE, Beckers J, Fernandez IE, Eickelberg O, Yildirim AÖ. EBioMedicine, 2019 (PMID: 31060902).

Paper 2: Female mice lacking Pald1 exhibit endothelial cell apoptosis and emphysema.
Egaña I, Kaito H, Nitzsche A, Becker L, **Ballester-Lopez C**, Niaudet C, Petkova M, Liu W, Vanlandewijck M, Vernaleken A, Klopstock T, Fuchs H, Gailus-Durner V, Hrabe de Angelis M, Rask-Andersen H, Johansson HJ, Lehtiö J, He L, Yildirim AÖ, Hellström M; German Mouse Clinic Consortium. Scientific Reports, 2017 (PMID: 29133847).

3. COPD DEFINITION AND ITS SOCIOECONOMIC STATUS

Chronic obstructive pulmonary disease is a non-communicable disease that today occupies third position as the leading cause of mortality worldwide [1]. It is mostly caused by exposure to exogenous particles, like cigarette smoke (CS) or household air pollution but there are other causes for example; genetic predisposition, age or infections. COPD patients suffer from chronic airflow limitation provoked by small airway fibrosis, loss of alveolar tissue and chronic inflammation. There are treatments to alleviate these symptoms, but there is currently no curative therapy [2]. The global prevalence of COPD is between 170 and 380 million cases, a number that fluctuates depending on the clinical criteria followed by the studies [3, 4]. Most of the mortality (90%) occurs in low- and middle-income countries [5] where they have the highest exposure to household air pollution and deep-seated smoking habits [6]. According to the Global Burden of Disease (GBD) database, in 2017, approximately 3.2 million people died from COPD worldwide, more than the 5% of the global population (Figure 1) [7].

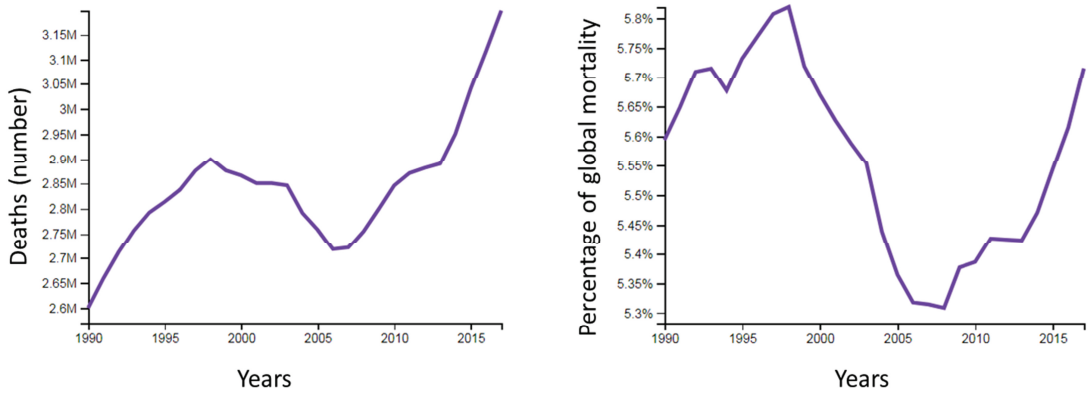

Figure 1: global number of deaths and mortality percentage caused by COPD in the last 27 years. Adapted from the GBD platform tool [7].

Despite being a dangerously growing pandemic, little consideration is given to the need of improving the management and treatment of COPD in comparison to other diseases like HIV or tuberculosis [6]. A one-year follow up study of therapy assignation for a large population of patients in the US [8], showed that health care personnel are not aware of the right guidelines to determine an appropriate treatment resulting in interrupted pharmacotherapy or simply incorrect medication like influenza vaccination. On the other hand, the histological and pathological heterogeneity that characterizes COPD, make the detection of the disease at an early stage very complex [9]. The lack of knowledge from medical personnel together with the poor prognosis leads to misdiagnosis and undertreatment [10], which further encourages the absence of recognition of COPD. A better understanding of the disease pathology is needed in order to identify novel biomarkers that could substantially contribute to

the improvement of early diagnosis.

Regarding the economic burden of this disease, it varies across different regions. In Europe, a person with COPD over 18 years generates a total cost (related to health care resources and lost production) of 2.989 euros per year [11]. Thus, the annual total costs due to COPD is approximately 48.4 billion euros [12]. Nevertheless, these numbers are underestimated since there are two important sources of expense that are usually overlooked in current studies: the non-diagnosed COPD subjects and those patients suffering from comorbidities [11, 13]. This fact is even more alarming when taking into account that exacerbations are predominantly responsible for COPD mortality [14]. Given the considerable socio-economic impact of COPD, additional effort is urgently needed to fill the current gaps in management and treatment. Indeed, the global initiative for chronic lung diseases (GOLD) 2019 reported that current strategies for COPD management are ineffective, highlighting the lack of personalized medicine. Today, the first treatment for a newly diagnosed COPD patient is established according to the severity of the disease, which is evaluated based on lung function performance. However, these patients are kept under the same treatment independently of the efficiency and impact of the prescribed medicaments. The GOLD 2019 report attempts for improved diagnoses and pharmacological follow up, where the treatment does not necessary fall in a specific category of disease severity but rather adapt to the needs of each patient [15]. Aiming towards personalized medicine as the future therapeutic strategy for COPD patients would not only improve life quality but also contribute to understanding better the disease progression.

4. COPD ETIOLOGY

The most common cause of COPD is the prolong inhalation of irritants, among which CS is the most prevalent. Despite the indisputable relevance of CS as a risk factor, only 20% of smokers develop COPD [16]. Moreover, there are other COPD irritants like air pollution, especially predominant in developing countries. Inhalation of products originated from partial combustion of biomass or solid fuel usually used as energy resources, is known to cause approximately 4 million deaths per year, including respiratory tract cancers and infections [6]. Furthermore, workplaces such as mines or in the chemical industry, also contain noxious inhaled substances that can cause what is termed occupational COPD [17]. Aside environmental factors, genetic factors can have a huge impact in determining COPD development. Indeed, COPD heritability is significantly high; first-degree relatives of COPD patients have approximately 3 times more risk of contracting the disease [18]. Specific mutations can strongly increase COPD predisposition. For example, this is the case for patients that develop COPD due to deficiency of alpha-1 antitrypsin (AAT), a serine-protease inhibitor really critical in protecting the lung against enzymatic proteolysis of extracellular matrix [19]. AAT deficiency is usually provoked by the presence of a single nucleotide polymorphism (SNP) in the encoding gene. However,

only one to two percent of COPD patients showed this mutation [20]. Thanks to the increasing number of genome wide association studies (GWAS) in the last years, more genetic risk factors with known function and contribution to COPD have been identified: *AGER*, *ELN*, *SFTD*, *TERT*, *NAF1*, *HHIP*, *FAM13A* and *IREB2* [16]. Nevertheless, further investigation is needed to understand the specific mechanism through which these genes entail a risk or susceptibility for COPD development. SNPs recurrence can also result in an increase of COPD susceptibility in combination with environmental factors. Indeed, COPD can persist and progress after smoking cessation and it is also known that smoker relatives of COPD patients have a higher risk to develop the disease than the non-smokers relatives [21]. These facts reflect the huge impact that the genetic component can have in COPD development.

5. PATHOLOGY OF COPD

COPD is generally defined as a chronic airflow limitation, but this is a strong oversimplification of a complex and heterogeneous pathological profile [22]. In COPD pathogenesis, several molecular processes come into play to advance the disease to the most severe stage. On one hand, peripheral airways undergo airway remodeling characterized by an increase of intimal thickness and fibrosis that results in obstruction and loss of small airways. These structural changes are believed to be mainly triggered by macrophages and epithelial cells that activate fibroblasts, which produce an excess of extracellular matrix via the TGFβ pathway and induce smooth muscle cell proliferation [21]. On the other hand, there is a destruction of alveolar walls (emphysema) provoked by different molecular events, whose underlying mechanisms are not yet completely understood. Abnormal accumulation of recruited immune cells leads to high levels of metalloproteinases (MMPs) [23], which leads to increased elastolysis of the alveolar walls. Oxidative stress is also an important driver of COPD pathology. Elevated levels of reactive oxygen species (ROS) released by macrophages and neutrophils also act as an anti-protease inhibitor and further can induce cell death of endothelial and epithelial cells by inducing mitophagy and subsequent necroptosis [21, 24]. In addition to the loss of epithelial cells and extracellular matrix, there is a reduction of blood vessels probably due to decreased expression of VEGF [18]. Loss of parenchyma elasticity results in an inability to exhale the trapped air and aggravates airway remodeling contributing to airflow limitation. Moreover, mucus hypersecretion caused by goblet cell hyperplasia together with cilia dysfunction also contributes to airway obstruction by filling the airways with mucus plugs [21]. COPD pathology is not only characterized by a destructive phenotype, but also by an inability to induce tissue repair. Indeed, activation of Wnt and TGFβ signaling, key pathways for tissue regeneration, promotes airway remodeling and emphysema development [25, 26]. Stem cell senescence and decreased activity of sirtuins like SRT1 in endothelial progenitor cells also lead to defective tissue repair [21].

These molecular events do not occur independently but rather crosstalk exacerbating the pathological phenotype. Moreover, there are additional factors that heavily influence the clinical phenotype, like age, gender, progression rate, incidence of exacerbations and the presence of co-morbidities [18]. Indeed, the elderly population is the most prone to develop COPD, and supporting evidence indicates that COPD can be the consequence of an accelerated lung aging [21, 25, 27]. Co-morbidities are usually observed in COPD patients, especially those associated with metabolic syndromes and cardiovascular diseases. Lung cancer, type 2 diabetes and pulmonary hypertension are some of the frequent diseases that appear as COPD co-morbidity given the overlap of pathological mechanisms [28]. One example is oxidative stress, which induces DNA damage that can promote lung cancer or carbonylation of proteins that can lead to production of autoantibodies and therefore autoimmune diseases [21]. Gender is another factor that influences COPD susceptibility. Several clinical studies have shown that women tend to have more severe emphysema than men with the same amount of tobacco exposure. Interestingly, these differences are more significant at the early stage, suggesting that disease progression is what differs among sexes [29].

5.1 Immunopathology

In COPD, lung inflammation predominantly occurs in the small airways although inflammatory changes can be also observed in the upper airways [21]. As the disease progresses, recruited immune cells accumulate and inflammation becomes chronic. Over the last decades, several studies have presented evidence that chronic inflammation is the main trigger of airway remodeling and emphysema [30]. For instance, mouse models have shown that overexpression of pro-inflammatory cytokines like IL-1β or IFNγ leads to spontaneous emphysema and airway remodeling in the adult murine lung [31, 32]. Moreover, a clinical study monitoring COPD patients based on CT scans suggest that airway fibrosis precedes emphysema [33], which together with the fact that inflammation induces fibrosis, supports the idea of inflammation as the first trigger of COPD pathogenesis. Once noxious particles or gases are inhaled, a substantial number of immune cells are recruited from the blood to the lung attracted by the local release of chemotactic molecules [18]. In fact, further studies have shown that increased numbers of macrophages and neutrophils correlates with disease severity and emphysema [30, 34]. Neutrophils release serine proteases (neutrophil elastase) and metalloproteinases (MMP8 and MMP9) that degrade matrix components destroying the alveolar walls are released by both cell types [35]. Inhaled irritants activate the lung epithelium to secrete cytokines such as TNFα, IL-8, IL-1β, IL-6 and GM-CSF. The remaining structural cells like endothelial cells and fibroblasts, and resident macrophages contribute to magnify the response by releasing more inflammatory mediators [18]. [30, 34]. Given the considerable release of chemokines, like CXCL13 and CCL19, increasing levels of B and T cells are recruited to the lung. Indeed, T cell number

correlates with the degree of emphysema and airway obstruction [30]. Infiltrates of CD8+ T cells, which exert cytotoxic activity by releasing perforins and granzymes B, is usually more predominant than CD4+ T cells in the COPD lung. Nevertheless, certain subtypes of CD4+ T cells like Th1 and Tregs, important for immune regulation and bacterial infections are also increased [36]. As the disease progresses, infiltrating T and B cells organize into tertiary lymphoid structures, called inducible bronchus-associated lymphoid tissue (iBALT), that accompanies emphysema in both humans [37] and mice [38]. The function of these follicles is not completely understood. On one side they accelerate the efficiency of the immune system to overcome infections. On the other, they exacerbate the immune response leading to a more chronic inflammatory state [39]. Indeed, in our group we have shown that B cell knock out mice are protected against iBALT formation and emphysema development after CS-exposure [40]. Furthermore, we demonstrated that B cells were necessary to trigger macrophage recruitment in response to CS and that B cells via IL-10 secretion stimulated MMP12 release by macrophages, suggesting a role for B cells in triggering macrophage-driven emphysema [40].

5.1.1 Subpopulations of lung macrophages

Macrophages are pleiotropic and plastic cells able to adapt and respond to the surrounding microenvironment. In order to simplify the distinct phenotypes that a macrophage can acquire, in vitro studies analyzing the type of cellular response, proposed the existence of two main types of macrophages: pro-inflammatory macrophages or M1 and anti-inflammatory macrophages or M2 [41]. M1 macrophages are known to secrete pro-inflammatory cytokines including TNFα, CXCL1, CXCL8, CCL2, lipid mediators and reactive oxygen species (ROS) that attract monocytes, neutrophils and promote Th1 responses [30]. They are professional phagocytes contributing to the clearance of the lung by degrading apoptotic bodies and bacteria. On the other hand, M2 macrophages control the immune response by releasing anti-inflammatory cytokines and promoting tissue repair and regeneration mainly via the TGFβ signaling pathway [42]. As experts in the macrophage field continuously highlight [42, 43], it should be considered that this classification is an oversimplification of what occurs *in vivo*, since it is originated in *in vitro* settings where the stimuli and conditions are under control. Indeed, given the complex immune profile of a COPD lung, it is probable that a macrophage is constantly shifting from one behavior to another (Figure 2). Added complexity to the topic is the diversity in origin of macrophage populations. In an inflamed lung there are two different origins to the macrophages observed: lung resident and recruited macrophages. In steady state, the lung is populated uniquely by self-renewing resident macrophages which derive from the fetal liver and the yolk sac [44]. Recruited macrophages are those originating from blood monocytes that come from the bone marrow and are recruited to the lung in response to an ongoing insult. These monocytes

infiltrate into the lung tissue and differentiate into macrophages [45]. Another relevant criterion for lung macrophage classification is the location, which in some studies is occasionally confused with the origin. A macrophage can be located in the alveoli lumen where they are highly exposed to air and environment; they are called alveolar macrophages. These macrophages are more active in phagocytosing inhaled particles and metabolizing the lung surfactant, necessary to prevent alveoli collapse [45]. Lung macrophages can also be embedded within the alveolar walls, and those are called interstitial macrophages, usually involved in tissue repair and antigen presentation [45].

Given that a macrophage can be classified according to three independent criteria, it should be highlighted that a lung macrophage falls into the three categories of phenotype, origin or location without following a specific pattern. Nevertheless, numerous studies have tried to better understand the behavior of distinct macrophage subpopulations [45-49]. In a COPD lung, it has been demonstrated that alveolar macrophages exhibit high phagocytic activity and release inflammatory cytokines, given their high exposure to environmental stimuli, showing a tendency to acquire a M1 phenotype [46-48]. Others also suggest that recruited macrophages tend to be pro-inflammatory since they infiltrate into the site of insult which is predominantly a pro-inflammatory microenvironment [46]. Nevertheless, this is still a debate and further investigation is needed to fully understand the dynamics of macrophage subpopulations. In COPD, several studies have shown that both M1 and M2 subpopulations are increased but they are defective in their ability to release cytokines, migrate or phagocytose foreign or apoptotic bodies [48, 49].

There are a considerable number of molecular pathways precisely controlling the phenotype that a macrophage can acquire. Intriguingly, the same molecular signaling pathway can skew the macrophage to one phenotype or another dependent upon the microenvironment [50]. For example, IRF/STAT signaling is one of the main pathways regulating M1/M2 polarization. IRF/STAT pathway activation via IFNs and TLR4 (STAT1) would trigger an M1 phenotype, while IRF/STAT activation by IL-4 and IL-13 (STAT6) would polarize macrophages towards M2 [50]. Other local conditions like hypoxia also significantly influence the phenotype [51]. Importantly, nuclear factor kappa B (NF-κB) is the predominant cell signaling pathway that induces the expression of pro-inflammatory cytokines in activated macrophages, including TNFα, IL1β, COX2 and IL12p40. Indeed, supremacy of STAT1 and NF-κB activation skews macrophages to an M1 phenotype [50]. Nevertheless, other pathways can also determine the macrophage phenotype. Notch signaling has been firstly linked to M1 polarization as an upstream pathway of the suppressor of cytokine signaling (SOCS) family [50]. However, additional studies have shown that Notch signaling can directly activate transcription of pro-inflammatory cytokines like *Il6*, *Il12b*, *Nos2* and *Tnf* in macrophages [52, 53]. Furthermore, Notch signaling can crosstalk with NF-κB by promoting translocation of p50 and RelB to the nucleus in macrophages following LPS stimulation [53]. Similarly in T cells, it has been shown that Notch intracellular domain 1 (NICD1) can directly bind to p50 and cRel NF-κB subunits to trigger *Ifng*

expression [54]. Indeed, specific blockade of Notch pathway in bone marrow derived macrophages (BMDM) inhibits M1 polarization [55].

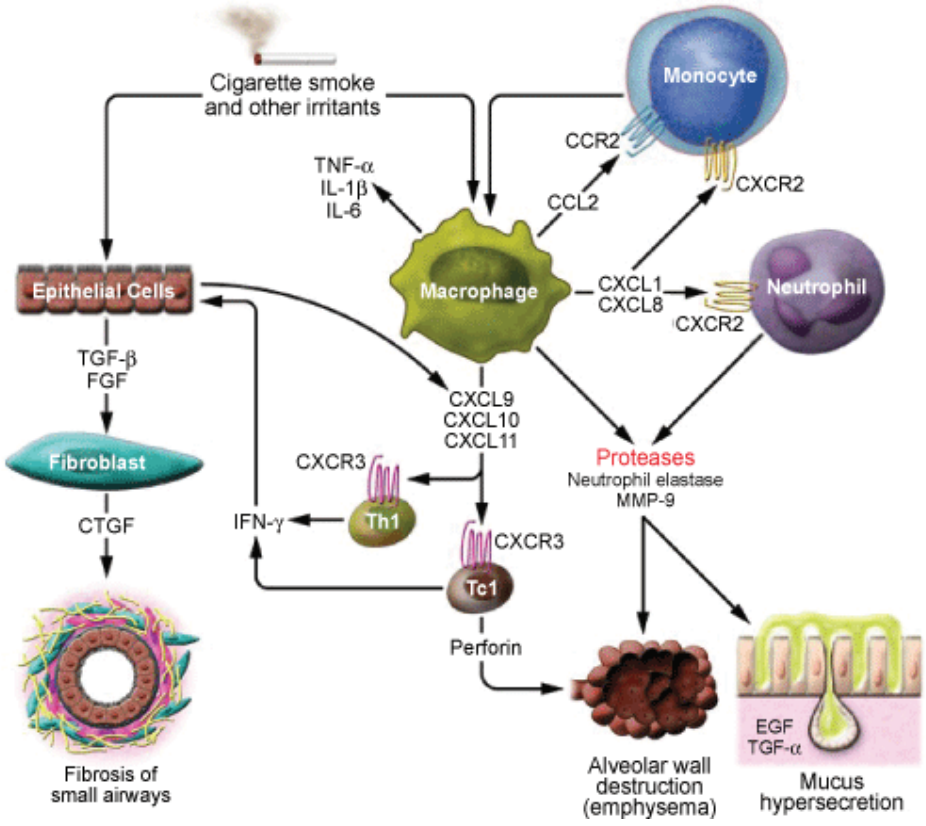

Figure 2: Schematic representation of the central role of lung macrophages during COPD immunopathogenesis. Adapted from Barnes, 2008 [56].

5.1.2 Relevance of IFNγ

IFNγ is a pro-inflammatory cytokine that was discovered firstly to be released by T cells, but later studies have shown that a wide variety of cell types are able to secrete this cytokine as well, including B, NK, Th1, $CD8^+$ T cells, dendritic cells, neutrophils and macrophages [57, 58]. The presence of IFNγ stimulates T cells to become Th1 cells and macrophages to acquire a M1 phenotype. Th1 cells and $CD8^+$ T cells secrete IFNγ in response to pathogen insult or chronic inflammation inducing tissue destruction by increasing the release of metalloproteinases in macrophages and other cell types and by inducing cell apoptosis [59-61]. It also promotes antigen presentation by dendritic cells and activates macrophages increasing expression of pro-inflammatory cytokines and TLR mediators [61, 62]. In addition, IFNγ can induce apoptosis of structural cells including endothelial and epithelial cells [58, 63]. Indeed, overexpression of IFNγ in mice, lead to the development of spontaneous emphysema by

enhancing cellular DNA injury, inflammation and production of proteases [32, 64]. Despite T cells and NK cells secreting the highest amount of IFNγ, T cell predominance in the COPD lung is much lower in comparison to macrophages. This suggests that although macrophages release less IFNγ, its contribution to total IFNγ in the lung is still considerable, given that the macrophage number vigorously increases in comparison to other cell types.

5.2 The role of endothelium in COPD pathogenesis

The vascular system plays a key role in COPD by regulating the vascular tone and vessel adaptation to increased flow and by overcoming hypoxia induced by the constricted vessels [65]. Furthermore, it also acts as a selective barrier for immune cells, nutrients, oxygen and waste products between the blood and the lung tissue [66]. As part of the COPD pathological profile, aggravated structural and molecular changes affect the endothelium. Aside airways, endothelial walls also become thicker due to artery remodeling leading to intimal hyperplasia, which is more pronounced in the region of small airways [65]. This is characterized by the presence of highly proliferative cells and excessive deposition of elastin and collagen fibers. These alterations usually induce pulmonary hypertension (PH), a frequent complication in COPD patients [24]. Furthermore, COPD patients exhibit areas of detached and apoptotic endothelial cells in lung arteries, evidenced by the increase of circulating endothelial microparticles (EMP), a vesicle released after apoptosis. The structural damage to the pulmonary vascular bed observed in COPD is strongly associated with emphysema development. Nevertheless, it is not clear which of these two pathological events is the predecessor [67]. Moreover, the molecular mechanism that triggers endothelial cell apoptosis in COPD pathogenesis it is not completely understood. One possibility is the impairment of vascular regeneration or angiogenesis. Angiogenesis is the de novo formation of capillary branches from pre-existing blood vessels mainly driven by vascular endothelial growth factor (VEGF) signaling [68]. In COPD pathogenesis, tissue inflammation and airway remodeling frequently lead to hypoxia, which could trigger the expression and activation of VEGF signaling [68]. Indeed, patients that suffer from moderate COPD or smokers with normal lung function, show an increase of VEGF expression in the lung arteries. On the contrary, patients with severe emphysema exhibit low levels of VEGF mediators and specific blockade of VEGF-A or VEGFR2 in mice or rats lead to cell death of alveolar cells and emphysema development [68-70]. This suggests that in early stage of the disease, there is an upregulation of VEGF in response to hypoxia and vascular remodeling to promote endothelial cell survival and migration, but it is not capable of overcoming the ongoing tissue destruction.

6. THERAPY OF COPD

6.1 Current therapeutic treatments

In order to overcome the heterogeneity of COPD, current treatment consists of a combination of pharmaceutical drugs where each of them alleviates a different symptom. Factors like frequency of exacerbations, age, gender and comorbidities should also be considered as they generate a huge variability in the clinical phenotype among subjects, and therefore there is no common therapy efficient for all COPD patients. To simplify the heterogeneity of COPD phenotypes among patients, in 1997 GOLD established a classification of disease severity consisting of 4 GOLD stages (0-IV) based on the forced expiratory volume after 1 second (FEV1), GOLD IV being the most severe. Since it was recognized that FEV1 was not properly correlating with symptoms, in 2011 a new classification criteria was formulated including exacerbations and comorbidities. The new GOLD categories A, B, C and D do not necessarily correlate with disease severity, but rather with symptom intensity and disease risk and move towards personalized medicine as the future for therapy [71].

The most common treatment to defeat respiratory difficulties is the use of inhaled long acting β adrenergic receptor (B_2) agonists (LABA) and long acting muscarinic antagonists (LAMA), drugs that induce the relaxation of airway smooth muscle acting as bronchodilators [72]. Usually these two inhalators are prescribed as a dual therapy to decrease bronchus obstruction and mucus hypersecretion. To palliate the exaggerated inflammation, inhaled corticosteroids (ICS) are usually added as a third drug in combination with LAMA and LABA. Given that a substantial number of COPD patients suffer from exacerbations, antibiotics are usually prescribed as well, and some of them like azithromycin have been shown to also act as an anti-inflammatory [73].

Despite the fact that these treatments reach certain efficiency in alleviating symptoms, they have some limitations. For example, despite that LAMA and LABA are the most efficient treatment for reducing exacerbations and hyperinflation [2, 73, 74], several studies have shown that they increase the risk for cardiovascular diseases, a frequent comorbidity found in COPD patients [75]. Regarding anti-inflammatory drugs, corticosteroids have exhibit a great performance in reducing the release of chemokines and cytokines in asthma, but unfortunately many COPD patients are insensitive to this treatment, probably due to the complex inflammatory pattern present in these subjects [76]. It is commonly known that an abuse of antibiotics influences the capability of the immune system to defeat infections by creating resistant bacteria. Nevertheless, a common disadvantage for all these treatments is their limitation when it comes to regulate disease changes or progression [73].

6.2 Current targets under investigation

As explained in previous sections, inflammation is the main driver of disease severity and therefore

COPD patients present a vast increase of pro-inflammatory cytokines in the lung. Some of them are known to be key for certain mechanisms, which make them attractive candidates for potential therapeutic targets. Therefore, considerable attention has been focus on exploring specific cytokines important for COPD pathogenesis. IL-1β is a pro-inflammatory cytokine and downstream target of the NF-κB cascade and is released by the bronchial epithelium in response to cigarette smoke in mice [73, 77]. Small clinical trials have been carried out to study the effect of blocking IL-1β in 147 COPD patients [73]. Unfortunately, no improvements were observed in lung function, although further studies are needed to completely discard IL-1β as a future therapeutic target. Another well-known cytokine with possible potential as a COPD therapy is IL-6, whose inhibition have been shown to protect against disease progression in mice models [78]. Despite the fact that clinical studies in COPD have not been performed yet, IL-6 blocking appeared to palliate symptoms in other inflammatory diseases like rheumatoid arthritis [73]. IL-8 is a key inducer of mucus hypersecretion during COPD development and its blockade has been evaluated in patients [73]. Although no improvements were observed, inhibition of CXCR2, an upstream regulator of IL-8 production, showed positive effects in lung function from COPD patients [76]. TNF is another pro-inflammatory cytokine responsible for amplifying neutrophilic recruitment and macrophage activation. Despite asthma patients showed improvement in exacerbation rate and airway hyperresponsiveness after TNF blockade, a small study in COPD patients failed in exhibiting beneficial effects. Nevertheless, additional studies are necessary to explore TNF as a therapeutic target [76].

Regardless of the effort by the scientific community to improve COPD therapy, the lack of knowledge in molecular mechanisms that drives COPD pathogenesis makes very difficult the discovery of therapeutic targets**.** Considering the last two sections, it is evident that there is an unmet need of finding new strategies for developing a curative therapy, and inflammation is one of the critical aspects to focus on.

6.3 The unmet need of druggable targets and biomarkers

Today, up to date approaches processing big clinical data intensely search for molecular or protein markers that associate to diseases and could be pharmaceutically targeted or could serve as a biomarker contributing to improved diagnosis. Nevertheless, the fact that COPD is progressive and very heterogeneous over time and among individuals makes the discovery of new biomarkers very difficult [79]. Moreover, the duration of most of the clinical studies is too short to properly evaluate the efficiency or prognosis value of a biomarker. In fact, lung function testing is the only biomarker that is currently in use for drug trials in COPD [79]. A very recent meta-analysis study proposed 6 min walk distance, heart rate, fibrinogen, CRP, WCC and IL6 as potential biomarkers that correlate with clinical outcomes [80]. However, the authors recognize the limitation of their study given the

short follow-up time and the exclusion of unstable COPD patients.

The heterogeneity and complexity of COPD is also a big obstacle for the exploration of novel druggable targets as illustrated in the previous section. Indeed, the idea of finding one single and common marker or target that could cure or predict COPD development is unrealistic. Likely, strategies for finding future therapies or early diagnoses should be focus on targeting more than one molecule. The discovery of new targets in combination with improved diagnosis would engender progress towards personalized medicine as the future of COPD therapy.

6.4 Strategies to identify new druggable targets

There are several strategies to find novel druggable targets; the conventional manner is from "bench to bedside" or "forward- translational" research, which starts with basic research providing promising proteins and terminates with clinical trials where those proteins are tested as druggable candidates in patients. However, new approaches are arising given the accumulation of clinical data that appear to be a valuable source of information which used to be overlooked. For example, therapeutic drugs that fail in clinical trials provide knowledge about new pathological mechanisms [81]. This is the most common example of reverse-translational research or so called "bedside to bench". An important tool related to this concept of reverse translation is genome wide association studies (GWAS). These analyses consist in the screening of large cohorts searching for single nucleotide polymorphisms (SNPs) that associate to complex diseases providing susceptibility to disease onset [16]. SNPs are genetic loci considered susceptible to single mutations when more than 1% of the studied population has a different nucleotide base in that specific genetic locus [82]. However, GWAS have limitations, being necessary the use of large datasets, usually possible by performing meta-analysis of several cohorts [16]. Thanks to the great increase of GWAS over the last years, the list of genes associated with COPD has considerably incremented. However, most of the identified targets remain unexplored given the lack of background knowledge that exists for most of the targets suggested by GWAS. The investigation of these novel proteins could provide new information on the mechanisms that perpetuate and magnify the disease pathology and even contribute to find new targets or biomarkers.

7. GOALS AND HYPOTHESES

In light of the unmet need of new therapeutic strategies for COPD patients and the lack of understanding of pathological mechanisms, these two papers presented in this thesis have the common goal of discovering the role of novel proteins potentially involved in the development of COPD pathogenesis.

Each paper focuses on a different protein, DNER and Paladin. The identification of these proteins as potential novel targets in COPD has evolved differently. Firstly, DNER was identified in a GWAS of

SNPs associated with lung function using data from 50,047 subjects of different cohort studies including COPD patients among others. Secondly, Paladin was identified as an important protein for angiogenesis in screening studies. As explained in previous sections, angiogenesis is a cellular mechanism of high relevance to COPD pathology. Given that the lung is the organ with the highest number of vessels, and that Paladin is expressed in embryonic and adult lung endothelial cells, the presented paper hypothesized a role for Paladin in COPD development.

Here, we propose two different approaches to reach a common goal: find new proteins involved in COPD pathogenesis. Our study on DNER function serves as an example of reverse translational research while the second paper about Paladin demonstrates forward translational research of bench to bedside.

The following section will discuss more in detail the background that led to the investigation of these two proteins.

- **Delta And Notch-Like Epidermal Growth Factor-Related Receptor (DNER)**

One of the problems of GWAS is that there is not much consistency between risk genes identified in GWAS and those shown in microarray expression studies [83]. Therefore, in the GWAS where *DNER* was identified as an associated gene to COPD [84], the authors incorporated SNP-by-environment interactions in order to identify SNPs that would not appear if only the main SNP effect is considered. This is especially important in the case of smoking, since genetic factors could have heterogeneous effects depending on the smoking habits. Therefore, 2 different SNP-by-environment interactions were considered in order to identify associations with lung function (FEV1/FVC or FEV1): SNP-by-ever smoking and SNP-by-pack years. The SNP located in *DNER* was the most significantly associated with lung function in the ever-smoking model as well as in the pack year model with highly conservative P values [84]. Furthermore, they also evaluate whether the identified SNPs in this study are related to smoking, by using results from a GWAS meta-analytic study of smoking related traits in 41,150 individuals (Oxford-GlaxoSmithKline Consortium) [85]. The authors conclude that the identified SNPs do not emerge from the main effects of smoking. To our understanding, this means that the SNP located in *DNER* is significantly associated with declined lung function independently of the presence of tobacco smoke. This strongly supports the idea of the involvement of DNER in COPD.

- **Paladin (PALD1)**

Angiogenesis is a process involved in COPD and many other lung diseases but the underlying mechanisms are unclear. In order to enlighten the field on novel proteins that could be critical during vessel formation, a meticulous screening of microarray data from different tissues and organs was

carried out [86]. A subset of well-established endothelial markers like *Tie1, Robo4, Notch4* were strategically chosen as reference to find new proteins that correlates with their expression pattern using the Pearson test. Interestingly, the lung was the tissue with the highest expression of endothelial markers and was correlating with the lung epithelium expression profile, meaning that the lung contains a much greater proportion of endothelial cells (50%) than the rest of the organs (5%). Using this strategy, a subset of 58 transcripts was identified to be highly expressed in the microvasculature across different murine organs. 26 transcripts were known markers for endothelial cells; *X99384* encoding for Paladin protein was among the other 32, which had never been related to angiogenesis before. Interestingly, *X99384* was also identified as a potential angiogenic factor in an independent reverse genetic screening using microvascular fragments from different species [66]. A third independent study performing bioinformatic analysis of microarray data showed that *X99384* was predominantly expressed in human endothelial cells [87]. Since these studies strongly suggest a role for Paladin in the endothelium, a further study was performed addressing the expression profile of Paladin across different embryonic stages.

8. CONTRIBUTION

Paper 1: The Notch ligand DNER regulates macrophage IFNγ release in chronic obstructive pulmonary diseases.

Together with my supervisor Ali Önder Yildirim I have conducted the experimental design of the paper. I have performed all the immunofluorescence staining and picture acquisition for human and murine tissue. I carried out the RNA isolations and quantifications by qPCR in human tissue and human and murine monocyte derived macrophages. I isolated brain tissue and perform end point PCRs of brain, lung and macrophages to analyse the efficiency of the knock out mice. I performed the dissection, FACS analysis and lung processing of the animal experiments with additional help of Christine Hollauer, Thomas Conlon and Zeynep Ertüez. I quantified the mean chord length of the obtained lungs. I carried out the gen set enrichment analysis (GSEA) of the microarray data on the M0, M1 and M2 macrophage populations. I did the differentiation of murine bone marrow derived macrophages and the quantification of protein levels by Western Blot with the help of Zeynep Ertüez. I carried out the ELISAs of the supernatants from the bone marrow derived macrophages. I wrote the paper with the help of Ali Önder Yildirim and Thomas Conlon.

Paper 2: Female mice lacking Pald1 exhibit endothelial cell apoptosis and emphysema.

I performed the quantification of the mean chord length and the septal thickness of wildtype and Paladin knock out adult lungs. I carried out immunohistochemistry of Caspase 3 on the same lung tissue. I contributed to the manuscript preparation and finalization.

EBioMedicine 43 (2019) 562–575

Contents lists available at ScienceDirect

EBioMedicine

journal homepage: www.ebiomedicine.com

EBioMedicine
Published by THE LANCET

Research paper

The Notch ligand DNER regulates macrophage IFNγ release in chronic obstructive pulmonary disease

Carolina Ballester-López [a], Thomas M. Conlon [a], Zeynep Ertüz [a], Flavia R. Greiffo [a], Martin Irmler [b], Stijn E. Verleden [c], Johannes Beckers [b,d,e], Isis E. Fernandez [a], Oliver Eickelberg [a,f], Ali Önder Yildirim [a,*]

[a] Comprehensive Pneumology Center (CPC), Institute of Lung Biology and Disease, Helmholtz Zentrum München, Member of the German Center for Lung Research (DZL), Munich, Germany
[b] Institute of Experimental Genetics (IEG), Helmholtz Zentrum München, Munich, Germany
[c] Division of Pneumology, KU Leuven, Leuven 3000, Belgium
[d] Chair of Experimental Genetics, Technische Universität München, Freising, Germany
[e] German Center for Diabetes Research (DZD), Germany
[f] Division of Pulmonary Sciences and Critical Care Medicine, University of Colorado, Denver, CO, USA

ARTICLE INFO

Article history:
Received 11 December 2018
Received in revised form 28 February 2019
Accepted 19 March 2019
Available online 4 May 2019

Keywords:
COPD
Macrophages
DNER
Notch signalling
IFNγ
Cigarette smoke
Lung
NFkB

ABSTRACT

Background: Chronic Obstructive Pulmonary Disease (COPD) is the third leading cause of death worldwide with no curative therapy. A non-canonical Notch ligand, DNER, has been recently identified in GWAS to associate with COPD severity, but its function and contribution to COPD is unknown.
Methods: DNER localisation was assessed in lung tissue from healthy and COPD patients, and cigarette smoke (CS) exposed mice. Microarray analysis was performed on WT and DNER deficient M1 and M2 bone marrow-derived macrophages (BMDM), and gene set enrichment undertaken. WT and DNER deficient mice were exposed to CS or filtered air for 3 day and 2 months to assess IFNγ-expressing macrophages and emphysema development. Notch and NFKB active subunits were quantified in WT and DNER deficient LPS-treated and untreated BMDM.
Findings: Immunofluorescence staining revealed DNER localised to macrophages in lung tissue from COPD patients and mice. Human and murine macrophages showed enhanced DNER expression in response to inflammation. Interestingly, pro-inflammatory DNER deficient BMDMs exhibited impaired NICD1/NFKB dependent IFNγ signalling and reduced nuclear NICD1/NFKB translocation. Furthermore, decreased IFNγ production and Notch1 activation in recruited macrophages from CS exposed DNER deficient mice were observed, protecting against emphysema and lung dysfunction.
Interpretation: DNER is a novel protein induced in COPD patients and 6 months CS-exposed mice that regulates IFNγ secretion via non-canonical Notch in pro-inflammatory recruited macrophages. These results provide a new pathway involved in COPD immunity that could contribute to the discovery of innovative therapeutic targets.
Funding: This work was supported from the Helmholtz Alliance 'Aging and Metabolic Programming, AMPro'.

1. Introduction

COPD is currently the third leading cause of death worldwide with 10% of people past forty affected [1,2]. Exposure to environmental particles, especially cigarette smoke, is the most common cause of COPD. These patients exhibit a progressive airflow obstruction provoked by small airway fibrosis, alveolar wall destruction (emphysema) and chronic inflammation [3]. In the last decades, it has become evident that inflammatory cells play a key role in initiating and perpetuating the disease pathology [4–9]. Firstly, inflammation is rapidly recognizable by an increase of neutrophils and macrophages in the lung. Indeed, macrophage-driven inflammation is one of the main triggers driving an abnormal immune response. It is believed that most of these macrophages are derived from bone marrow-derived blood monocytes that have been quickly recruited to the site of injury rather than expansion of lung tissue resident macrophages [10]. In a disease context, macrophages can acquire distinct phenotypes attending to the local microenvironmental needs. It is generally accepted the existence of two main phenotypes: activated (M1) and alternative (M2) macrophages,

* Corresponding author at: Comprehensive Pneumology Center (CPC), Institute of Lung Biology and Disease, Helmholtz Zentrum München, Ingolstädter Landstraße 1, Neuherberg 85764, Germany.
E-mail address: oender.yildirim@helmholtz-muenchen.de (A.Ö. Yildirim).

https://doi.org/10.1016/j.ebiom.2019.03.054

Research in context

Evidence before this study

COPD is a complex and progressive disease whose pathology is mainly driven and perpetuated by chronic inflammation. In fact, current treatments are mainly immunosuppressive drugs in combination with bronchodilators that mitigate the symptoms but do not cease disease progression. Hence, there is an urgent need of finding new molecular targets that can be implicated in disease development. Therefore, we searched for recent GWAS studies with healthy and COPD patients using PubMed and the GWAS central database (search terms: "GWAS COPD" "SNP COPD"). We found DNER as a potential genetic risk confirmed by 2 independent GWAS. Additionally, *DNER* gene expression was upregulated in smoker patients analysed in the GWAS studies. However, we could not find any study addressing DNER lung cell localisation and function (sources: Pubmed, UniProt, NextBio). Thus, our aim was to unravel how DNER is implicated in COPD development.

Added value of this study

Here we showed that DNER is expressed in pro-inflammatory recruited alveolar macrophages where it regulates IFNγ release during chronic inflammation in a CS-induced COPD mouse model. Furthermore, we provided the first evidence of DNER as a regulator of Notch1-NFKB crosstalk in activated macrophages.

Implications of all the available evidence

Today there are few studies dedicated to following up new gene candidates obtained from GWAS, usually due to the considerable lack of knowledge about these novel proteins. DNER is a protein well described in the nervous system but no detailed research has been investigated in other organs or cell types. This is the first study showing a functional role and molecular mechanism for DNER in lung macrophages, regulating IFNγ release. Moreover, the controversial and little understanding of the non-canonical Notch pathway entails an additional novel angle to our research, since the molecular mechanism of DNER published in neurons was not observed in macrophages. Lastly, it is known that cigarette smoke IFNγ-driven inflammation is the main trigger of COPD immunopathology, mostly released by macrophages and Th1 cells. Here we showed that DNER regulates IFNγ expression in macrophages during CS-induced chronic inflammation. Taken altogether, our study offers new molecular and functional knowledge on DNER and non-canonical Notch signalling as well as contributes to enlightening novel therapeutic strategies for COPD patients.

originally defined based on in vitro settings [11]. M1 are responsive to type 1-driven inflammation by secreting inflammatory cytokines like IL-12a or TNFα, while M2 are induced by type 2 stimulation and are involved in tissue remodelling, anti-inflammatory response and efferocytosis [12]. During COPD, the altered biology of the lung together with the pleiotropic effects and plasticity of macrophages, results in a continuous phenotype shifting that makes it difficult to discriminate M1 and M2 [13]. Indeed, it has been postulated the existence of at least 8 different phenotypes [10]. However, it is known in COPD that M1 and M2 subpopulations are defective in their ability to respond to the environment although it is not clear if there is a dominant phenotype [14,15]. Nevertheless, as the disease progresses, dysfunctional macrophages lead to an exacerbated and inefficient inflammatory response contributing to tissue damage and enhanced susceptibility to bacterial and virus infections [14,16]. Macrophage responses are thus precisely controlled by a wide range of cellular pathways [17], among them Notch signalling [18], although further investigation is needed to fully understand the molecular mechanisms.

Given the complexity and heterogeneity of COPD pathology, there is an unmet therapeutic need since current treatments only alleviate the symptoms but do not interrupt or reverse disease progression [1]. This lack of a curative therapy leads to the necessity of searching new targets. Hancock and colleagues in 2012 identified a SNP located in the intronic region of *DNER* (Delta Notch like epidermal growth factor related receptor), as the most significant SNP associated with the FEV1/FVC ratio and FEV1 [19]. Indeed, a further GWAS using an expanded cohort (16,707 subjects) confirmed the relevance of this SNP as a genetic risk for COPD and pulmonary function [20].

DNER is a transmembrane protein that belongs to the non-canonical Notch ligand family and binds to the Notch1 receptor [21,22]. In contrast to canonical, the non-canonical pathway is triggered by a different family of ligands that differ in their protein structure and whose downstream cascade leads to CSL (CBF1, Suppressor of Hairless, Lag-1) independent Notch activation. DNER was first described to be highly expressed by Purkinje neurons where it played a key role in cerebellum development [23,24], but it is also involved in differentiation and proliferation during cancer and stemness [25,26]. Nevertheless, its function in other cell types or in lung disease is completely unknown. Moreover, implication of the non-canonical Notch pathway in the immunopathogenesis of COPD has never been elucidated. Therefore, we hypothesize that the non-canonical Notch ligand DNER contributes to the promotion of pro-inflammatory responses during the progression of COPD pathogenesis.

Here, we demonstrate that DNER is expressed and localised to macrophages of experimental and human COPD. Furthermore, we provided evidence ex vivo and during disease pathogenesis that downstream DNER signalling is crucially involved in IFNγ secretion by pro-inflammatory murine macrophages via activation of Notch1-NFκB crosstalk. Collectively, this study is the first to describe the function and mechanism of DNER in macrophages in the context of chronic lung inflammation and opens new avenues to discover novel therapeutic targets for COPD patients.

2. Material and methods

2.1. Human tissue samples

Lung core samples from COPD patients (Supplementary Table 1) prior to lung transplantation were provided by Dr. Stijn Verleden (University of Leuven, Belgium), following ethical approval of the University of Leuven Institutional Review Board (S52174). All participants gave written consent and experiments were carried out following the principles described in the Declaration of Helsinki. COPD patients were explanted between 2009 and 2015. Controls were obtained from lungs not suitable for transplantation due to different reasons (kidney tumor, logistics, presence of microthrombi). Lung conditions were evaluated based on stereology/morphology parameters and CT. According to Belgian law, declined donor lungs can be designated for research after second opinion examination. Control subjects were explanted between 2011 and 2018. After organ removal, lungs were air-inflated at 10 cm H_2O pressure and fixed with liquid nitrogen vapour. Lungs were then cut into pieces with a band saw and sampled with a core bore. For paraffin embedding, lung pieces were sliced and fixed in 4% paraformaldehyde. For isolation of total RNA (peqGOLD Total RNA Kit, Peqlab), lung cores were snap frozen in liquid nitrogen.

2.2. Human monocyte derived macrophages

Human macrophages were differentiated from PBMCs of four healthy donors. Informed written consent was provided by all

participants and the local ethical review board approved the use of human tissue (180–14 LMU board). Briefly, 5×10^6 PBMCs were cultured in amino acids, 1 mM sodium pyruvic acid, 9 mg of bovine insulin (Sigma Chemical Co., St Louis, Mo) and the presence of 100 ng/ml M-CSF for 7 days. After differentiation, macrophages were treated for 24 h with 1 μg/ml LPS (*E. coli* O55:B5, Sigma-Aldrich) and 5% cigarette smoke extract (CSE).

2.3. Mice

C57BL/6 N *Dner*$^{tm3b(EUCOMM)Hmgu}$ (*Dner*$^{-/-}$) mice were obtained from the German Mouse Clinic (GMC), Helmholtz Zentrum München. Mice were allowed food and water ad libitum, kept at a constant temperature and humidity, with a 12-h light cycle, under specific pathogen free conditions. All animal experiments were performed following strict governmental and international guidelines and were approved by the local government for the administrative region of Upper Bavaria, Germany.

2.4. Cigarette smoke exposure

8–12 weeks old C57BL/6 N and *Dner*$^{-/-}$ mice were exposed to 100% mainstream of 500 mg/m^3 cigarette smoke (CS) [57], using 3R4F research cigarettes (Filter removed, Tobacco Research Institute, University of Kentucky), for 50 min twice/day, for 3 days, and 5 days/week for 2 months or 6 months. Mice exposed to filtered air were used as controls.

2.5. Lung function test

Lung function analysis was performed as previously described [4]. In summary, anaesthetised mice were tracheostomized and cannulated before the test. Respiratory function (forced expiratory volume after 100 ms, FEV100) was analysed using a forced pulmonary maneuver system [5] (Buxco Research Company, Data Sciences International) running FinePointe Software (version 6, Data Sciences International) and the quasistatic PV maneuver protocol.

2.6. Bronchoalveolar lavage (BAL)

Lungs were washed three times with 500 μl of sterile PBS (Gibco, Life Technologies) supplemented with Complete Protease Inhibitor Cocktail tablets (Roche Diagnostics). BAL cells were pelleted and resuspended in 500 μl RPMI-1640 medium (Gibco, Life Technologies) for the total cell count. Cytospins of the cell suspensions were prepared and stored at −80 °C for immunofluorescence staining.

2.7. Mouse lung processing

The two right lower lung lobes were stored in liquid nitrogen for RNA and protein isolation. The right upper two lobes were dissociated into single cell suspensions in MACS buffer using the lung dissociation kit and gentleMACS Dissociator (Miltenyi Biotec) for flow cytometry analysis. The left lung was fixed with 6% paraformaldehyde under a pressure of 20 cm inflation and paraffin embedded.

2.8. Flow cytometry

10^6 cells from filtered single cell lung homogenates or BAL cell pellets were blocked with purified anti-mouse CD16/CD32 (Clone: 93, eBioscience) for 20 min followed by 30 min incubation with antibody cocktails on ice. For intracellular staining, cells were fixed with 4% PFA for 10 min and then permeabilized with 1% BSA/0.5% Saponin/PBS buffer followed by 10 min incubation with anti-mouse CD16/CD32 and a second incubation of antibody cocktails in the permeabilization buffer. After washing and re-suspending in MACS buffer (Miltenyi Biotec), cells were analysed on a BD FACSCanto II flow cytometer (BD Biosciences) running BD FACSDiva software. B cell and T cell staining was performed with: APC-conjugated anti-CD19 (clone: 6D5, Miltenyi Biotec), APC-Vio770-conjugated anti-CD3e (clone: 17A2, Miltenyi Biotec), PE-Vio770-conjugated anti-CD22 (clone: Cy34.1, Miltenyi Biotec), PE-conjugated anti-CD80 (clone: 16-10A1, Miltenyi Biotec), PerCP-Vio700-conjugated anti-MHCII (clone: M5/114.15.2, Miltenyi Biotec), VioGreen-conjugated anti-CD69 (clone: H1.2F3, Miltenyi Biotec), FITC-conjugated anti-IgG (Biolegend). For the macrophage profile: VioGreen-conjugated anti-CD45 (clone: 30F11, Miltenyi Biotec), APC-Vio770-conjugated anti-Ly6C (clone: 1G7.G10, Miltenyi Biotec), VioBlue-conjugated anti-Ly6G (clone: 1A8, Miltenyi Biotec), FITC-conjugated anti-MHCII (clone: M5/114.15.2, Miltenyi Biotec), PerCP-Vio700-conjugated anti-F4/80 (clone: REA126, Miltenyi Biotec), PE-Vio770 conjugated anti-Siglec-F (clone: ES22-10D8, Milteyi Biotec), PE-conjugated anti-CD11b (clone: M1/70.15.11.5, Miltenyi Biotec), APC-conjugated anti-CD11c (clone: N418, Miltenyi Biotec). For intracellular staining: APC conjugated anti-IL-4 (clone: 11B11, BIOZOL Diagnostica) and FITC conjugated anti-IFNγ (clone: XMG1.2, Life Technologies).

2.9. Immunofluorescence

3 μm murine or human lung tissue sections were deparaffinized and rehydrated followed by heat-induced epitope retrieval using HIER Citrate Buffer (pH 6.0, Zytomed Systems). For the cytospins, cells were fixed by incubation with methanol for 10 min followed by 1 min of acetone. Sections or cytospins were blocked with 5% BSA for 30 min, incubated overnight at 4 °C with primary antibodies and 1 h at room temperature with secondary antibodies (anti-goat Alexa Fluor 568, anti-rabbit Alexa Fluor 488, anti-mouse Alexa Fluor 488 and anti-rabbit Alexa Fluor 555, Life Technologies) diluted in 1% BSA. Images at different magnifications were captured using Axio Imager with an M2 microscope (Zeiss) and processed with ImageJ 1.x [58]. Primary antibodies common for human and murine tissue: Galectin-3 (1:50 sc-32790, Santa Cruz), CD31 (1:50 ab28364, Abcam), ACTA-2 (1:600 ab5694, Abcam), Pro-SPC (1:100 AB3786, Chemicon International). Human tissue: DNER (1:100 AF3646, R&D Systems), CC10 (1:100 sc-365992), NOS2 (1:20 sc-8310). Murine tissue: DNER (1:50 AF2254, R&D Systems), NICD1 (1:25 ab8925, Abcam).

2.10. Quantitative morphometry

Design-based stereology was used to analyse mean chord length in H&E stained tissue sections using the new Computer Assisted Stereological Toolbox (newCAST, Visiopharm) and an Olympus BX51 light microscope as described [5]. In brief, 20 frames were randomly selected by the software across multiple sections under the x20 objective and superimposed by a line grid and points. The intercepts of lines with alveolar wall (I_{septa}) and points localised on air space (P_{air}) were counted and calculated as $MCL = \sum P_{air} \times L(p) / \sum I_{septa} \times 0.5$, where L(p) is the line length per point.

2.11. Professional APC isolation and stimulation

Bone marrow was flushed from femurs and tibias of C57BL/6 N and *Dner*$^{-/-}$ mice with RPMI-1640 medium. Bone marrow cells were passed through 40 μm filters (Miltenyi Biotec), counted and resuspended in 5% fetal bovine serum, 50 μM β-mercaptoethanol and 100 U/ml penicillin and streptomycin RPMI-1640 medium. 2×10^6 cells/ml were plated in T25 Flasks for protein isolation and nuclear extractions or in 24 well plates for RNA isolation. Medium was additionally supplemented with 20 ng/ml of murine recombinant M-CSF to generate bone marrow derived macrophages (BMDM) or 20 ng/ml murine recombinant GM-CSF for bone marrow derived dendritic cells (BMDC). Medium was changed every 2–3 days carefully discarding non-

adherent cells. For BMDM, on day 7 fresh medium without M-CSF was added and left overnight. For BMDCs, on day 7 to 8 adherent cells were harvested and 1×10^7 cells were seeded in 100 mm petri dishes to keep them in culture for an additional 24-48 h. The non-adherent maturing DCs were collected as they were released. BMDM were stimulated with 1 μg/ml LPS (from E.coli 0111:B4, Sigma-Aldrich) and 20 ng/ml of recombinant murine IFNγ (M1 phenotype) or with 20 ng/ml of recombinant murine IL-4 (M2 phenotype) for 24 h. BMDCs were treated with 1 μg/ml LPS for 24 h. All cytokines were purchased from ImmunoTools.

2.12. Th differentiation

Naive CD4 T cells were purified from total murine splenocytes using the $CD4^+$ $CD62L^+$ T cell Isolation Kit II (Miltenyi Biotec) and cultured at 1.5×10^6/ml in RPMI1640 medium supplemented with 10%FCS, 0.1 mM beta-mercaptoethanol, 100 U/ml penicillin Streptomycin, 10 mM HEPES, 1 mM Sodium Pyruvate, 0.1 mM non essential amino acids and 1 × MEM Vitamin Solution. These were then stimulated for 48 h with anti-CD3/anti-CD28 coupled beads, along with recombinant human TGFβ (10 ng/ml, R&D Systems, Wiesbaden, Germany), IL-6 (60 ng/ml, R&D Systems), anti-IL-4 (10 μg/ml, BioLegend, San Diego, CA), anti-IL-12 (10 μg/ml, BioLegend), anti-IFNγ (5 μg/ml, BioLegend) and anti-IL-2 (2.5 μg/ml, Miltenyi Biotec) for Th17 differentiation. For Th2, anti-CD3/anti-CD28 coupled beads were supplemented with recombinant mouse IL-4 (20 ng/ml, R&D systems, anti-IL12 (10 μg/ml) and anti-IFNgamma (5 μg/ml) for 96 h. For Th1, with recombinant IL-12p70 (10 ng/ml, BD Pharmingen) and anti-IL-4 (10 μg/ml) for 96 h. For Treg differentiation anti-CD3/anti-CD28 coupled beads were supplemented with recombinant human TGFβ (10 ng/ml, R&D Systems) and 1000 IE/ml recombinant human IL-2 (ProleukinS, Novartis) for 72 h. Th0 control cells were stimulated with anti-CD3/anti-CD28 coupled beads alone for a comparable period of time. For Th1 and Th2 differentiation and their Th0 control, the culture volume was doubled with medium containing 1000 IE/ml recombinant human IL-2 at 40 h and at 80 h the medium was replaced with medium lacking IL-2.

2.13. Cell lysates

To obtain whole cell lysates, BMDM were washed with ice-cold PBS and collected by scraping into RIPA buffer. Samples were incubated for 30 min on ice mixing every 5 min. Lysates were centrifuged at 13000 rpm for 15 min at 4 °C and supernatants retained. To perform cytoplasmic and nuclear extractions from BMDM, a commercial kit was used and undertaken as per manufacturers instructions (Nuclear Extract Kit 40010 and 40410, Active Motif).

2.14. Western blotting

20 μg of cell lysates were diluted in Laemmli Buffer (BioRad) containing β-mercaptoethanol (Gibco, Life Technologies) and incubated for 10 min at 95 °C. Protein samples were separated on a 10% sodium dodecyl sulfate–polyacrylamide gel by electrophoresis and wet-transferred to a PVDF membrane (BioRad). Membranes were blocked with Roti buffer (Roti®-Block protein free, Roth) for 1 h, then incubated with primary antibody overnight at 4 °C followed by 1 h incubation with secondary antibody at room temperature. Primary antibodies: NICD1 (1:500, ab8925, Abcam), RelB (1:200, sc-226, Santa Cruz), cRel (1:100, sc-6955, Santa Cruz), p105/50 (1:100, sc-1190, Santa Cruz), p65 (1:500, sc-372, Santa Cruz), pIKKα/β (1:1000 #2697, Cell Signalling), IKKα (1:1000 #2682S, Cell Signalling), IKKβ (1:1000 clone D30C6, #8943, Cell Signalling). Secondary antibodies: rabbit anti-goat IgG-HRP (1:5000, 2768 Santa cruz), Anti-rabbit IgG-HRP (1:3000, 7074P2 New England Biolabs), and anti-mouse (1:3000, NA931V GE Healthcare).

2.15. Cigarette smoke extract (CSE) preparation

CSE was prepared as previously described [4]. Briefly, cigarette smoke from 3 cigarettes (3R4F, Tobacco Research Institute, University of Kentucky) was bubbled through 30 ml of cell culture medium at a constant speed, in a closed environment. The resultant solution was considered as 100% CSE.

2.16. ELISA

Total IFNγ cytokine levels were measured in BAL from 3 days and 2 months CS exposed C57BL/6 N and *Dner*$^{-/-}$ mice and in cell supernantants from BMDMs using a commercial kit following the manufacturer's instructions (murine IFNγ PEP-900-K98, Preprotech).

2.17. RNA isolation and quantitative real time RT-PCR and end point PCR

RNA from tissue or cells was isolated as described using the peqGOLD total RNA kit (Peqlab). 0.5-1 μg RNA was reverse transcribed using Random Hexamers and MuLV Reverse Transcriptase (Applied Biosystems). To analyse gene expression, Platinum™ SYBR™ Green qPCR SuperMix-UDG (Thermo Fisher) on a StepOnePlus 96 well Real-Time PCR System (Applied Biosystems) was used. Primer sequences can be found in Supplementary Table 2. Gene relative expression was calculated using *HPRT1* or *Hprt1* as housekeeping genes ($2^{-\Delta Ct}$). For end point PCR, cDNA fragments were amplified in a thermo cycler using Green GoTaq Polymerase (Promega) and separated in a 2% agarose gel. Primer sequence: *Dner* 5′-CAT AAT CCT GCC CCG CTC TC-3′, 3′-TCATTTGAGTGGCTGTCCCC-5′.

2.18. Microarray

Total RNA from C57BL/6 N and *Dner*$^{-/-}$ M0, M1 and M2 BMDM was isolated with peqGOLD total RNA kit (Peqlab) including digestion of remaining genomic DNA. The Agilent 2100 Bioanalyzer was used to assess RNA quality and only high quality RNA (RIN > 7) was used for microarray analysis. For the expression profiling, about 30 ng of RNA was amplified using the Ovation Pico WTA System V2 in combination with the Encore Biotin Module (NuGEN Technologies, Inc., San Carlos, CA, USA). Amplified cDNA was hybridized on a mouse Gene 2.0 ST array (Affymetrix, Santa Clara, CA, USA). Staining and scanning (Scanner 3000 7G) was done according to the Affymetrix expression protocol including minor modifications as suggested in the Encore Biotion protocol (NuGEN Technologies, Inc). Array data has been submitted to GEO (GSE119257).

2.19. Transcriptome analysis

Expression console (v.1.4.1.46, Thermo Fisher Scientific Inc.) was used for quality control and to obtain annotated normalized RMA gene-level data (standard settings including median polish and sketch-quantile normalisation). Statistical analyses were performed by utilizing the statistical programming environment R (R Development Core Team [59]). Genewise testing for differential expression was done employing the (limma) *t*-test ($p < 0.05$) and cut-offs for ratio (>1.3-fold) and expression levels (average > 16 in at least one experimental group per comparison) were applied. PCA was done in R and the upstream regulator analysis was generated through the use of QIAGEN's Ingenuity Pathway Analysis (IPA®, QIAGEN Redwood City, www.qiagen.com/ingenuity).

2.20. Gene set enrichment analysis (GSEA)

Enrichment of defined sets of genes in our microarray data and data obtained from series matrix files downloaded from the NCBI GEO database (GSE8608) was performed using the GSEA software from the

Broad Institute (http://www.gsea-msigdb.org/gsea/index.jsp) [60]. The following molecular signature databases obtained from the GSEA collection were examined; canonical pathways (CP) REACTOME (gene set size filters: 30–500 genes, 270 gene sets), gene ontology (GO) molecular function (gene set filters: 15–500 genes, 659 gene sets).

2.21. Statistical analysis

No statistical procedure was applied to define the number of samples. GraphPad Prism (Version 6, GraphPad Software) was used for all statistical analysis. Data are presented as mean ± SD with sample size and number of repeats indicated in the Figure legends. For comparison between two groups statistical significance was analysed with Student's *t*-test *p* values <.05 were considered significant. For multiple comparisons, one-way ANOVA (one variable) or two-ways ANOVA (two variables) and Tukey's multiple comparisons test were used ($^{*}P < 0.05$, $^{**}P < 0.01$, $^{***}P < 0.001$, $^{****}P < 0.0001$).

3. Results

3.1. DNER is localised to activated macrophages in COPD patients

To determine the relevance of DNER in COPD evidenced by the GWAS studies [19,20], we assessed *DNER* expression in whole lung homogenates from healthy and COPD patients. *DNER* transcription was significantly increased in COPD patients compared to healthy controls independently of both gender and age (Fig. 1a, Supplemental Fig. 1a-b). In human lung histological sections, DNER co-localised with the macrophage marker Galectin-3 in both healthy and COPD patients (Fig. 1b, Supplemental Fig. 1c), suggesting that macrophages are the predominant DNER-expressing cells. Given the predominance of inflammation in a COPD lung, human monocyte derived macrophages (MDM) were treated with LPS plus cigarette smoke extract (CSE) to mimic the COPD microenvironment in vitro. Interestingly, *DNER* expression was significantly induced as well as the pro-inflammatory marker, *TNF* (Fig. 1c). Supporting this data, DNER co-localised with the pro inflammatory M1 marker NOS2 in human lung tissue (Fig. 1d). These results strongly suggest that pro-inflammatory human macrophages are the main cell type expressing DNER in the human lung and likely harbour DNER function during COPD development.

3.2. DNER is expressed in murine M1 macrophages and regulates IFNγ signalling

The cigarette smoke (CS)-induced COPD mouse model was used to further investigate the role of DNER in the immunopathogenesis of COPD. After 6 months of CS exposure, wild-type (WT) mice develop emphysema, airway remodelling and chronic lung inflammation [4], the main characteristic pathological changes observed in human COPD patients [3,27]. Immunofluorescence staining revealed that DNER localised to macrophages of CS-exposed COPD mice (Fig. 2a), supporting the previous findings in human tissue. As already mentioned, macrophage-driven inflammation in the context of COPD plays an important role in disease onset. Therefore, we next exposed bone marrow derived macrophages (BMDM) from WT mice to pro (M1) or anti- (M2) inflammatory stimuli and assessed *Dner* expression. Validation of BMDM differentiation was confirmed by FACS analysis (90.7% of the obtained population was F4/80^{+} CD11b^{+} CD11c^{-} Ly6g^{-} Ly6c^{-}, Supplementary Fig. 1d). Interestingly, M1 BMDM revealed significantly increased expression of *Dner* (Fig. 2b). In contrast, bone marrow derived DCs (BMDC) treated with LPS did not increase *Dner* levels, suggesting that murine macrophages are the only antigen presenting-cell that express *Dner* in response to inflammation (Supplementary Fig. 1e). To address whether DNER has a role in macrophage polarisation, microarray analysis of WT and DNER deficient BMDM polarised populations was performed. DNER deficient mice were created by deletion of *Dner* exon 3 using the Cre-LoxP system and knock out efficiency was confirmed by the absence of DNER transcript and protein in brain tissue and macrophage lysates from knock out mice (Supplementary Fig. 2a-c). Principal component analysis (PCA) revealed that M0, M1 and M2 populations were similarly clustered for both WT and DNER deficient BMDM, indicating that global macrophage polarisation is not affected by the absence of DNER (Supplementary Fig. 2d). Likewise, M1 (*Tnf*, *il12a*) and M2 (*Fizz1*, *Arg1*) markers exhibited comparable expression levels in both genotypes, confirming similar polarisation (Supplementary Fig. 2e).

Even though DNER did not influence macrophage polarisation, its expression levels are significantly elevated in M1 macrophages (Fig. 2b), which could suggest a role in signalling pathway regulation. To further analyse the downstream cascade of DNER in M1 macrophages, we performed gene set enrichment analysis (GSEA). Investigating a combination of 270 REACTOME pathway gene sets, revealed that interferon signalling was the most enriched pathway in WT M1 compared to DNER deficient M1 BMDM (Fig. 2c, d). Given the diversity and complexity of interferon signalling, we next determined which type of interferon pathway is impaired in DNER deficient mice. Interestingly, induction of type II interferon (*Ifng*), but not type I (*Ifnb1*), was significantly abrogated in M1 polarised DNER deficient compared to WT BMDM (Fig. 2e). Supporting the idea of *Ifng* as a possible downstream target of DNER, IFNγ signalling was found to be enriched in WT M1 (Fig. 2f, Supplementary Fig. 2f). Furthermore, GSEA from an online available dataset of monocyte derived macrophages (MDM) obtained from healthy and COPD patients (GSE8608) [28], revealed an enriched IFNγ pathway in COPD MDM (Fig. 2g). It should be considered that T cells, specifically Th1 cells, serve as a major source of IFNγ. However, in vitro differentiated WT T cell subpopulations showed very low expression of *Dner*, therefore making it unlikely that DNER regulates IFNγ in T cells (Supplementary Fig. 3f). Hence, these data indicated that DNER is significantly enhanced in M1 macrophages where it specifically regulates IFNγ expression.

3.3. DNER regulates IFNγ in recruited macrophages during chronic CS exposure

The persistent inflammation observed in COPD is mainly caused by the continuous secretion of pro-inflammatory cytokines, among them IFNγ is essential to maintain cytokine production and immune cell recruitment and polarisation [29]. To investigate whether in vivo DNER deficiency affects the release of IFNγ during acute and chronic inflammation, WT and DNER deficient mice were exposed to CS for 3 days (acute) or 2 months (chronic) (Supplementary Fig. 3a). Immunofluorescence staining of the bronchoalveolar lavage (BAL) macrophages from 3 days and 2 months of CS exposure revealed increased DNER expression in macrophages compared to filtered air treated animals (Fig. 3a), confirming that DNER expression is triggered in pro-inflammatory macrophages (M1). Similarly, in BAL fluid from 2 month CS-exposed mice, IFNγ levels were significantly induced in WT mice but this was not significantly enhanced in DNER deficient animals (Fig. 3b). To clarify whether DNER regulates macrophage IFNγ secretion during chronic inflammation, we analysed the lung macrophage population from chronic CS-exposed mice by flow cytometry. In line with the in vitro results, CD45^{+} Ly6g^{-} F4/80^{+} alveolar macrophages from WT mice exhibited significant IFNγ induction after chronic CS exposure which was diminished in DNER deficient mice (Fig. 3c).

To elucidate whether recruited or resident macrophages differentially secrete IFNγ in the absence of DNER, we analysed both populations by gating on CD45^{+}Ly6g^{-} F4/80^{+} SiglecF^{-} (recruited) or CD45^{+}Ly6g^{-} F4/80^{+}SiglecF^{+} (resident) populations (Fig. 3d). Strikingly, recruited macrophages from DNER deficient mice were unable to secrete IFNγ in response to CS exposure, as determined by both the percentage of IFNγ positive cells and the mean fluorescence intensity (MFI) (Fig. 3e). In contrast, resident macrophages did not show any

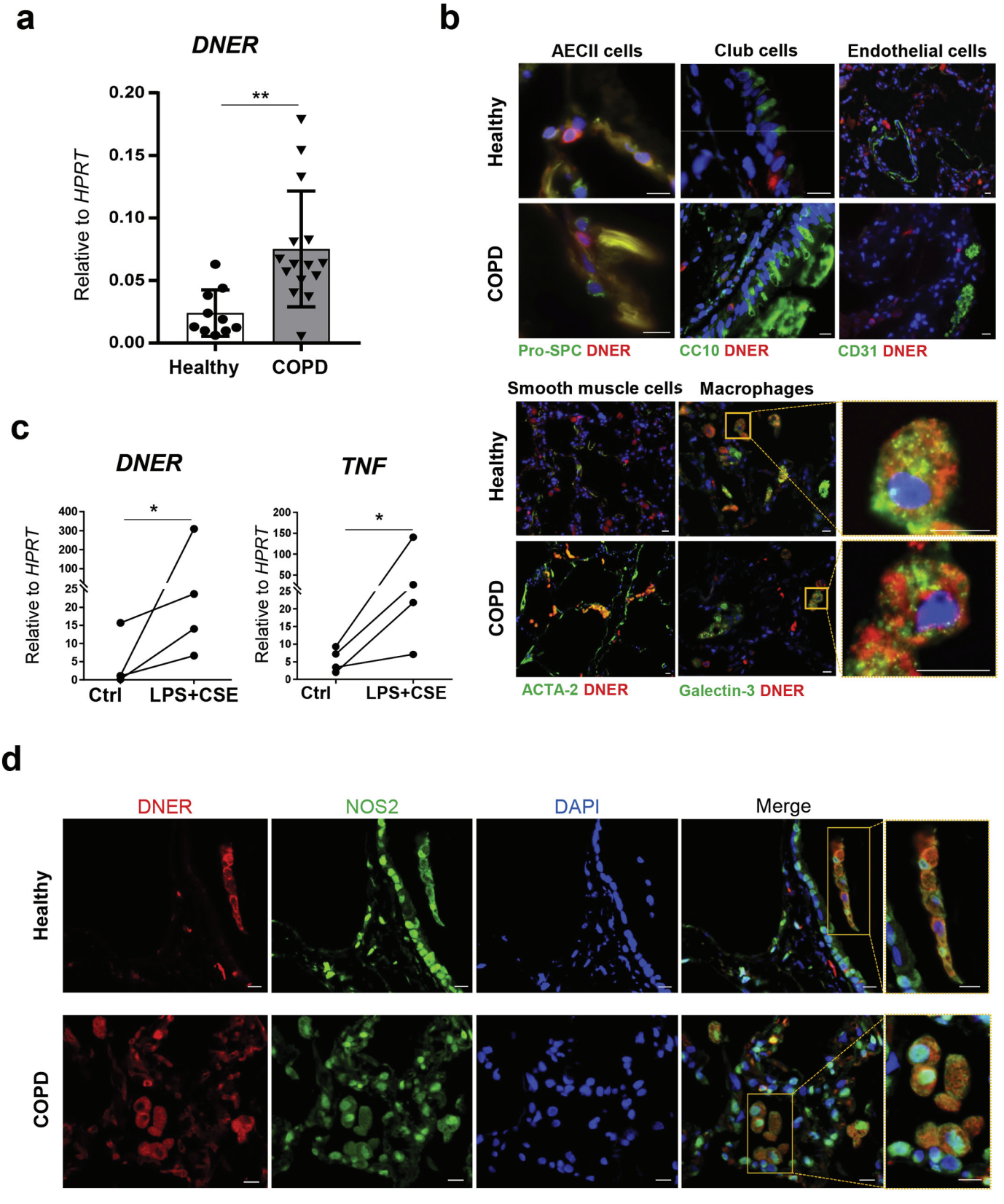

Fig. 1. *DNER* is significantly upregulated in lung tissue from COPD patients and localised to pro-inflammatory macrophages. (a) *DNER* mRNA abundance in lung tissue from healthy subjects ($n = 10$) and COPD patients ($n = 15$). $^{**}p$-value = 0.003, unpaired *t*-test. Data shown mean values ± SD. (b) Representative immmunofluorescence images from healthy and COPD lung tissue ($n = 2/3$) stained to detect localisation of DNER (red), DAPI (blue) and Pro-SPC/CC10/CD31/Acta2/Galectin-3 (green). Scale bar, 10 μm. (c) *DNER* and *TNF* mRNA abundance in human monocyte derived macrophages obtained from PBMCs of healthy subjects ($n = 4$) and treated with 1 μg/ml LPS in combination with cigarette smoke extract (CSE) 5% for 24 h. Paired *t*-test, $^{*}p = 0.0408$. (d) Representative immunofluorescence pictures of DAPI (blue), NOS2 (green) and DNER (red) staining in healthy and COPD lung tissue ($n = 3$). Scale bar, 10 μm.

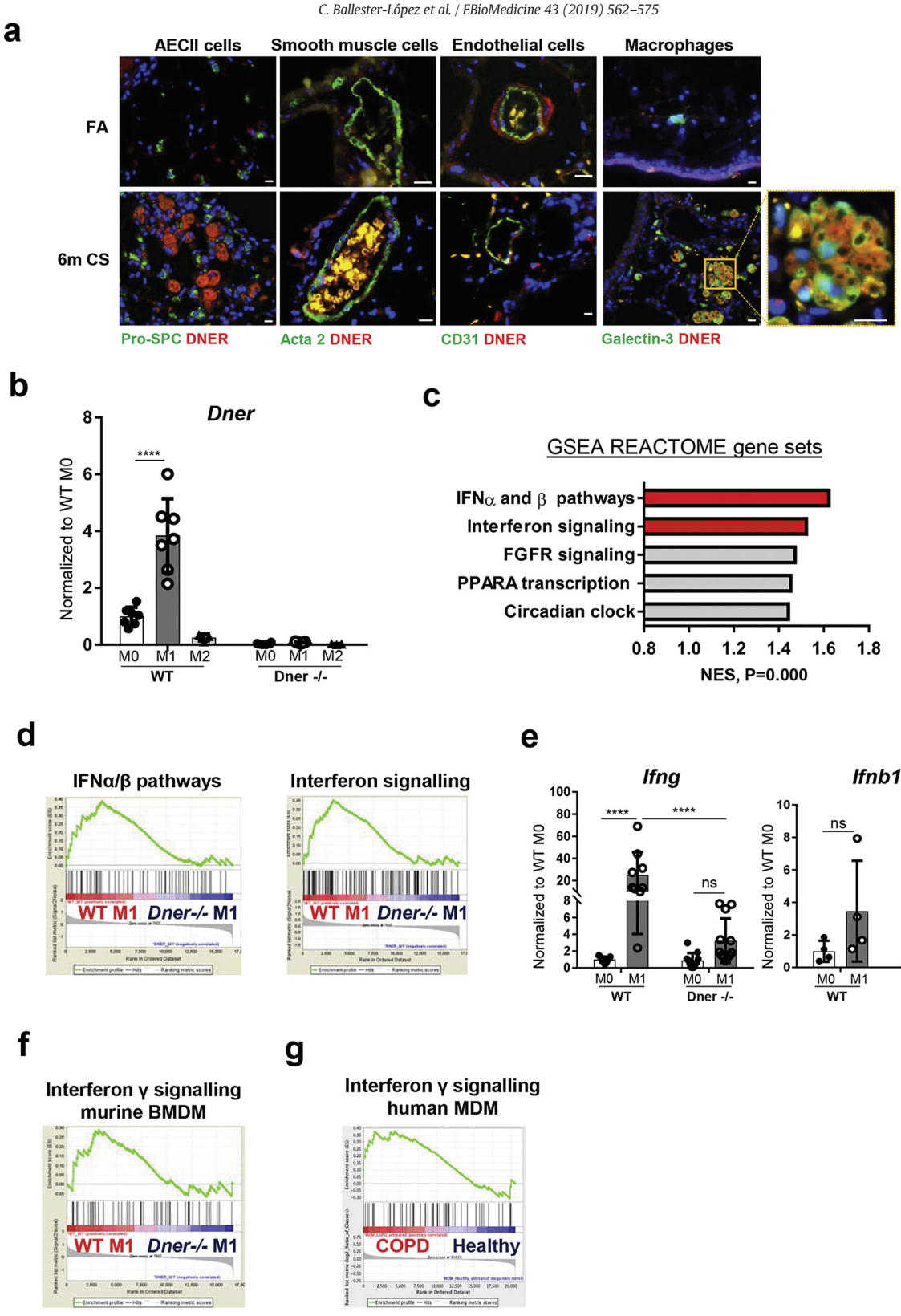

Fig. 2. DNER is localised to macrophages in 6 m CS-exposed mice and regulates IFNγ response in M1 BMDM. (a) Representative immmunofluorescence images of lung tissue from filtered air (FA) and 6 month CS-exposed mice stained with DNER (Red), DAPI (Blue) and Galectin-3/Pro-SPC/Acta-2/CD31 (green) (n = 2–3 mice per group). Scale bar, 10 μm. (b) *Dner* mRNA levels in WT and DNER deficient bone marrow derived macrophages (BMDM) treated with 1 μg/ml LPS and 20 ng/ml IFNγ (M1) or 20 ng/ml IL-4 (M2) or untreated (M0). (c) Top 5 pathways with the highest Normalized Enriched Scores (NES) in Gene set enrichment analysis (GSEA) of the microarray data from WT M1 vs DNER deficient M1 BMDM using a list of 270 REACTOME pathway gene sets obtained from the Broad Institute software. (d) Enrichment plots from (2c) of WT M1 vs DNER deficient M1 BMDM. (e) mRNA levels of *Ifnb1* and *Ifng* in M0 and M1 BMDM populations. (f) Enrichment plot of IFNγ signalling following GSEA analysis of the microarray data from WT M1 vs DNER deficient M1 BMDM. (g) Enrichment plot of IFNγ signalling from the GSEA analysis of Monocyte Derived Macrophages (MDM) obtained from healthy and COPD patient microarray data (NCBI GEO dataset, GSE8608). Two-way ANOVA, Tukey's multiple comparisons test, $^{****}P < 0.0001$ (b, e). Representative 2 independent experiments out of 5, $n = 3$ mice, 2–3 replicates per mouse (b, e). One experiment, $n = 3$ (c-d, f-g). Data shown mean values ± SD.

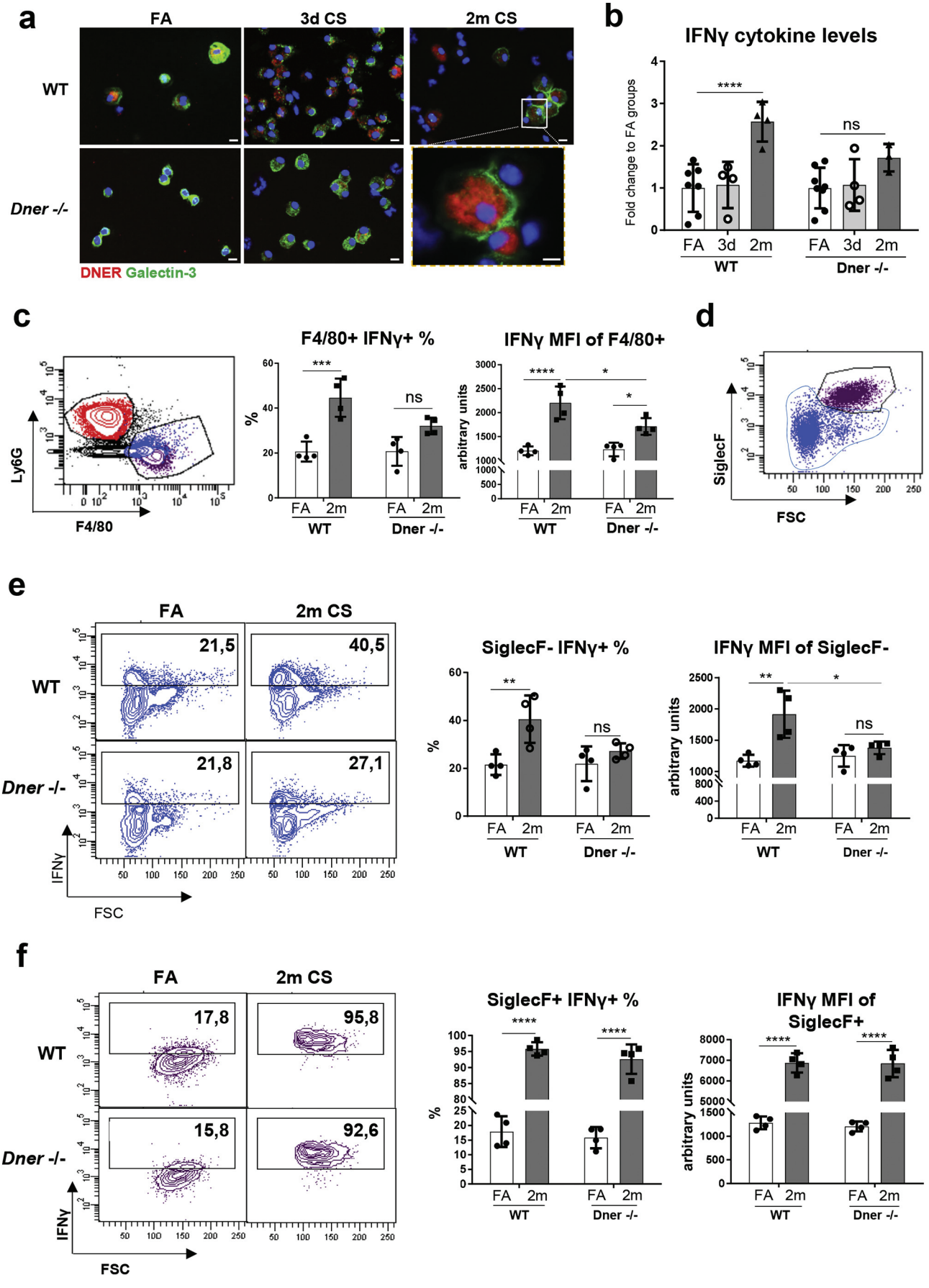
a
FA
3d CS
2m CS
WT
Dner -/-
DNER Galectin-3
b
IFNγ cytokine levels
Fold change to FA groups
****
ns
FA 3d 2m
WT
FA 3d 2m
Dner -/-
c
Ly6G
F4/80
F4/80+ IFNγ+ %
%
***
ns
FA 2m
WT
FA 2m
Dner -/-
IFNγ MFI of F4/80+
arbitrary units
****
*
*
FA 2m
WT
FA 2m
Dner -/-
d
SiglecF
FSC
e
FA
2m CS
WT
Dner -/-
21,5
40,5
21,8
27,1
IFNγ
FSC
SiglecF- IFNγ+ %
%
**
ns
FA 2m
WT
FA 2m
Dner -/-
IFNγ MFI of SiglecF-
arbitrary units
**
*
ns
FA 2m
WT
FA 2m
Dner -/-
f
FA
2m CS
WT
Dner -/-
17,8
95,8
15,8
92,6
IFNγ
FSC
SiglecF+ IFNγ+ %
%
****
****
FA 2m
WT
FA 2m
Dner -/-
IFNγ MFI of SiglecF+
arbitrary units
****
****
FA 2m
WT
FA 2m
Dner -/-

difference in IFNγ secretion between both genotypes after CS exposure (Fig. 3f). Along similar lines, innate and adaptive immune populations after CS exposure were not altered in the lungs of DNER deficient mice compared to WT (Supplementary Fig. 3d, e). Thus, explaining the partial enhancement of total IFNγ levels in BAL from 2 month CS-exposed DNER deficient mice (Fig. 3b). Previous studies have shown that high levels of IFNγ leads to significant emphysema development [30]. Interestingly, 2 months CS exposed DNER deficient mice showed a significantly retained lung function, measured as FEV100, compared to CS exposed WT mice (Supplementary Fig. 3b). This was further supported by an absence of emphysema development in DNER deficient mice after 2 months CS exposure (Supplementary Fig. 3c). Taken together, these results revealed that DNER regulates IFNγ secretion in lung recruited macrophages and is crucial for CS-induced emphysema development.

3.4. DNER activates Notch1 signalling in response to CS

Several studies have shown that Notch-NFκB crosstalk signalling regulates IFNγ transcription [31,32]. To determine whether DNER deficiency affects Notch signalling in lung macrophages, we quantified the number of nuclear NICD1$^+$ Gal3$^+$ cells (white arrows, Fig. 4a) in lung sections from FA and 2 months CS-exposed mice. Interestingly, DNER deficient mice revealed significantly reduced nuclear translocation of NICD1 in macrophages after 2 months of CS exposure in comparison to WT mice (Fig. 4a-b). In support, the Notch1 signalling pathway was enriched in WT M1 compared to DNER deficient M1 macrophages (Fig. 4c, Supplementary Fig. 4a) and a similar pattern was observed in MDM from COPD patients (Fig. 4d). This could suggest that COPD macrophages have an altered Notch signature similar to the one observed in WT versus DNER deficient lung macrophages after CS exposure. Taken altogether, this data demonstrated that CS induced Notch1 activity in alveolar macrophages in vivo via DNER.

Further, to decipher whether DNER regulates IFNγ expression via Notch1-NFκB crosstalk, WT and DNER deficient BMDM were treated with LPS ex-vivo. First, we evaluated our previous results (Fig. 2e, f) by measuring IFNγ cytokine levels in the cell supernatants. As expected, IFNγ concentration after LPS stimulation was significantly reduced in the DNER deficient BMDM cell medium compared to the WT BMDM (Supplementary Fig. 4b). Upon LPS stimulation, DNER deficient BMDM showed reduced release of NICD1 to the cytoplasm and complete absence of NICD1 nuclear translocation in contrast to WT BMDM (Fig. 5a). *Notch1* expression was similarly increased after LPS treatment in both genotypes suggesting that reduced NICD1 in DNER deficient BMDM is not due to lower Notch1 receptor levels (Fig. 5b). Likewise, the gene expression of other Notch family members expressed in macrophages was not affected in the DNER deficient BMDM (Fig. 5b).

Consistent with this, we found that the quantification of NFκB subunits revealed that cytoplasmic levels of c-Rel, p105 and p50 were reduced in DNER deficient BMDM compared to WT before and after LPS treatment (Fig. 5c). Interestingly, there was no nuclear translocation of the NFκB subunits in DNER deficient BMDM with the exception of RelB, whose levels were reduced, compared to WT BMDM (Fig. 5c). This pronounced inhibition of the NFκB pathway was independent of IKKα/β activity, as its phosphorylation levels were unaltered (Fig. 5d). Together, this data clearly indicated that DNER is necessary for Notch activation and essential for nuclear activation of NFkB signalling after LPS treatment of pro-inflammatory macrophages. Transcriptomic analysis by GSEA and upstream regulator prediction using Ingenuity Pathway Analysis (IPA) supported this data. GSEA revealed enrichment of the NFκB downstream cascade in WT M1 compared to DNER deficient M1 BMDM (Fig. 5e and Supplementary Fig. 4c) and IPA predicted, with the lowest negative *Z*-score, the NFκB complex to be the most inhibited upstream regulator in DNER deficient M1 BMDM (Supplementary Fig. 4d). Taken all together, we have demonstrated that DNER is activating the Notch1-NFκB crosstalk pathway in BMDM after LPS activation.

4. Discussion

The absence of a curative therapy for COPD, make necessary the exploration of new targets. This is the first study that investigates the role of DNER, a novel non-canonical Notch ligand that appeared to be significantly associated with COPD patients in recent GWAS studies [19]. Here, we showed that *DNER* is upregulated in COPD human lung homogenates and localised to pro-inflammatory human and murine macrophages. In a CS-induced COPD mouse model, induced DNER expression is necessary for IFNγ production in lung recruited macrophages during chronic inflammation. This was further supported in vitro, where M1 polarised DNER deficient BMDM failed to induce *Ifng* transcription in response to pro-inflammatory stimulus due to an aberrant activation of Notch1-NFκB crosstalk.

In sections of COPD and healthy lung tissue, we observed that DNER is predominantly expressed by NOS2 positive macrophages and that its mRNA levels are induced in human primary macrophages after an inflammatory stimulus. This might lead to the debate of whether *DNER* upregulation is related to COPD or is a smoking effect. Nevertheless, the authors from the GWAS also presented evidence of a lack of association between DNER and distinct smoking phenotypes, concluding that the SNP is associated with declined lung function rather than smoking. These findings together with our results, suggest that the presence of the SNP entails susceptibility for *DNER* expression in COPD patients. Indeed, exploration of the SNP genomic region using the ENSEMBL database showed that the SNP is located in a methylation-sensitive histone site and 286 bp upstream to transcription factor binding motifs (data not shown). However, it should be considered that smoking drives inflammation in the lung, and this can lead to DNER induction as well [19], independently of the presence of the SNP. In contrast to a previous study showing a positive correlation between gender and DNER expression, we did not observe any gender nor age effect on DNER levels (Supplementary Fig. 1a-b). Additionally, the use of inhaled corticosteroids (ICS), a common immunosuppressive medicament for COPD patients, did not seem to affect lung DNER expression either (data not shown). These data suggest that the increased *DNER* expression in COPD lung homogenates is most likely due to an increase in pro-inflammatory macrophages. Supporting this idea, a very recent proteomic analysis of sputum from asthmatic patients showed that DNER was increased among 15 other markers implicated in macrophage-related inflammation [33].

The predominance and contribution of different macrophage subpopulations to the immunopathogenesis of COPD is unclear, especially given the complexity and diversity that entails the macrophage population [34,35]. Regarding origin, some studies suggest that lung resident macrophages have greater ability to phagocytose and secrete anti-inflammatory cytokines, meanwhile recruited macrophages tend to have a more pro-inflammatory phenotype. Indeed, it is believed that

Fig. 3. DNER regulates IFNγ secretion in lung recruited macrophages during CS-induced chronic inflammation. (a) Representative immunofluorescence images of bronchoalveolar lavage (BAL) cells obtained from filtered air (FA) and 3 day or 2 month CS-exposed WT and DNER deficient mice stained to detect DNER (red), Galectin-3 (green) and DAPI (blue) (n = 2–3 mice per group). (b) Total IFNγ levels quantified by ELISA in BAL from FA, 3 day and 2 month CS-exposed WT and DNER deficient mice (n = 4 mice per group). (c, d, e and f) Flow cytometric analysis of Ly6g$^-$ F4/80$^+$ macrophage populations from the whole lung of FA and 2 month CS-exposed WT and DNER deficient mice (n = 4 mice per group). (c) Percentage of IFNγ$^+$ cells gated from Ly6g$^-$ F4/80$^+$ macrophages and the MFI of IFNγ staining in the Ly6g$^-$ F4/80$^+$ population. (d) Gating strategy for Ly6g$^-$ F4/80$^+$ SiglecF$^+$ and SiglecF$^-$ populations. (e) Percentage of IFNγ$^+$ cells gated from SiglecF$^-$ Ly6g$^-$ F4/80$^+$ macrophages (blue from d) and the MFI of IFNγ staining in the SiglecF$^-$ Ly6g$^-$ F4/80$^+$ population. (f) Percentage of IFNγ$^+$ cells gated from SiglecF$^+$ Ly6g$^-$ F4/80$^+$ macrophages (burgundy population from d) and the MFI of IFNγ staining in the SiglecF$^+$ Ly6g$^-$ F4/80$^+$ population. Two-way ANOVA, Tukey's multiple comparisons test, $^*p < 0.05$, $^{**}p < 0.01$, $^{***}p < 0.001$, $^{****}p < 0.0001$. Each data point represents an individual mouse. Data shown mean values ± SD. (b-c, e-f).

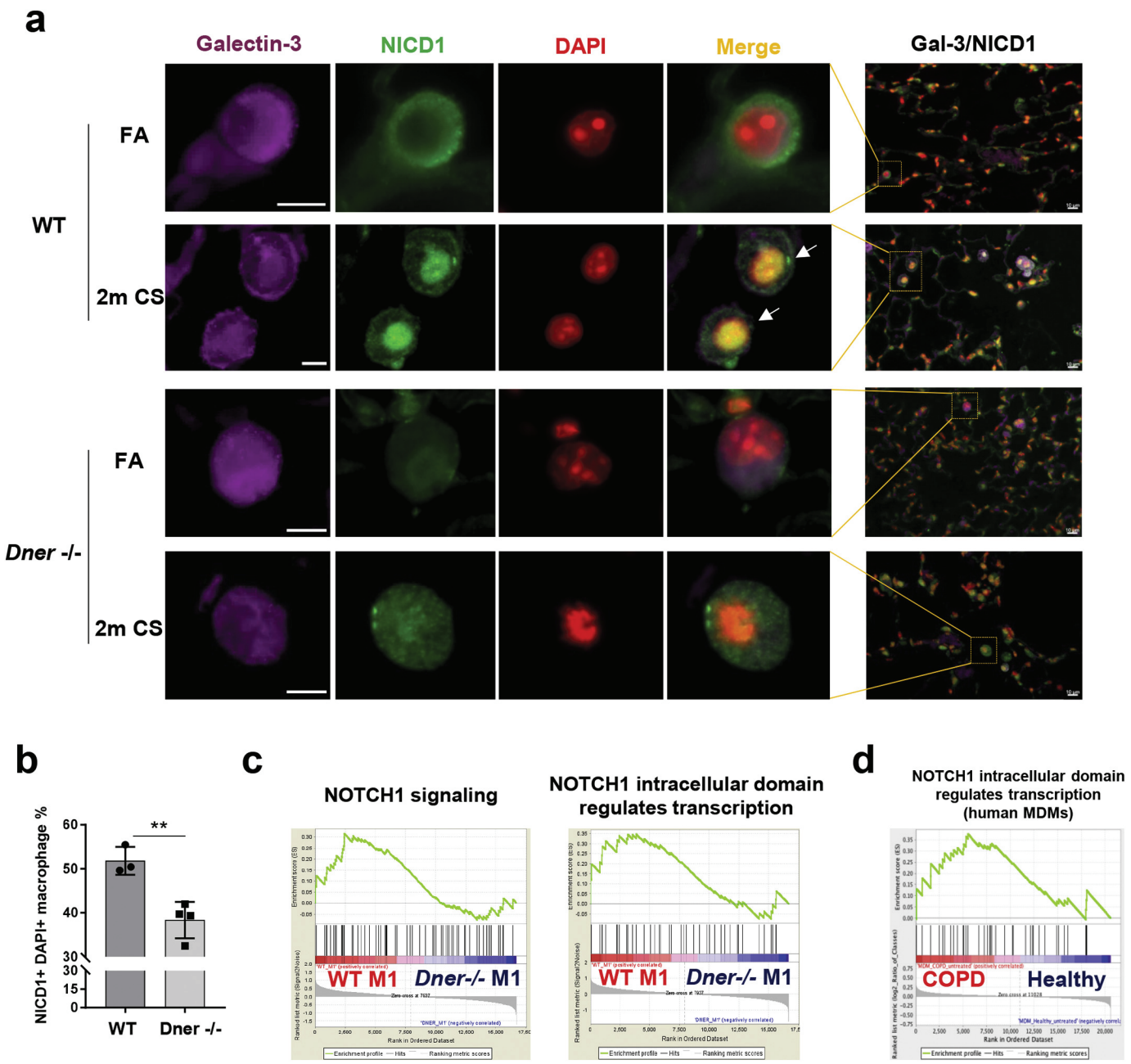

Fig. 4. DNER activates Notch1 signalling in alveolar macrophages from 2 month CS exposed mice. (a) Representative immunofluorescence images of lung tissue from FA and 2 m CS-exposed WT and DNER deficient mice (n = 3–4 mice per group), Galectin-3 (purple), NICD1 (green) and DAPI (red), high magnification, scale bars 5 μm; low magnification, 10 μm. Yellow squares indicate tissue location of the amplified macrophages. (b) Quantification of Galectin3$^+$ cells showing NICD1$^+$ DAPI overlap (white arrows shown in 4a) from staining in (a). 12 pictures at 20× magnification were taken from each mouse sample of each group. Unpaired t-test, $^{**}p$-value = 0.0055. No significant difference was found between FA groups. (c) Enrichment plots of Notch1 signalling from GSEA analysis of the microarray data from WT M1 vs DNER deficient M1 BMDM. (d) Enrichment plot of Notch1 signalling from the GSEA analysis of Monocyte Derived Macrophages (MDM) obtained from healthy and COPD patient microarray data (GSE8608).

when recruited macrophages enter the inflammatory zone, they become M1 in response to the ongoing insult, contributing to the exaggerated production of pro-inflammatory cytokines [10]. Concerning the macrophage phenotypes in the lung, recent reviews point to a direction of dysfunctionality in both phenotypes, M1 and M2, which results in defective cytokine secretion, migration and efferocytosis [14,15]. Nevertheless, it should be taken into account that the concept of M1/M2 emerged from an in vitro setting where the stimuli are known and stable [11]. Thus, it becomes controversial whether there is the existence of well-defined M1 and M2 subpopulations in a disease context, where the microenvironment constantly changes [10,34]. Together with the lack of appropriate markers to track these macrophage subpopulations, leads us to question whether in vitro findings can be extrapolated to what occurs during disease development. Nevertheless, we do believe that in vivo, a macrophage phenotype can be more pro than anti-inflammatory or vice-versa at a certain time and place, and this is what we would consider "M1" or "M2" in a disease context.

Several studies have shown that blockade of the Notch pathway improves disease resolution by regulating macrophage polarisation in autoimmune and inflammatory diseases [36,37]. Most of the published data consistently supports that Notch promotes a pro-inflammatory response in macrophages mainly by enhancing TLR and NFκB signalling [38,39]. Interestingly, our GSEA on monocyte derived macrophages (MDM) from COPD and healthy subjects showed an enrichment of the

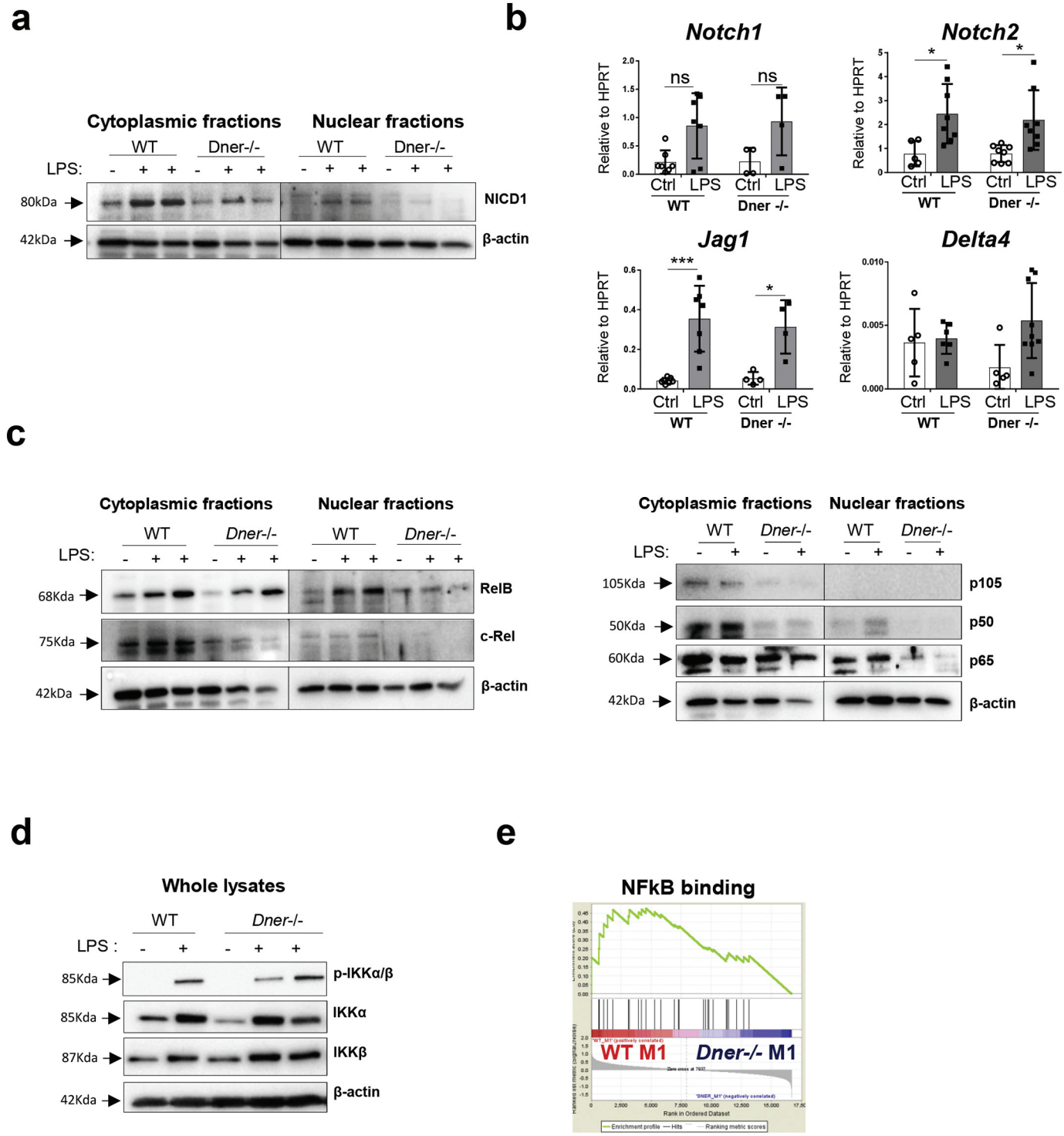

Fig. 5. Nuclear translocation of Notch1 and NFκB active subunits was abrogated in LPS treated BMDM from DNER deficient mice. (a) Representative Western blot of NICD1 protein levels in cytoplasmic and nuclear extracts of samples from WT and DNER deficient BMDM treated with LPS (1μg/ml) for 24 h and untreated (2 independent experiments, 2/3 biological replicates). (b) mRNA abundance of Notch receptors (*Notch1, Notch2*) and ligands (*Delta4, Jag1*) in the samples from (a). Two-way ANOVA, Tukey's multiple comparisons test, $^{*}P < 0.05$, $^{***}P < 0.001$. Data shown mean values ± SD. (c) Cytoplasmic and nuclear RelB, c-Rel, p105, p50 and p65 from samples described in (a). (d) Representative Western blots of phosphorylated (p)-IKKα/β, IKKα and IKKβ from 15 min LPS (1μg/ml) treated WT and DNER deficient BMDM. 2 independent experiments and 2/3 biological replicates, n = 3 (e) Enrichment plot of NFkB signalling (GO:0051059) following GSEA analysis of the microarray data from WT M1 vs DNER deficient M1 BMDM.

Notch pathway in COPD MDM. Here, we showed that DNER is essential for a fully functioning IFNγ driven M1 pro-inflammatory response in murine macrophages even though it was not crucial for delineating the distinct phenotypes.

IFNγ is one of the most upregulated cytokines in the lung of COPD patients [40,41]. Indeed, COPD MDM showed an enrichment of IFN pathways compared to healthy subjects. On the one hand, it plays a key role in promoting inflammation and tissue damage by polarising macrophages and T cells towards a type 1 response [29]. On the other, it induces bacterial clearance by activating phagocytosis and enhancing antigen presentation and nitric oxide production, important defence mechanisms during disease exacerbation [42,43]. Therefore, it should

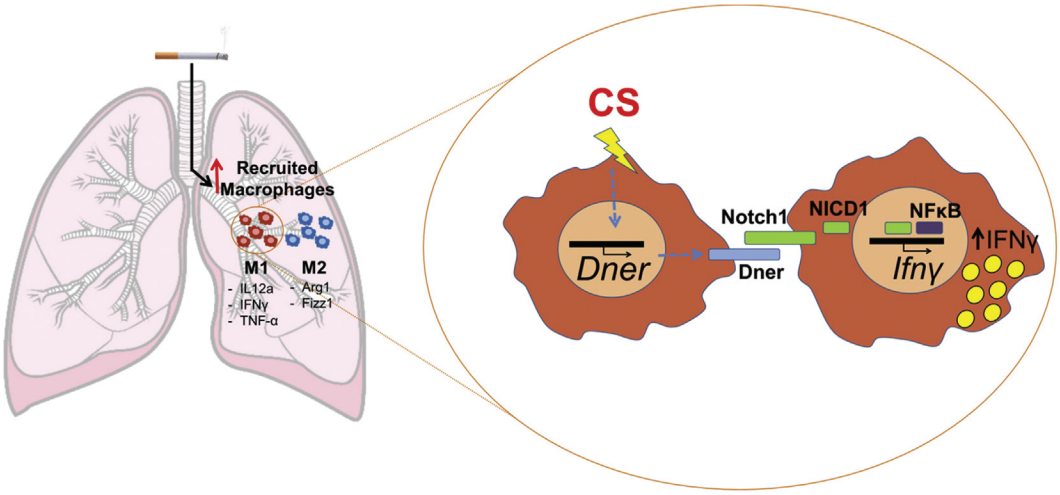

Fig. 6. Proposed role for DNER in macrophages during COPD inflammatory responses.

be considered that IFNγ may be beneficial as well as detrimental to the lung. Neutrophils, dendritic cells, NK, B, Th1 and $CD8^+$ T cells are all known to release IFNγ in response to infections and macrophage-driven inflammation [44,45]. Despite the fact that T cells are the most common IFNγ-producing cells [46], macrophages are the dominant cell population in a COPD lung [8], suggesting that macrophage contribution to IFNγ levels is likely considerable. Moreover, macrophages play a pivotal role in promoting inflammation at the early stage of disease, when IFNγ is involved [42,47,48]. Additionally, high levels of IFNγ can alleviate tissue injury by inducing TGFβ in macrophages [42] but it can also induce epithelial cell apoptosis and subsequent emphysema [30]. Thus, the precise regulation of IFNγ in COPD is essential to resolve infection without provoking an exaggerated inflammatory response. This would mean that dampening excessive levels of IFNγ, but not complete abrogation, could improve COPD patient outcomes. Here, we showed that IFNγ production is abrogated in recruited but not in resident macrophages from DNER deficient mice during chronic inflammation. In COPD, it has been suggested that recruited macrophages tend to acquire a pro-inflammatory phenotype, while resident macrophages become anti-inflammatory and pro-resolving cells [49]. Thus one could hypothesize that the blockage of DNER may modulate IFNγ levels and therefore control the exaggerated immune response in pro-inflammatory macrophages, without affecting the potential beneficial effects that IFNγ could exert in other cell types. Indeed, we showed that DNER deficiency in mice prevented CS induced emphysema and improved lung function (FEV100), without affecting the percentage or activation of the immune cell populations.

Currently, the molecular mechanism of non-canonical Notch signalling is controversial and poorly understood. It has been shown that DNER specifically interacts with the first and second EGF-like repeat of the extracellular domain of Notch1 by cell-cell contact, and activates gene transcription in a CSL-independent manner during Bergmann glia differentiation [21]. In this process, DNER cell location is precisely controlled by endocytosis to regulate its availability to interact with other neighbouring cells [50–52]. This explains why DNER, as a transmembrane protein, showed a cytoplasmic localisation in our immunofluorescence analysis. Indeed, previous analysis of DNER in neurons, showed a similar cellular distribution to the one we observe in macrophages [50,51].

Non-canonical Notch is characterized for being independent of CSL, and instead, regulating other signalling proteins such as the NFκB subunits [22]. Indeed, the presence of nuclear NICD1 is essential for NFκB signalling in T cells and macrophages to regulate transcription of pro-inflammatory cytokines. In Th1 cells, interaction of NICD1 with p50 and c-Rel regulates transcription of IFNγ in response to CD3/CD28 co-stimulation [31,32]. In the case of macrophages, it has been shown that NICD1 regulates nuclear translocation of NFκB subunits and it is able to directly bind to TNF and INOS promoters [39,53]. However, the Notch ligands upstream of these responses remains poorly understood. It has been suggested that Jag1 and Delta4 can trigger and maintain Notch signalling by the activation of a positive feedback loop in pro-inflammatory macrophages [54]. In order to undertake molecular studies to address the DNER induced signalling cascade in activated BMDM, macrophages were stimulated with LPS alone instead of the combination with IFNγ as performed for M1 polarisation, since IFNγ activates other pathways and a positive feedback loop [44], that could make it difficult to interpret the results. In contrast to previous studies, our data revealed that induced levels of Jag1 and Delta4 in LPS treated DNER deficient BMDM are not able to compensate for the reduction in IFNγ expression. Here, we showed that the non-canonical Notch ligand DNER regulates IFNγ transcription via NICD1 and NFκB signalling in primary murine macrophages upon LPS stimulation and in vivo chronic inflammation. Supporting these findings, quantification of triple nuclear $NICD1^+$ macrophages, revealed that DNER deficient 2 month CS-exposed mice exhibited reduced nuclear NICD1 translocation compared to WT macrophages which was accompanied by impaired nuclear translocation of the NFκB subunits in LPS stimulated BMDM from DNER deficient mice. In keeping with NFκB regulating the expression of the majority of cytokines in activated macrophages [55], gene levels of NFκB downstream targets, aside from IFNγ, was observed to be dampened in DNER deficient M1 macrophages as evidenced by GSEA and predictive upstream regulator analysis. Nevertheless, we would have expected a more pronounced reduction in cytokine expression given the strong abrogation of NFκB in LPS-treated DNER deficient BMDM. However, it should be taken into account that other key pathways for cytokine expression like MAPK cascade, ERK or JAK/STAT1 could partially compensate the absence of NFκB activation [56].

Taken all together, we speculate that exposure of lung recruited macrophages to the ongoing inflammatory insult during COPD progression, leads to increased levels of DNER and subsequent induction of IFNγ expression via a non-canonical Notch NFκB cross talk pathway in Notch1 positive macrophages (Fig. 6). This study not only adds new molecular insights to the complexity of Notch and the involvement of non-canonical signalling in COPD pathogenesis, but also opens new directions to further investigate novel targets for the treatment of COPD.

Author contributions

CBL and AÖY conceived the study and experimental design. CBL conducted the experiments. TMC contributed to FACS experiments, animal

preparation and GSEA analysis. ZE performed BMDM culture and cell fractioning. SEV provided the human samples. FG and IEF undertook experiments with human monocyte derived macrophages. MI and JB performed microarray analysis. CBL, TMC, OE and AÖY analysed and interpreted the data. CBL, TMC and AÖY wrote the manuscript. All authors read and edited the manuscript.

Declaration of interests

The authors declare no competing interests.

Acknowledgements

The authors acknowledge the technical assistance of Christine Hollauer (Helmholtz Zentrum München). We thank Dr. Stephanie J. London and Dr. Matthias Wjst for stimulating discussion. We gratefully acknowledge the provision of human biomaterial and clinical data from the CPC-M bioArchive and its partners at the Asklepios Biobank Gauting, the Klinikum der Universität München and the Ludwig-Maximilians-Universität München. This work was supported from the Helmholtz Alliance 'Aging and Metabolic Programming, AMPro' (J.B.). The funding bodies did not have any role in study design, data collection, data analysis, interpretation or writing of the report.

Appendix A. Supplementary data

Supplementary data to this article can be found online at https://doi.org/10.1016/j.ebiom.2019.03.054.

References

[1] Barnes PJ. Targeting cytokines to treat asthma and chronic obstructive pulmonary disease. Nat Rev Immunol 2018;1.
[2] Burney PG, Patel J, Newson R, Minelli C, Naghavi M. Global and regional trends in COPD mortality, 1990-2010. Eur Respir J 2015;45:1239–47.
[3] Barnes PJ. Cellular and molecular mechanisms of asthma and COPD. Clin Sci 2017; 131:1541–58.
[4] Jia J, Conlon TM, Sarker RS, Tasdemir D, Smirnova NF, Srivastava B, et al. Cholesterol metabolism promotes B-cell positioning during immune pathogenesis of chronic obstructive pulmonary disease. EMBO Mol Med 2018;10.
[5] John-Schuster G, Hager K, Conlon TM, Irmler M, Beckers J, Eickelberg O, et al. Cigarette smoke-induced iBALT mediates macrophage activation in a B cell-dependent manner in COPD. Am J Physiol Lung Cell Mol Physiol 2014;307:L692–706.
[6] Bhat TA, Panzica L, Kalathil SG, Thanavala Y. Immune dysfunction in patients with chronic obstructive pulmonary disease. Ann Am Thorac Soc 2015;12(Suppl. 2): S169–75.
[7] Barnes PJ. Immunology of asthma and chronic obstructive pulmonary disease. Nat Rev Immunol 2008;8:183–92.
[8] Finkelstein R, Fraser RS, Ghezzo H, Cosio MG. Alveolar inflammation and its relation to emphysema in smokers. Am J Respir Crit Care Med 1995;152:1666–72.
[9] Maeno T, Houghton AM, Quintero PA, Grumelli S, Owen CA, Shapiro SD. CD8+ T cells are required for inflammation and destruction in cigarette smoke-induced emphysema in mice. J Immunol 2007;178:8090–6.
[10] Yamasaki K, Eeden SFV. Lung macrophage phenotypes and functional responses: role in the pathogenesis of COPD. Int J Mol Sci 2018;19.
[11] Mills CD. Anatomy of a discovery: m1 and m2 macrophages. Front Immunol 2015;6: 212.
[12] Wang N, Liang H, Zen K. Molecular mechanisms that influence the macrophage m1-m2 polarization balance. Front Immunol 2014;5:614.
[13] Byrne AJ, Mathie SA, Gregory LG, Lloyd CM. Pulmonary macrophages: key players in the innate defence of the airways. Thorax 2015;70:1189–96.
[14] Kapellos TS, Bassler K, Aschenbrenner AC, Fujii W, Schultze JL. Dysregulated functions of lung macrophage populations in COPD. J Immunol Res 2018;2018:2349045.
[15] Vlahos R, Bozinovski S. Role of alveolar macrophages in chronic obstructive pulmonary disease. Front Immunol 2014;5:435.
[16] High M, Cho HY, Marzec J, Wiltshire T, Verhein KC, Caballero MT, et al. Determinants of host susceptibility to murine respiratory syncytial virus (RSV) disease identify a role for the innate immunity scavenger receptor MARCO gene in human infants. EBioMedicine 2016;11:73–84.
[17] Shaykhiev R, Krause A, Salit J, Strulovici-Barel Y, Harvey BG, O'Connor TP, et al. Smoking-dependent reprogramming of alveolar macrophage polarization: implication for pathogenesis of chronic obstructive pulmonary disease. J Immunol 2009; 183:2867–83.
[18] Walter W, Alonso-Herranz L, Trappetti V, Crespo I, Ibberson M, Cedenilla M, et al. Deciphering the dynamic transcriptional and post-transcriptional networks of macrophages in the healthy heart and after myocardial injury. Cell Rep 2018;23:622–36.
[19] Hancock DB, Soler Artigas M, Gharib SA, Henry A, Manichaikul A, Ramasamy A, et al. Genome-wide joint meta-analysis of SNP and SNP-by-smoking interaction identifies novel loci for pulmonary function. PLoS Genet 2012;8:e1003098.
[20] Busch R, Hobbs BD, Zhou J, Castaldi PJ, McGeachie MJ, Hardin ME, et al. Genetic association and risk scores in a chronic obstructive pulmonary disease meta-analysis of 16,707 subjects. Am J Respir Cell Mol Biol 2017;57:35–46.
[21] Eiraku M, Tohgo A, Ono K, Kaneko M, Fujishima K, Hirano T, et al. DNER acts as a neuron-specific notch ligand during Bergmann glial development. Nat Neurosci 2005;8:873–80.
[22] D'Souza B, Meloty-Kapella L, Weinmaster G. Canonical and non-canonical Notch ligands. Curr Top Develop Biol 2010;92:73–129.
[23] Eiraku M, Hirata Y, Takeshima H, Hirano T, Kengaku M. Delta/notch-like epidermal growth factor (EGF)-related receptor, a novel EGF-like repeat-containing protein targeted to dendrites of developing and adult central nervous system neurons. J Biol Chem 2002;277:25400–7.
[24] Tohgo A, Eiraku M, Miyazaki T, Miura E, Kawaguchi SY, Nishi M, et al. Impaired cerebellar functions in mutant mice lacking DNER. Mol Cell Neurosci 2006;31:326–33.
[25] Wang L, Wu Q, Zhu S, Li Z, Yuan J, Yu D, et al. Delta/notch-like epidermal growth factor-related receptor (DNER) orchestrates stemness and cancer progression in prostate cancer. Am J Transl Res 2017;9:5031–9.
[26] Sun P, Xia S, Lal B, Eberhart CG, Quinones-Hinojosa A, Maciaczyk J, et al. DNER, an epigenetically modulated gene, regulates glioblastoma-derived neurosphere cell differentiation and tumor propagation. Stem Cells 2009;27:1473–86.
[27] Tanabe N, Vasilescu DM, Kirby M, Coxson HO, Verleden SE, Vanaudenaerde BM, et al. Analysis of airway pathology in COPD using a combination of computed tomography, micro-computed tomography and histology. Eur Respir J 2018;51.
[28] Hofer TP, Frankenberger M, Mages J, Lang R, Meyer P, Hoffmann R, et al. Tissue-specific induction of ADAMTS2 in monocytes and macrophages by glucocorticoids. J Mol Med (Berl) 2008;86:323–32.
[29] Barnes PJ. Inflammatory mechanisms in patients with chronic obstructive pulmonary disease. J Allergy Clin Immunol 2016;138:16–27.
[30] Wang Z, Zheng T, Zhu Z, Homer RJ, Riese RJ, Chapman Jr HA, et al. Interferon gamma induction of pulmonary emphysema in the adult murine lung. J Exp Med 2000;192: 1587–600.
[31] Palaga T, Miele L, Golde TE, Osborne BA. TCR-mediated Notch signaling regulates proliferation and IFN-gamma production in peripheral T cells. J Immunol 2003; 171:3019–24.
[32] Shin HM, Minter LM, Cho OH, Gottipati S, Fauq AH, Golde TE, et al. Notch1 augments NF-kappaB activity by facilitating its nuclear retention. EMBO J 2006;25:129–38.
[33] Kasaian MT, Lee J, Brennan A, Danto SI, Black KE, Fitz L, et al. Proteomic analysis of serum and sputum analytes distinguishes controlled and poorly controlled asthmatics. Clin Exp Allergy 2018;48:814–24.
[34] Xue J, Schmidt SV, Sander J, Draffehn A, Krebs W, Quester I, et al. Transcriptome-based network analysis reveals a spectrum model of human macrophage activation. Immunity 2014;40:274–88.
[35] Franke-Ullmann G, Pfortner C, Walter P, Steinmuller C, Lohmann-Matthes ML, Kobzik L. Characterization of murine lung interstitial macrophages in comparison with alveolar macrophages in vitro. J Immunol 1996;157:3097–104.
[36] Zhang W, Xu W, Xiong S. Blockade of Notch1 signaling alleviates murine lupus via blunting macrophage activation and M2b polarization. J Immunol 2010;184:6465–78.
[37] Yin J, Hu H, Li X, Xue M, Cheng W, Wang Y, et al. Inhibition of Notch signaling pathway attenuates sympathetic hyperinnervation together with the augmentation of M2 macrophages in rats post-myocardial infarction. Am J Physiol Cell Physiol 2016;310:C41–53.
[38] Xu J, Chi F, Guo T, Punj V, Lee WN, French SW, et al. NOTCH reprograms mitochondrial metabolism for proinflammatory macrophage activation. J Clin Invest 2015; 125:1579–90.
[39] Monsalve E, Ruiz-Garcia A, Baladron V, Ruiz-Hidalgo MJ, Sanchez-Solana B, Rivero S, et al. Notch1 upregulates LPS-induced macrophage activation by increasing NF-kappaB activity. Eur J Immunol 2009;39:2556–70.
[40] Panzner P, Lafitte JJ, Tsicopoulos A, Hamid Q, Tulic MK. Marked up-regulation of T lymphocytes and expression of interleukin-9 in bronchial biopsies from patients with chronic bronchitis with obstruction. Chest 2003;124:1909–15.
[41] Reeves EP, Williamson M, Byrne B, Bergin DA, Smith SG, Greally P, et al. IL-8 dictates glycosaminoglycan binding and stability of IL-18 in cystic fibrosis. J Immunol 2010; 184:1642–52.
[42] Wang G, Lin A, Han Q, Zhao H, Tian Z, Zhang J. IFN-gamma protects from apoptotic neutrophil-mediated tissue injury during acute Listeria monocytogenes infection. Eur J Immunol Sep 2018;48(9):1470–80.
[43] Todisco T, Vecchiarelli A, Dottorini M, Eslami A, Bertotto A, Massucci M, et al. Interferon-gamma (r-IFN-gamma) induced activation of alveolar macrophages (AM) from anergic patients with chronic obstructive pulmonary disease (COPD). J Biol Regul Homeost Agents 1992;6:87–92.
[44] Hu X, Ivashkiv LB. Cross-regulation of signaling pathways by interferon-gamma: implications for immune responses and autoimmune diseases. Immunity 2009;31: 539–50.
[45] Wang G, Lin A, Han Q, Zhao H, Tian Z, Zhang J. IFN-gamma protects from apoptotic neutrophil-mediated tissue injury during acute listeria monocytogenes infection. Eur J Immunol 2018;48:1470–80.
[46] Schroder K, Hertzog PJ, Ravasi T, Hume DA. Interferon-gamma: an overview of signals, mechanisms and functions. J Leukoc Biol 2004;75:163–89.
[47] Sun K, Metzger DW. Inhibition of pulmonary antibacterial defense by interferon-gamma during recovery from influenza infection. Nat Med 2008;14:558–64.
[48] Wang F, Zhang S, Jeon R, Vuckovic I, Jiang X, Lerman A, et al. Interferon gamma induces reversible metabolic reprogramming of M1 macrophages to sustain cell viability and pro-inflammatory activity. EBioMedicine 2018;30:303–16.

[49] Aberdein JD, Cole J, Bewley MA, Marriott HM, Dockrell DH. Alveolar macrophages in pulmonary host defence the unrecognized role of apoptosis as a mechanism of intracellular bacterial killing. Clin Exp Immunol 2013;174:193–202.
[50] Fukazawa N, Yokoyama S, Eiraku M, Kengaku M, Maeda N. Receptor type protein tyrosine phosphatase zeta-pleiotrophin signaling controls endocytic trafficking of DNER that regulates neuritogenesis. Mol Cell Biol 2008;28:4494–506.
[51] Kurisu J, Fukuda T, Yokoyama S, Hirano T, Kengaku M. Polarized targeting of DNER into dendritic plasma membrane in hippocampal neurons depends on endocytosis. J Neurochem 2010;113:1598–610.
[52] Du J, Wang X, Zhang X, Zhang X, Jiang H. DNER modulates the length, polarity and synaptogenesis of spiral ganglion neurons via the Notch signaling pathway. Mol Med Rep 2018;17:2357–65.
[53] Boonyatecha N, Sangphech N, Wongchana W, Kueanjinda P, Palaga T. Involvement of Notch signaling pathway in regulating IL-12 expression via c-Rel in activated macrophages. Mol Immunol 2012;51:255–62.
[54] Palaga T, Wongchana W, Kueanjinda P. Notch Signaling in macrophages in the context of Cancer immunity. Front Immunol 2018;9:652.
[55] Hayden MS, West AP, Ghosh S. NF-kappaB and the immune response. Oncogene 2006;25:6758–80.
[56] Oeckinghaus A, Hayden MS, Ghosh S. Crosstalk in NF-kappaB signaling pathways. Nat Immunol 2011;12:695–708.
[57] John G, Kohse K, Orasche J, Reda A, Schnelle-Kreis J, Zimmermann R, et al. The composition of cigarette smoke determines inflammatory cell recruitment to the lung in COPD mouse models. Clin Sci 2014;126:207–21.
[58] Schneider CA, Rasband WS, Eliceiri KW. NIH image to ImageJ: 25 years of image analysis. Nat Methods 2012;9:671–5.
[59] Team RC. R: A Language and Environment for Statistical Computing; 2014.
[60] Subramanian A, Tamayo P, Mootha VK, Mukherjee S, Ebert BL, Gillette MA, et al. Gene set enrichment analysis: a knowledge-based approach for interpreting genome-wide expression profiles. Proc Natl Acad Sci U S A 2005;102:15545–50.

Supplementary Table 1

		Healthy	COPD
Subjects (n)		10	15
Mean age years		45.7 ± 4.65	57.2 ± 1.31
Sex	**Male**	6	6
	Female	4	9
Height (m)		1.72 ± 0.03	1.64 ± 0.02
Weight (kg)		77 ± 4.22	60.4 ± 3.21
Smoking (packs/year)			41.6 ± 7.57
FEV1 (%)			35 ± 5.89
FVC (%)			83.35 ± 6.24
FEV1/FVC (%)			33.80 ± 3.10
Bronchodilators only (subjects)			4 (26.6%)
Bronchodilators + ICS (subjects)			10 (66.6%)

Supplementary Table 2

Gene	Forward primer	Reverse Primer
DNER	CGA CCT GTG CCC AGC TTA TT	AGG CCA TGG TAA CCT GGA TCA
TNF	GCC TCT TCT CCT TCC TGA TCG	AGC TTG AGG GTT TGC TAC AAC A
HPRT1	AGG AAA GCA AAG TCT GCA TTG TT	GGT GGA GAT GAT CTC TCA ACT TTA A
Dner	AAT GGC ACT TGC TAC GTG GA	GGC CAT GGT AAC CTG GAT CG
Tnf	CAC CAC GCT CTT CTG TCT	GGC TAC AGG CTT GTC ACT C
Il12p35	ACT AGA GAG ACT TCT TCC ACA ACA AGA G	GCA CAG GGT CAT CAT CAA AGA C
Fizz1	TGC CAA TCC AGC TAA CTA TCC C	ACG AGT AAG CAC AGG CAG TT
Arg1	GGA ACC CAG AGA GAG CAT GA	TTT TTC CAG CAG ACC AGC TT
Ifnb1	CAG CTC CAAG AAA GGA CGA AC	GGC AGT GTA ACT CTT CTG CAT
Ifng	TCA AGT GGC ATA GAT GTG GAA GAA	TGG CTC TGC AGG ATT TTC ATG
Notch1	ACA GTG CAA CCC CCT GTA TG	AGT TGT TCC GTA GCT GGT CG
Notch2	AGC AGG AGG TGA TAG GCT CT	TGG GCG TTT CTT GGA CTC TC
Jag1	AGC CAA GGT GTG CGG G	ACG CGG GAC TGA TAC TCC TT
Delta4	TTC CAG GCA ACC TTC TCC GA	ACT GCC GCT ATT CTT GTC CC
Hprt1	AGC TAC TGT AAT GAT CAG TCA ACG	AGA GGT CCT TTT CAC CAG CA
Tbet	TCA GGA CTA GGC GAA GGA GA	TAG TGG GCA CCT TCC AAT TC
Gata3	GTC ATC CCT GAG CCA CAT CT	TAG AAG GGG TCG GAG GAA CT
Rorgt	TTTGGAACTGGCTTTCCATC	AAGATCTGCAGCTTTTCCACA
Foxp3	AGA GCC CTC ACA ACC AGC TA	CCA GAT GTT GTG GGT GAG TG

Supplementary Figure 1

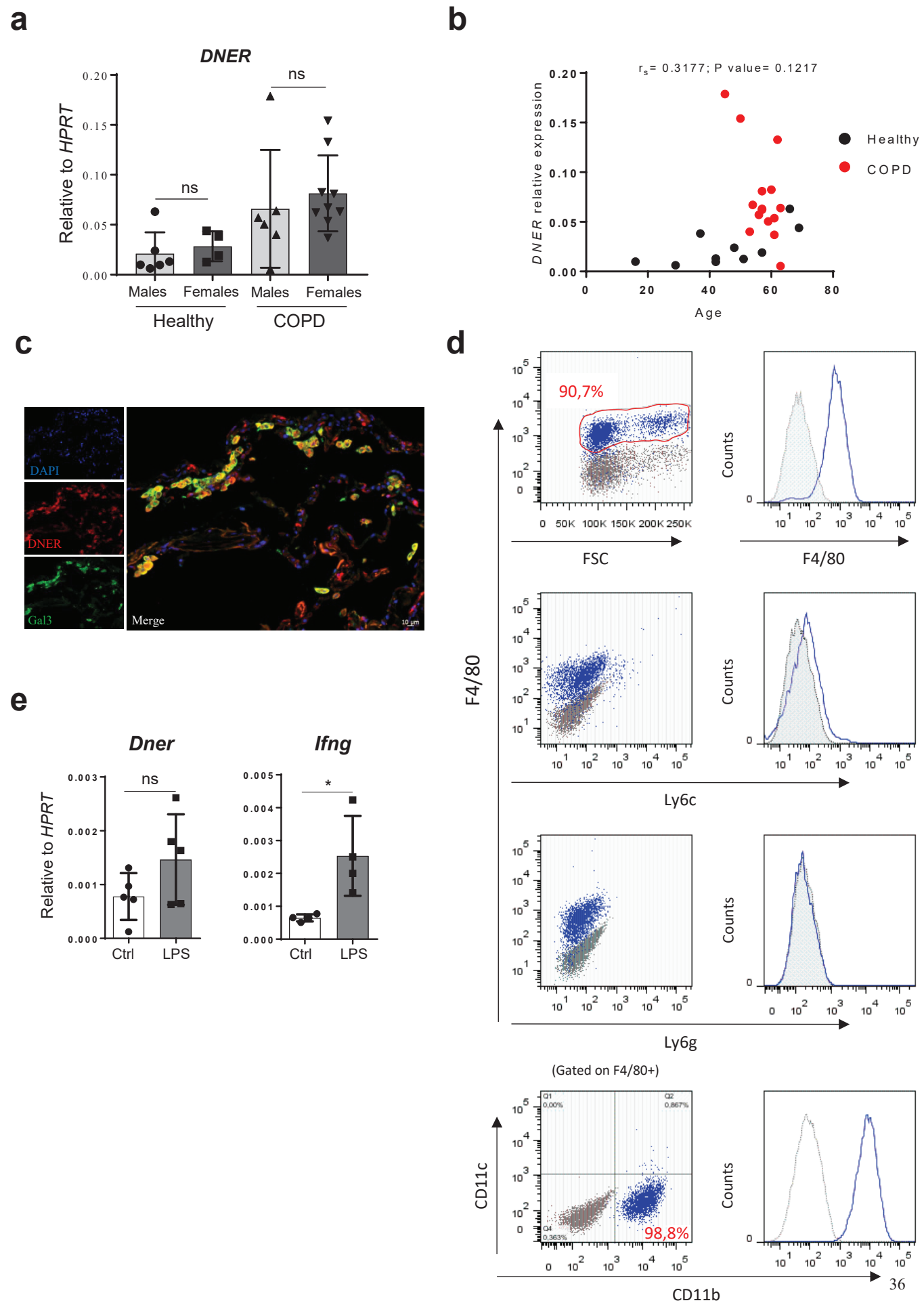

Supplementary Figure 2

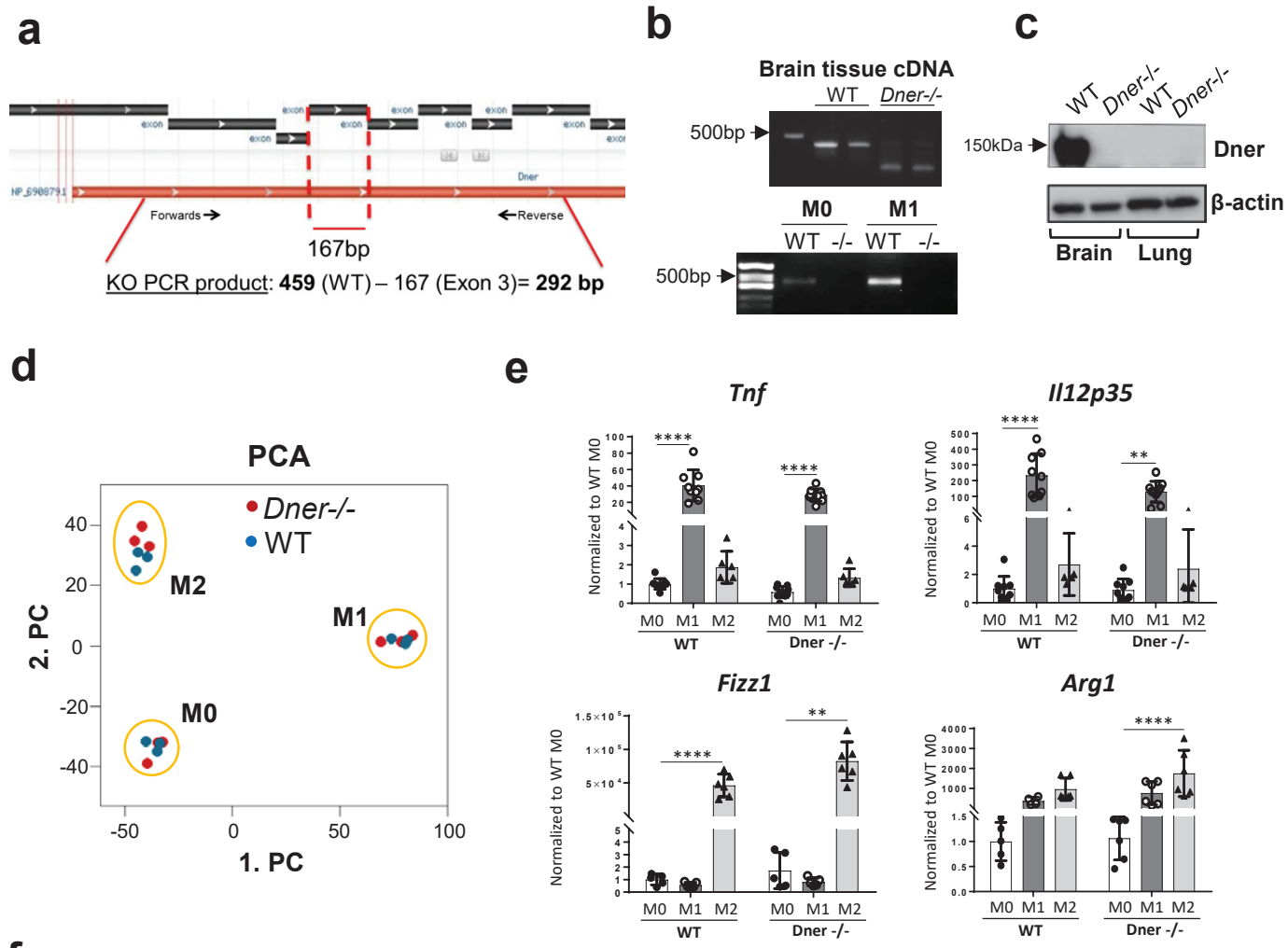

f

Enriched genes in IFNγ signalling dataset (from Fig 2F)

GENE SYMBOL	RANK METRIC SCORE	RUNNING ES	CORE ENRICHMENT
IFNGR1	0,555793166	0,016395938	Yes
SUMO1	0,555555582	0,06843433	Yes
FCGR1A	0,548780501	0,11730901	Yes
OAS2	0,476190478	0,14225388	Yes
PTAFR	0,454545468	0,17979813	Yes
PTPN1	0,384615391	0,18147604	Yes
GBP5	0,33427763	0,18348804	Yes
OAS1	0,317919075	0,20190263	Yes
PRKCD	0,306122452	0,22340244	Yes
JAK2	0,294117659	0,24346457	Yes
SOCS3	0,292035401	0,2672922	Yes
IFNGR2	0,276280522	0,28188163	Yes
VCAM1	0,255033553	0,28695264	Yes

Supplementary Figure 3

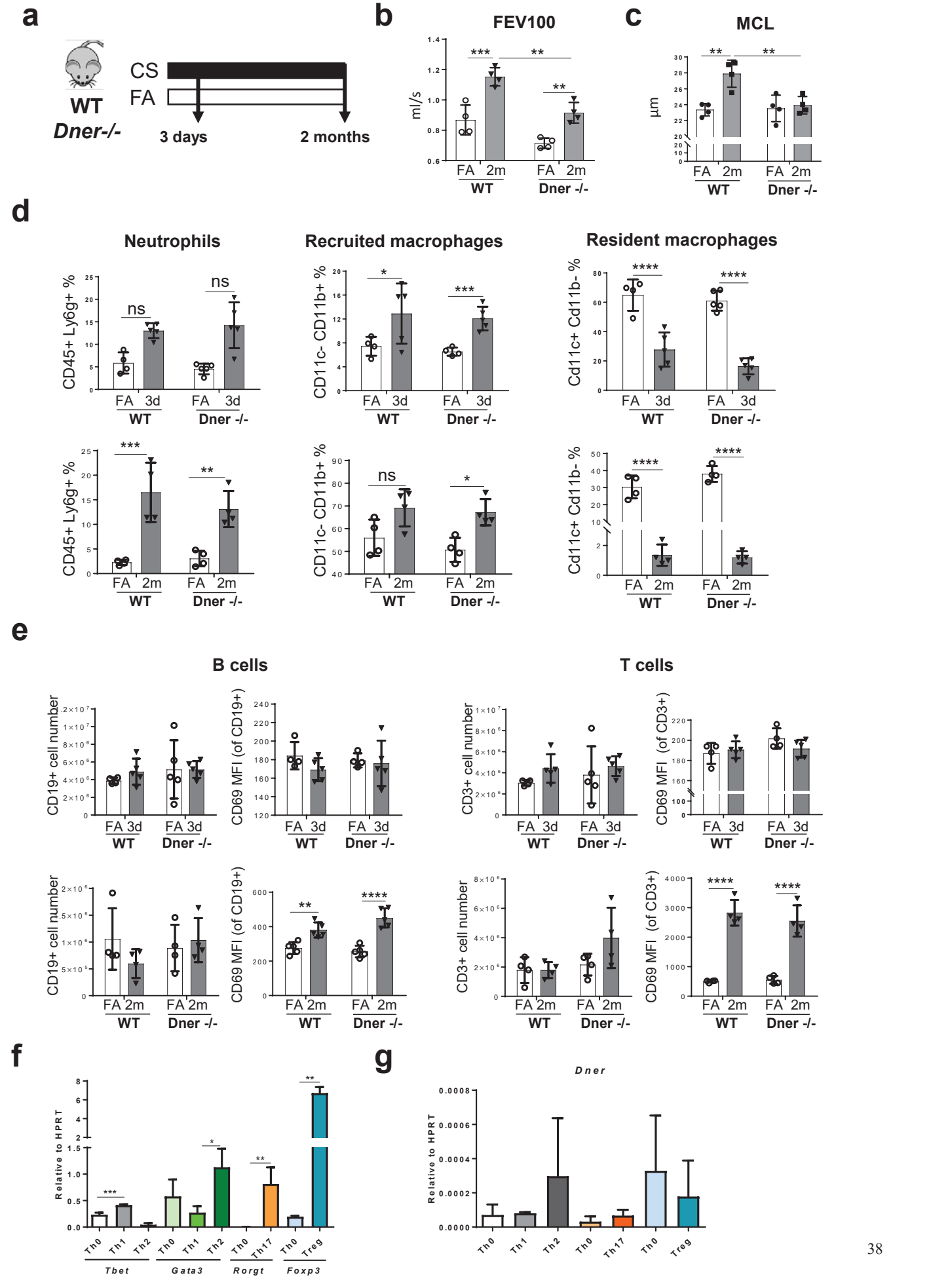

Supplementary Figure 4

a

Enriched genes of Notch1 pathway in WT M1 (Fig. 4e)

GENE SYMBOL	RANK METRIC SCORE	RUNNING ES	CORE ENRICHMENT
HDAC3	1.296296239	0.1251865	Yes
CREBBP	0.814317822	0.19795468	Yes
HIF1A	0.518518507	0.20764284	Yes
null	0.483870953	0.24362169	Yes
HDAC2	0.47356829	0.28676453	Yes
TLE4	0.434964508	0.3138684	Yes
MYC	0.333333343	0.2899674	Yes
NCOR1	0.32764855	0.3188046	Yes
TLE2	0.3125	0.33849412	Yes
SNW1	0.263157904	0.32508263	Yes
HDAC1	0.257731944	0.3445112	Yes
HDAC10	0.2360515	0.3449183	Yes
TBL1X	0.217391297	0.3469396	Yes

b

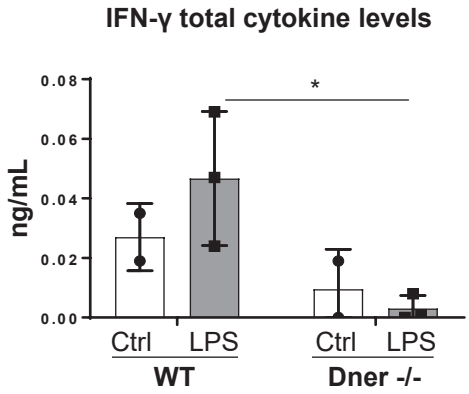

c

Enriched genes of NFkB pathway in WT M1 (Fig. 5c)

GENE SYMBOL	RANK METRIC SCORE	RUNNING ES	CORE ENRICHMENT
HDAC3	1.296296239	0.20311034	Yes
FOXP3	0.555555582	0.2531114	Yes
RELA	0.543243885	0.33511746	Yes
HDAC2	0.47356829	0.38970152	Yes
RPS3	0.428571433	0.43746465	Yes
COMMD7	0.373134315	0.46795464	Yes
ANXA4	0.263157904	0.43196097	Yes
HDAC1	0.257731944	0.4682062	Yes
FAF1	0.209026173	0.4539978	Yes
PPARD	0.196257785	0.47010383	Yes
TAF4B	0.175315574	0.47596845	Yes

d

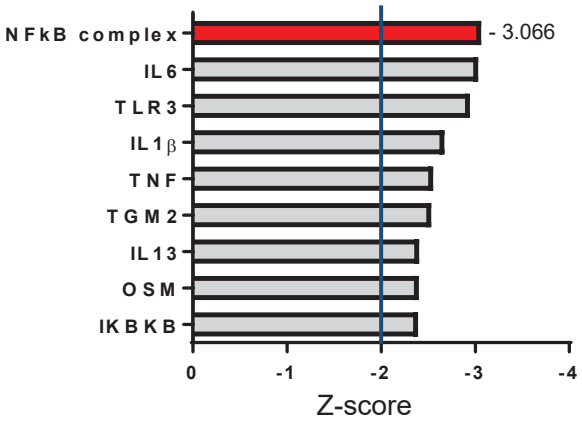

Supplementary Fig. 1. DNER expression in human lung and murine bone marrow derived dendritic cells. **(a)** Lung *DNER* mRNA levels in males versus females subjects used in Fig. 1a. One-way ANOVA. **(b)** Correlation between age and *DNER* expression in human samples used in Fig. 1a. Spearman test. **(c)** Representative picture of immunofluorescence staining of DNER and Galectin 3 in lung tissue from an additional COPD patient. **(d)** BMDM characterization by FACS analysis with markers for macrophages (F4/80, CD11b), DC (Ly6c, CD11c) and neutrophils (Ly6g). 1 experiment, *n*=1. **(e)** *Dner* and *Ifng* mRNA abundance in 24h LPS (1µg/ml) treated murine bone marrow derived dendritic cells isolated from WT mice. 1 experiment, n=5. Unpaired t-test, *p=0.0213. Data shown mean values ± SD.

Supplementary Fig. 2. Efficiency of *Dner* deletion in C57BL/6 mice and cellular phenotype of Dner-/- BMDM. **(a)** Schematic representation of *Dner* gene deletion strategy in Dner deficent mice. **(b)** Dner mRNA abundance in brain tissue and untreated or M1 (LPS 1µg/ml + IFNγ) BMDM from WT and Dner deficient mice quantified by end point PCR. **(c)** Protein levels of Dner in brain and lung tissue from WT and Dner deficent mice. **(d)** Principal component analysis of Dner-/- vs. WT BMDM microarray data. **(e)** mRNA levels of M1 (*Tnf, Il-12a*) and M2 (*Arg1, Fizz1*) markers in WT and Dner deficient BMDM. Two-way ANOVA, Tukey's multiple comparisons test, **p<0.01, ****p<0.0001. Data shown mean values ± SD. **(f)** List of genes enriched in WT M1 from the IFNγ signaling dataset of the GSEA analysis shown in Fig. 2f.

Supplementary Fig. 3. The pathophysiological and immunophenotypic analysis of Dner deficient mice after CS exposure. **(a)** Schematic representation of experimental design. **(b)** Forced expiratory volume after 100ms of FA and 2 months CS exposed Dner deficient and WT mice. **(c)** Mean chord length measurement of lung tissue sections from same samples as in b. **(d)** Percentages of innate immune cell populations in whole lung from FA, 3 days and 2 month CS-exposed WT and Dner deficient mice analyzed by flow cytometry. **(e)** Cell numbers and MFI values of adaptive immune cell populations in whole lung from samples shown in e. **(f)** mRNA levels of positive markers for *in vitro* differentiated T cell subpopulations: Th1 (*Tbet*), Th2 (*Gata3*), Th17 (*Rorgt*) and Treg (*Foxp3*) (see more details in materials and methods). n=2/3, 1 experiment. **(g)** *Dner* expression in T cell subpopulations from f. Two-way ANOVA, Tukey's multiple comparisons test, *p<0.05, **p<0.01, ***p<0.001, ****P<0.0001. (b-e). One-way ANOVA, Tukey's multiple comparisons test, Th1***p-value=0.0008, Th2 *p-value=0.0231, Th17** p-value=0.0019, Treg** p-value=0.0048 (f-g). Data shown mean values ± SD.

Supplementary Fig. 4. Gene datasets of enriched Notch1 and NFKB signalling in M1 WT BMDM compared to Dner deficient M1 BMDM. **a)** List of enriched genes in WT M1 BMDM from the Notch1 pathway dataset of the GSEA analysis shown in Fig. 2C. **b)** IFNγ cytokine concentration in cell supernatants obtained from WT and Dner deficient BMDM treated with LPS (1ug/ml) for 24h and untreated (2 independent experiments, n=3). Two-way ANOVA, Tukey's multiple comparisons test, *p<0.05. Data shown mean values ± SD. **c)** Enriched genes in WT M1 BMDM from NFKB binding dataset (GO:0051059) from the GSEA analysis of the WT M1 vs Dner deficient M1 microarray data . **d)** Upstream regulator prediction based on 614 significantly (p<0.05) regulated genes between Dner deficient M1 vs WT M1 in our microarray analysis. The plot represents the top 9 inhibited regulators with the lowest activation z-scores.

Supplementary Table 1. Demographics and clinical characteristics of healthy and COPD transplant patients (Mean ± SEM). **FEV1**: Forced expiratory volume in the first second; **FVC**: Forced vital capacity; ICS: inhaled corticosteroids.

Supplementary Table 2. Primer sequences used for RT-PCR.

SCIENTIFIC REPORTS

OPEN

Female mice lacking *Pald1* exhibit endothelial cell apoptosis and emphysema

Received: 16 February 2017
Accepted: 18 October 2017
Published online: 13 November 2017

Isabel Egaña[1], Hiroshi Kaito[1], Anja Nitzsche[1,12], Lore Becker[2,3], Carolina Ballester-Lopez[2,4], Colin Niaudet[1], Milena Petkova[1], Wei Liu[5], Michael Vanlandewijck[1], Alexandra Vernaleken[2,3], Thomas Klopstock[3,6,7,8], Helmut Fuchs[2], Valerie Gailus-Durner[2], Martin Hrabe de Angelis[2,9,10], Helge Rask-Andersen[5], Henrik J. Johansson[11], Janne Lehtiö[11], Liqun He[1], Ali Ö. Yildirim[2,4], Mats Hellström[1] & German Mouse Clinic Consortium*

Paladin (*Pald1*, *mKIAA1274* or x99384) was identified in screens for vascular-specific genes and is a putative phosphatase. Paladin has also been proposed to be involved in various biological processes such as insulin signaling, innate immunity and neural crest migration. To determine the role of paladin we have now characterized the *Pald1* knock-out mouse in a broad array of behavioral, physiological and biochemical tests. Here, we show that female, but not male, *Pald1* heterozygous and homozygous knock-out mice display an emphysema-like histology with increased alveolar air spaces and impaired lung function with an obstructive phenotype. In contrast to many other tissues where *Pald1* is restricted to the vascular compartment, *Pald1* is expressed in both the epithelial and mesenchymal compartments of the postnatal lung. However, in *Pald1* knock-out females, there is a specific increase in apoptosis and proliferation of endothelial cells, but not in non-endothelial cells. This results in a transient reduction of endothelial cells in the maturing lung. Our data suggests that *Pald1* is required during lung vascular development and for normal function of the developing and adult lung in a sex-specific manner. To our knowledge, this is the first report of a sex-specific effect on endothelial cell apoptosis.

Paladin or Pald1 is a phosphatase-domain containing protein and we have identified it in two independent screens for novel regulators of angiogenesis and vascular function[1,2]. Pald1 expression is prominent in developing endothelial cells during early embryonic development and, in certain vascular beds, Pald1 expression shifts to mural cells as the vasculature matures, e.g. in the CNS[3]. Furthermore, Pald1 was also found in hematopoietic cells and other non-vascular cells, such as neural crest cells[3,4]. A role of *Pald1* as a regulator for neural crest cell formation and migration in the chick embryo has been shown by morpholino knock-down experiments. It was suggested that Pald1 would not require any catalytic activity for its role in neural crest migration since mutation of the putative catalytic cysteine to serine still affected neural crest migration after over expression[4].

[1]Science for life laboratory, Department of Immunology, Genetics and Pathology, The Rudbeck laboratory, Uppsala University, Uppsala, Sweden. [2]German Mouse Clinic, Institute of Experimental Genetics, Helmholtz Zentrum München, German Research Center for Environmental Health (GmbH), Neuherberg, Germany. [3]Department of Neurology, Friedrich-Baur-Institut, Ludwig-Maximilians-Universität München, Munich, Germany. [4]Comprehensive Pneumology Center, Institute of Lung Biology and Disease, Helmholtz Zentrum München, German Research Center for Environmental Health (GmbH), The German Center for Lung Research (DZL), Munich, Germany. [5]Department of Surgical Sciences, Head and Neck Surgery, Section of Otolaryngology, Uppsala University Hospital, Uppsala, Sweden. [6]German Center for Vertigo and Balance Disorders, Munich, Germany. [7]Deutsches Zentrum für Neurodegenerative Erkrankungen e. V. (DZNE), Munich, Germany. [8]German Network for Mitochondrial Disorders (mitoNET), Munich, Germany. [9]Experimental Genetics, Center of Life and Food Sciences Weihenstephan, Technical University of Munich, Neuherberg, Germany. [10]German Center for Diabetes Research (DZD), Neuherberg, Germany. [11]Cancer Proteomics Mass Spectrometry, Science for Life Laboratory, Department of Oncology-Pathology, Karolinska Institutet, Stockholm, Sweden. [12]Present address: INSERM U970, 56 rue Leblanc, F-75015, Paris, France. *A comprehensive list of consortium members appears at the end of the paper. Correspondence and requests for materials should be addressed to M.H. (email: mats.hellstrom@igp.uu.se)

Pald1 has also been shown to negatively regulate expression and phosphorylation of the insulin receptor, as well as phosphorylation of its downstream target kinase Akt in cell culture, even though no phosphatase activity could be detected *in vitro*[5]. Pald1 has therefore been proposed to be a pseudo-phosphatase, and as such been implicated to indirectly regulate cell signaling[5–7]. However, others have predicted that Pald1 can possess catalytic activity, even though this have not been shown experimentally yet[8]. Furthermore, Pald1 has been suggested to affect another type of receptor signaling, acting as a negative regulator of Toll-like receptor 9[9].

While there is a strong expression of *Pald1* in both the prenatal and adult lung[3], its role in lung development or function is unknown. A central role for angiogenesis has been proposed for lung diseases like chronic obstructive pulmonary disease (COPD) and emphysema[10]. COPD is a chronic progressive disease characterized by clinical symptoms such as dyspnea and coughing, due to obstruction of the airways. COPD is a major cause of death worldwide and it is estimated that COPD will become the third leading cause of death by 2020[11,12]. COPD is frequently accompanied by emphysema, i.e. the destruction of the alveolar walls and the consequential dilation of the distal airways[10]. Alterations of mRNA and protein expression of vascular endothelial growth factor A (VEGF-A) and its receptor VEGF receptor 2 (VEGFR2) are associated with patients exhibiting COPD and emphysema[13]. Experimental disruption of VEGF-A/VEGFR2 signaling has also been shown to be sufficient to induce emphysema and COPD-like changes in mice and rats through apoptosis[14–16]. There are sex-specific differences in COPD and emphysema in humans where subsets of women develop more severe emphysema than men. Female smokers with early onset COPD or severe emphysema have smoked significantly less than their male counterparts[17]. It has also been shown that female mice develop earlier and more severe emphysema than male mice in response to cigarette smoke[18]. However, the mechanisms responsible for this apparent sex-linkage remain unclear.

Here we describe the phenotype of *Pald1*$^{+/-}$ and *Pald1*$^{-/-}$ mice[19,20] and characterize lung defects linking *Pald1* to sex-specific endothelial cell apoptosis, development of emphysema and COPD-like changes in females. To our knowledge, this is the first report of a sex-specific effect on endothelial cell apoptosis.

Results

Pald1$^{-/-}$ mice exhibit an obstructive lung phenotype. In order to characterize the *Pald1*$^{-/-}$ mouse, we performed a wide array of behavioral, physiological and biochemical tests at the German Mouse Clinic (GMC). Although most of the results turned out normal for *Pald1*$^{-/-}$ mice (Table S1 and Figure S1), it was noteworthy that female, but not male, *Pald1*$^{-/-}$ mice exhibited increased lung volumes and compliance and decreased resistance, which are changes also observed in elastase-induced emphysema mouse model[21] (Table 1).

Paladin is expressed broadly in the adult lung. We have previously shown that Pald1 protein is abundant in the mesenchymal compartment of embryonic lungs and that *Pald1* is also highly expressed in the adult lung[3]. Single cell sorting and sequencing from mouse embryonic lung strongly supports the conclusion that *Pald1* is exclusively expressed in endothelial cells during embryonic development[22,23].

To begin to understand the role of *Pald1* in postnatal lung development and function, we mapped *Pald1* expression in detail. We analyzed the expression at three distinct time points during postnatal development and in the adult, postnatal day 5 (P5), 4 and 19 weeks of age as it covers main aspects of postnatal development of the major gas exchange unit of the lungs – the alveoli. The tremendous increase in gas exchange surface that occurs postnatally by formation of alveoli is accelerated from P5 until 2 weeks of age and peaks at 5–6 weeks. It is then stable until 40 weeks of age, and subsequently there is a gradual loss of alveoli. The decrease in alveolar septal thickness, that also facilitates gas exchange, continues from P5 until 4 weeks of age. Therefore, we decided to map the expression of *Pald1* and assess the phenotype of *Pald1*$^{-/-}$ animals at P5, 4 and 19 weeks of age, to cover the dynamic process of postnatal lung development[24]. First we isolated single endothelial cells and pneumocytes type II from lungs using mT/mG reporter mice expressing Cre-recombinase under the endothelial Tie2 promoter and under the pneumocyte type II-specific surfactant protein C (SPC) promoter, respectively[25,26]. mRNA isolation and quantitative PCR for *Pald1* showed that *Pald1* is expressed in endothelial cells, but also in type II pneumocytes (Fig. 1a). To map the expression of *Pald1* at cellular resolution, we took advantage of the LacZ reporter of *Pald1* knock-out construct[3]. Murine *Pald1* heterozygous (*Pald1*$^{LacZ/+}$) and homozygous mutant (*Pald1*$^{LacZ/LacZ}$) lungs were harvested at postnatal day (P) 5, week 4 and week 19. The LacZ reporter indicated a broad expression of *Pald1* in the murine lung in both males and females across all ages analyzed apart from bronchiolar epithelium. LacZ expression pattern was the same in *Pald1*$^{LacZ/+}$ and *Pald1*$^{LacZ/LacZ}$ lungs (Fig. 1b and Figure S2). Combining LacZ staining with antibodies specific for each of the main cell types in the alveoli revealed that *Pald1* can be detected at all stages in the endothelial cells forming the capillaries around the alveoli but is less frequently detected in the endothelium of larger vessels (Fig. 2, and Figure S3). Paladin was also detected in vascular smooth muscle cells, macrophages, pneumocytes type I and II and Platelet-derived Growth Factor Receptor α (PDGFRα)-positive mesenchymal cells (Fig. 2). However, the surfactant protein positive type II pneumocytes were not LacZ positive at P5.

Taken together, *Pald1* mRNA and protein are strongly expressed in endothelial cells as well as in other cell types in the postnatal lung, except for bronchial epithelial cells.

Lack of _Pald1_ leads to enlarged distal airspaces in female mice. COPD in humans is often accompanied by emphysema, characterized by destruction of alveolar walls and distal airspace enlargement[27]. Histological analysis of *Pald1* wild type and knock-out lungs revealed enlarged distal airspaces in female mice, but not in males, assessed by both blinded lung pathologist and quantification of mean linear intercept (MLI) (Fig. 3a–c). Increase in MLI, i.e. increase in distance between airway walls, was seen already at P5, at the end of the saccular stage and before alveolarization[28]. The distal airway dilation was still present at 4 and 19 weeks of age. Interestingly, we observed that female *Pald1*$^{+/-}$ mice also exhibited a significant increase in distal airspace

	Female			Male		
	***Pald1*$^{+/+}$ (n = 6)**	***Pald1*$^{-/-}$ (n = 6)**	**p-value**	***Pald1*$^{+/+}$ (n = 7)**	***Pald1*$^{-/-}$ (n = 5)**	**p-value**
	Median	Median		Median	Median	
	[25%; 75%]	[25%; 75%]		[25%; 75%]	[25%; 75%]	
Body weight (g)	**26.2**	**25.6**	0.623	**34.9**	**33.4**	0.093
	[24.4, 27.7]	[23.6, 27.4]		[34.1, 36.4]	[32.8, 33.0]	
Tidal volume (ml)	**0.21**	**0.22**	0.056	**0.19**	**0.20**	0.374
	[0.21, 0.21]	[0.22, 0.22]		[0.18, 0.21]	[0.20, 0.20]	
Inspiratory capacity (ml)	**0.695**	**0.885**	**0.026**	**0.871**	**1.340**	**0.026**
	[0.650, 0.755]	[0.832, 0.982]		[0.650, 0.755]	[1.320, 1.253]	
Expiratory Reverse Volume (ml)	**0.26**	**0.29**	0.323	**0.24**	**0.26**	0.425
	[0.25, 0.29]	[0.28, 0.30]		[0.21, 0.26]	[0.24, 0.28]	
Vital Capacity (ml)	**0.97**	**1.17**	**0.026**	**1.23**	**1.09**	0.779
	[0.90, 1.01]	[1.12, 1.29]		[0.90, 1.46]	[1.12, 1.29]	
Functional Residual Capacity (ml)	**0.295**	**0.310**	0.370	**0.325**	**0.295**	0.980
	[0.290, 0.308]	[0.292, 0.328]		[0.329, 0.369]	[0.275, 0.365]	
Residual Volume (ml)	**0.025**	**0.035**	0.649	**0.029**	**0.056**	0.649
	[0.020, 0.053]	[0.030, 0.040]		[0.025, 0.035]	[0.030, 0.040]	
Total lung capacity (ml)	**1.005**	**1.190**	**0.022**	**1.472**	**1.695**	0.096
	[0.962, 1.032]	[1.137, 1.302]		[1.362, 1.532]	[1.137, 1.859]	
Forced Vital Capacity (ml)	**0.895**	**1.065**	**0.026**	**1.099**	**1.160**	0.323
	[0.828, 0.925]	[1.015, 1.175]		[0.828, 1.125]	[1.015, 1.175]	
Forced Expiratory Volume in 100 ms (ml)	**0.885**	**1.030**	**0.028**	**1.058**	**1.097**	0.507
	[0.802, 0.915]	[0.982, 1.145]		[0.976, 1.129]	[0.872, 1.201]	
Peak Expiratory Flow (ml/sec)	**30.1**	**30.7**	0.141	**33.6**	**31.7**	0.092
	[30.1, 30.5]	[30.6, 30.9]		[33.1, 34.5]	[30.8, 32.7]	
Static lung compliance (ml/cm H_2O)	**0.050**	**0.070**	**0.039**	**0.056**	**0.053**	0.384
	[0.050, 0.058]	[0.063, 0.070]		[0.051, 0.059]	[0.051, 0.055]	
Dynamic lung compliance (ml/cm H_2O)	**0.02**	**0.03**	**0.015**	**0.04**	**0.03**	0.370
	[0.02, 0.02]	[0.03, 0.03]		[0.03, 0.05]	[0.03, 0.03]	
Resistance (cm H_2O/ml/sec)	**1.40**	**1.27**	**0.013**	**0.98**	**1.11**	0.652
	[1.35, 1.45]	[1.23, 1.31]		[0.96, 1.11]	[1.01, 1.31]	

Table 1. Functional lung tests in 20-week old *Pald1*$^{+/+}$ and *Pald1*$^{-/-}$ mice. Lung function was assessed by a forced maneuver system and a Fine-Pointe RC system. Differences between genotypes were evaluated by Wilcoxon test. Data are presented as median values ± interquartile range.

enlargement as quantified by MLI (Fig. 3d). However, no difference in alveolar septal thickness was detected (*Pald1*$^{+/+}$ 2,67+/− 0,14 vs. *Pald1*$^{-/-}$ 2,48+/−0,07 µm^3/µm^2, P = 0,13).

Reduced number, increased apoptosis and proliferation of endothelial cells in female *Pald1* knock-out lungs. To further dissect the lung phenotype of female *Pald1* knock-out mice, we used cell type-specific markers to assess the relative contribution in the lung. Cell type-specific markers for pneumocytes type I or II, macrophages or PDGFRα-positive cells did not reveal any differences of cell number between wild type and *Pald1* knock-out mouse lungs over time (Fig. 4c–e and Figure S4). However, using the endothelial cell nuclei-specific marker Erg showed a reduction of endothelial cell number in the vascular compartment in females at 4 weeks of age by 14% (Fig. 4a and b).

Given the reduced number of endothelial cells at 4 weeks, we determined the frequency of apoptotic cells by cleaved caspase-3 (CC3) staining in both endothelial and non-endothelial cells in these lungs (Figure S5). There was a more than six-fold increase in apoptotic cells (0.75% ± 0.41% (SD) vs. 4.90% ± 0.76% CC3+ cells, $p < 0.0001$) in the endothelial compartment in female *Pald1*$^{-/-}$ compared to *Pald1*$^{+/+}$ mice at 4 weeks of age. However, there were no differences in non-endothelial cell apoptosis or apoptosis comparing male wild type and knock-out mice. The increase in cleaved caspase-3 was still more than two-fold at both P5 and 19 weeks of age comparing wild type and knock-out *Pald1* females (Fig. 5a and b). The enhanced endothelial apoptosis in female *Pald1*$^{-/-}$ was also accompanied by an increase of proliferation, as assessed by Ki-67 staining (Fig. 5c and Figure S5).

Sex-dependent protein expression differences in lung tissue. To begin to understand the mechanism of sex-specific phenotype in *Pald1* knock-out lungs, we employed lung proteome analysis using mass spectrometry based proteomics[29]. We identified in total 10099 proteins at 1% protein false discovery rate, and 8,635 proteins were quantified in all 16 lung samples (n = 4 per sex and genotype) from 4 weeks old mice. One female *Pald1* knock-out sample was excluded from further analyses because of contamination as described in

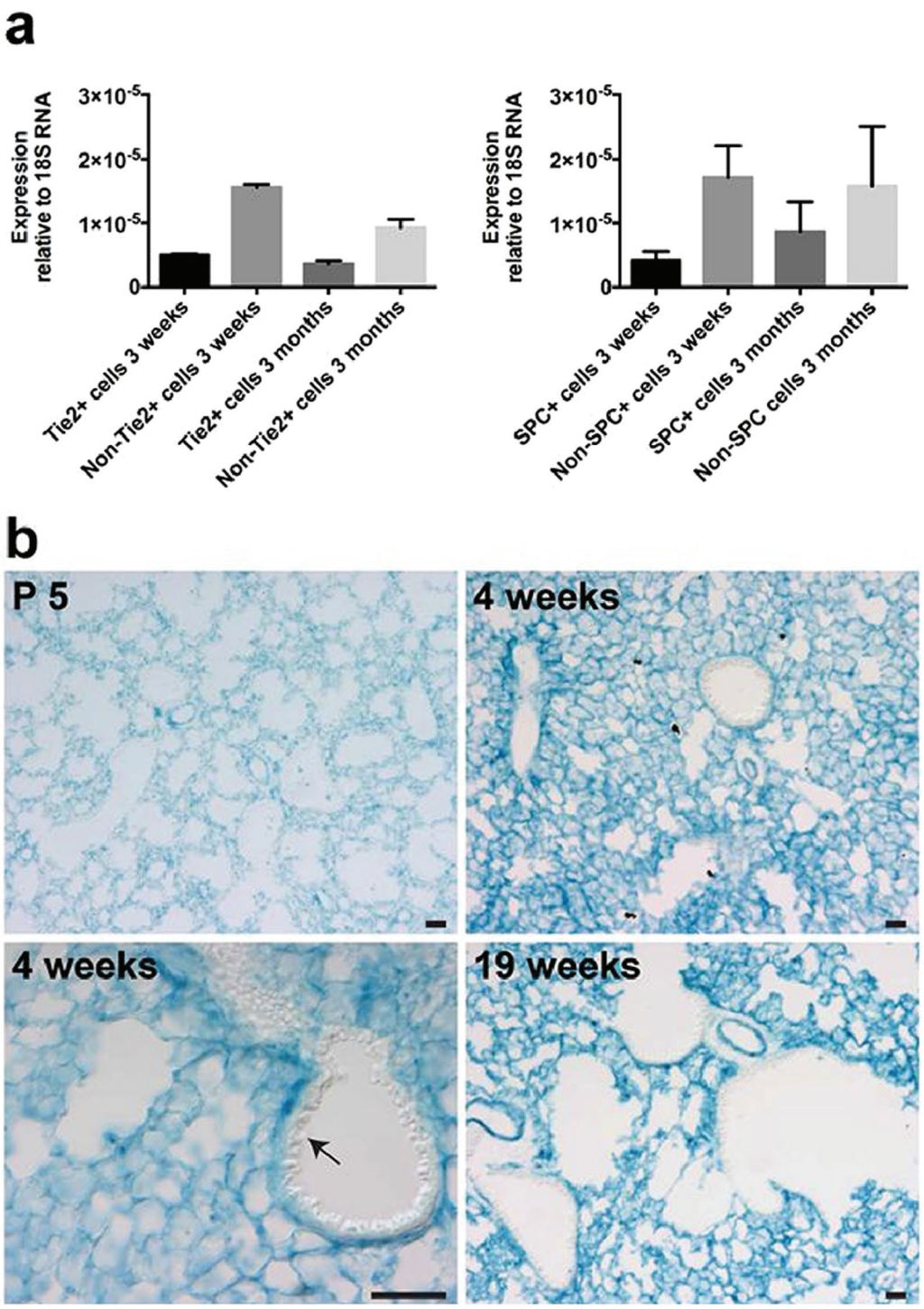

Figure 1. Paladin has a broad expression in the postnatal lung. (**a**) Endothelial cells and pneumocytes type II were isolated from lungs of mT/mG mice expressing endothelial-specific Tie2-Cre (left) or pneumocyte type II-specific SPC-Cre (right). Q-PCR of sorted single cells indicates *Pald1* mRNA expression in both endothelial cells and non-endothelial cells, including pneumocytes type II, both at 3 weeks and 3 months of age. Expression was normalized to 18 S RNA. (**b**) *Pald1* LacZ reporter activity (blue) is detected in *Pald1*$^{LacZ/LacZ}$ mice, 5 days, 4 weeks and 19 weeks after birth. LacZ is broadly expressed in the lung tissue, except for the bronchial epithelium, which shows no reporter activity (arrow). Scale bar = 200 μm.

Materials and Methods. Hierarchical clustering based on the expression of all proteins showed that the major factor for clustering is sex, and not genotype (Fig. 6a). Three proteins including Pald1 showed significantly altered expression between wild type and knock-out mice in a sex-independent manner. Hpgd (hydroxyprostaglandin

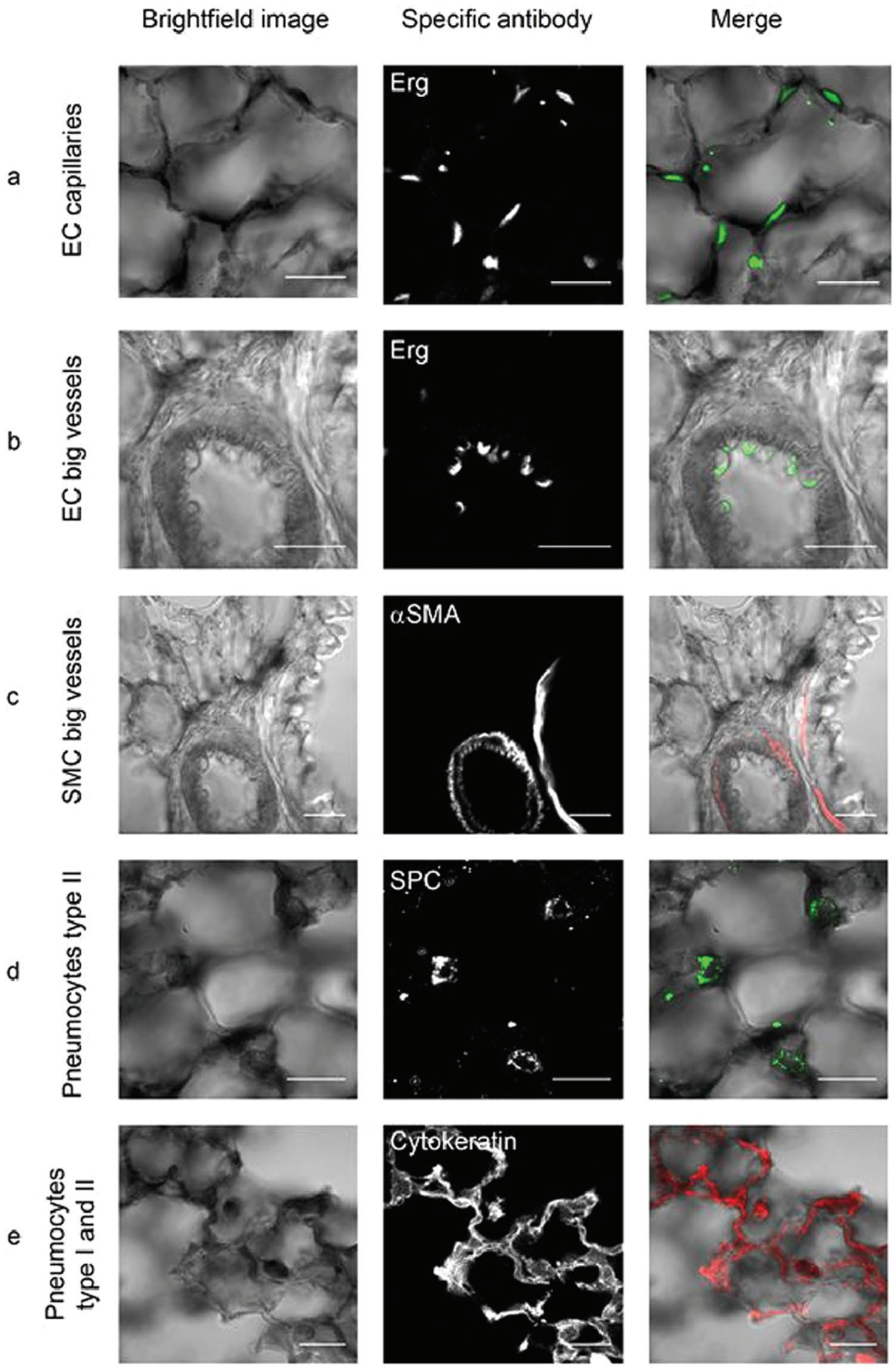

Figure 2. Paladin is expressed both in the epithelial and mesenchymal compartment of the postnatal lung (4 weeks). (**a**–**e**) Combined X-gal (black) and immunofluorescence staining of *Pald1*$^{LacZ/LacZ}$ mice show *Pald1* LacZ expression in the vasculature, i.e. endothelial cells in capillaries (**a**) but to a lesser extent in endothelial cells of larger blood vessels (**b**) as indicated by Erg staining (endothelial cell nuclei, green). In large blood vessels LacZ expression can be detected in vascular smooth muscle cells (**c**, α-smooth muscle actin, red). Paladin LacZ reporter is also active in pneumocytes type II (**d**, SPC, green) and pneumocytes type I/II (**e**, cytokeratin, red). Scale bar = 20 μm.

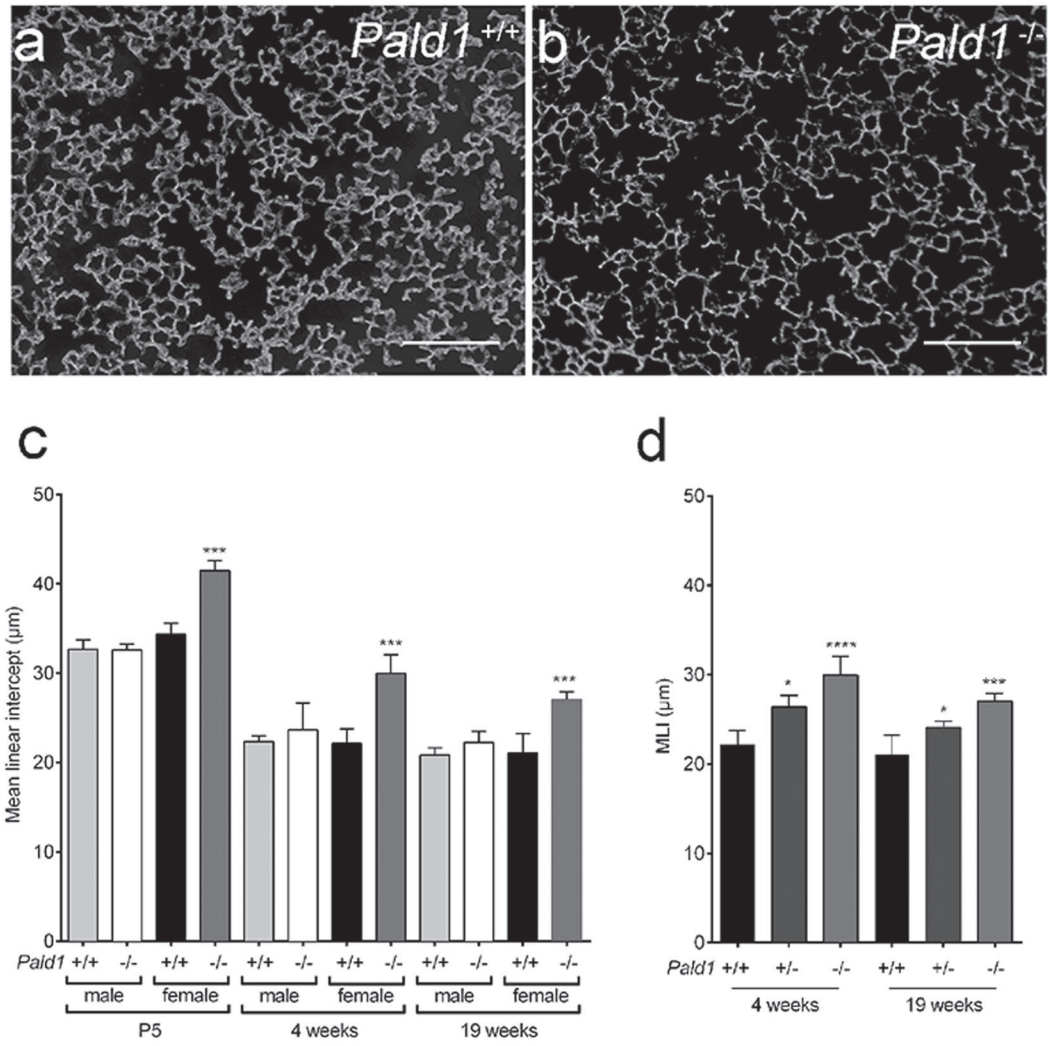

Figure 3. *Pald1*$^{-/-}$ mice show reduced complexity of the lung tissue. (**a**,**b**) Dark field images of distal airspace from 4 weeks old female *Pald1* wild type (**a**) and knock-out animals (**b**), suggest a general airspace enlargement in the *Pald1* knock-out lungs. Scale bars = 200 µm. (**c**) Quantification of interseptal alveolar distance using Mean Linear Intercept (MLI) of hematoxylin-eosin stained lung tissue at P5 (n = 3), 4 (n = 5) and 19 weeks (n = 4) shows increased air spaces in female knock-out animals at all stages, but was particularly increased at 4 weeks. ANOVA per age group: P5 $p < 0.0001$; 4 weeks $p = 0.0002$; 19 weeks $p = 0.0004$. *Pald1*$^{-/-}$ was compared to *Pald1*$^{+/+}$ of the same sex within each age group. (**d**) MLI of *Pald1* wild type, heterozygous and knock-out female mice at the indicated ages. ANOVA per age group: 4 weeks $p = 0.0001$, 19 weeks $p = 0.0007$. *Pald1*$^{-/-}$ and *Pald1*$^{+/-}$ were compared to *Pald1*$^{+/+}$ within each age group. Error bars: SD, *$p \leq 0.05$, ***$p \leq 0.001$, ****$p \leq 0.0001$.

dehydrogenase 15 (NAD)), showed higher expression in knock-out lungs than wild type, which was confirmed by Western blot (Fig. 6b and Figure S6). In addition, Mycbp2, MYC binding protein 2, as well as Pald1 was significantly down regulated (Figure S7). The most differentially expressed protein between wild type male and female lungs was HSD17B7, a protein essential for cholesterol biosynthesis and with the capacity to catalyze conversion of estrone to estradiol[30]. There were no statistically significant protein expression changes that were specific to female knock-out mice, after correction for multiple testing.

Discussion

Several independent groups have identified *Pald1* as a vascular enriched gene[1,2,31] and we have previously shown that *Pald1* is expressed in both endothelial and mural cells in the vasculature[3].

Extensive phenotypic screening revealed morphological and functional lung defects in female *Pald1*$^{-/-}$ mice. This was accompanied by increased distal air spaces and elevated apoptosis and proliferation exclusively in the endothelial compartment of female mice. It is tempting to speculate, that *Pald1* has a unique role in the vasculature of the lung, as this is where we observe the strongest phenotype, even though the expression of *Pald1* is broader and we cannot exclude that the increased endothelial turnover is secondary to alteration in other cell types.

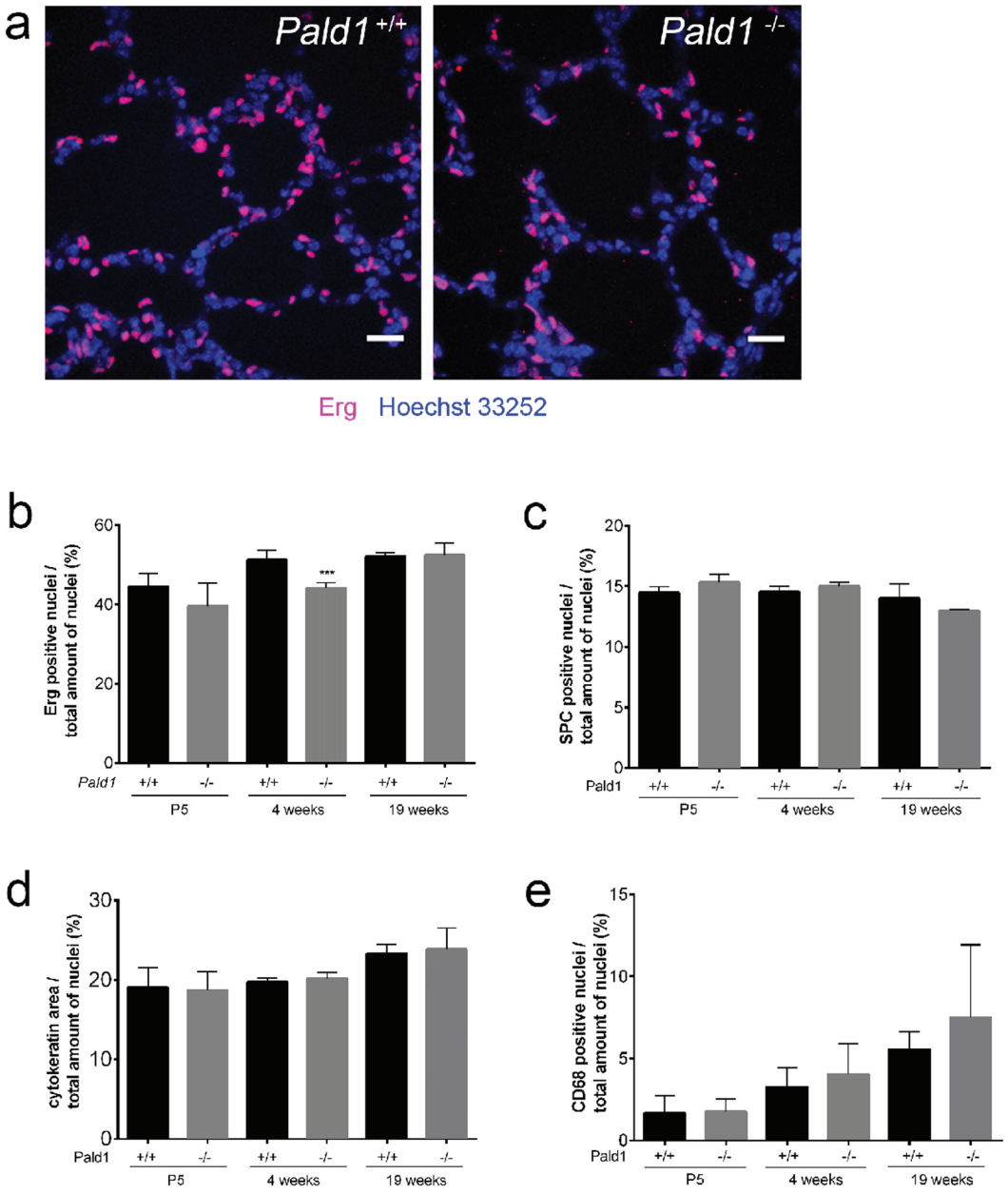

Figure 4. *Pald1*$^{-/-}$ show a decrease in the endothelial cell population at 4 weeks. (**a**–**e**) Quantification of the relative proportion of endothelial cells (**a**,**b**, Erg, n = 3–5), pneumocytes type II (**c**, SPC, n = 3), pneumocytes type I/II (**d**, cytokeratin, n = 3), and macrophages (**e**, CD68, n = 3–7). The specific cell type contribution was unaltered in *Pald1*$^{-/-}$ mice except for a 15% decrease of the endothelial cell population at 4 weeks in *Pald1*$^{-/-}$ mice. Scale bar = 20 µm, Error bars: SD, t-test between genotypes of each age group. ***$p \leq 0.001$.

A central role for endothelial cell apoptosis in the development of emphysema has been proposed. This is based on both the correlation of increased endothelial cell apoptosis and down regulation of VEGF in human patients exhibiting emphysema[13], and experimental evidence in animal models. Genetic ablation of VEGF-A in the lung using adenoviral Cre led to endothelial and non-endothelial cell apoptosis, without a compensatory increase in proliferation[16]. Inhibition of VEGFRs using either low molecular weight kinase inhibitors or specific VEGFR2 (but not VEGFR1) blocking antibodies was also sufficient to trigger alveolar apoptosis and development of emphysema in mice and rats[14,15]. In addition, direct induction of lung endothelial cell apoptosis using an endothelial-homing peptide triggers development of emphysema[32], suggesting that alveolar structures cannot be maintained without endothelial cells, as well as that endothelial cell apoptosis in the lung culminates in emphysema. Comparison of MLI measurements in the above-mentioned VEGF-A/VEGFR2 targeted mice and rats shows that the emphysema development in *Pald1*$^{-/-}$ female mice is comparable to what is seen in those models. However, alterations of VEGF and VEGFR levels were not the reason to emphysema in the *Pald1* knock-out mice as no differences in VEGFA or VEGFR2 protein levels were detected in the proteomic analysis, or by western blot.

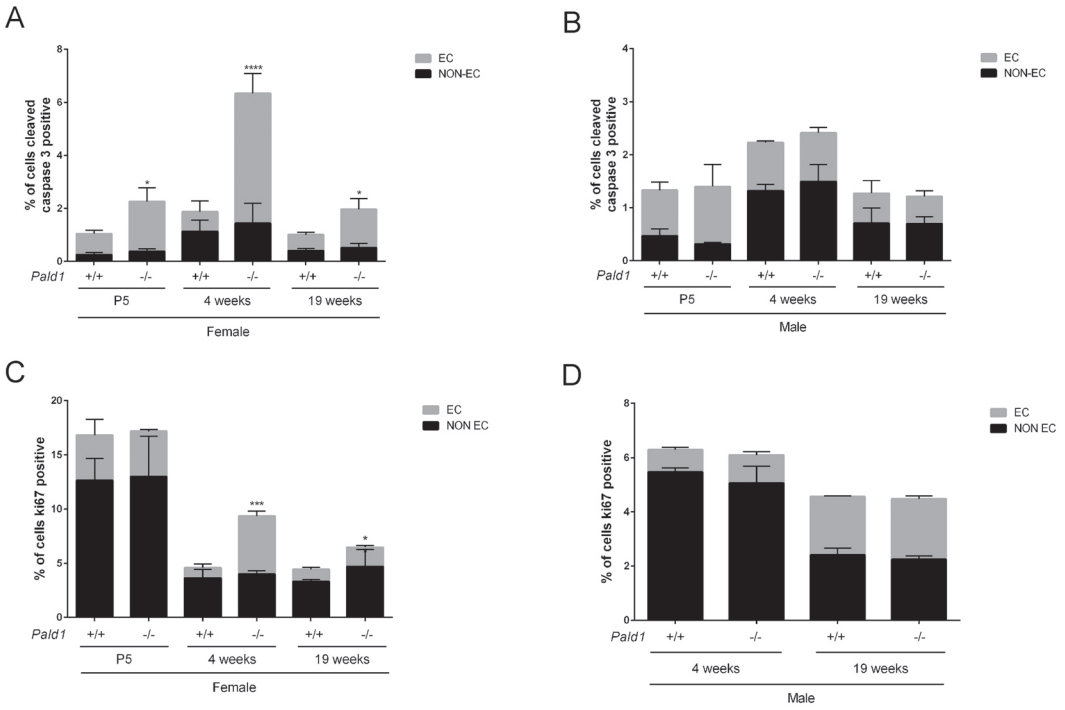

Figure 5. Increased apoptosis and proliferation of endothelial cells in *Pald1* knock-out female lungs. (**a**,**b**) Quantification of cleaved caspase-3 positive (CC3+) cells in 4 and 19-week old lungs revealed a significant increase in the number of cleaved caspase-3 positive endothelial cells (Erg positive) at 4 weeks of age and at 19 weeks in female (**a**, n = 3–4), but not in male *Pald1*$^{-/-}$ mice (**b**, n = 3–4). There was no significant increase in non-endothelial cells (Erg negative) at both 4 and 19 weeks. (**c**,**d**) Quantification of Ki67 positive cells in 4 and 19-week old lungs revealed an increased number of Ki67-positive endothelial cells (Erg positive) in female (**c**, n = 3–4), but not in male *Pald1*$^{-/-}$ mice (**d**, n = 3–4). There was no significant increase in non-endothelial cells (Erg negative) at both 4 and 19 weeks. Error bars: SD, t-test between genotypes within each age group. * = $p \leq 0.05$, **** = $p \leq 0.0001$.

The increase in distal airspace in female *Pald1* knock-out mice is stable from early postnatal stage to 19 weeks of age. The mechanism of airspace enlargement must be distinct from emphysematous development in adult humans as it occurs already before alveolar septation and is non-progressive. Despite this, further studies into this phenotype, might provide additional information on what type of cellular changes and biochemical pathways that can lead to the end stage phenotype that we refer to as emphysema. Further studies will also be necessary to pinpoint the mechanism whereby *Pald1* regulates endothelial cell survival and proliferation in a sex-specific fashion. The proteomics data showed that sex, but not genotype, was the most significant factor for differential protein expression. This is consistent with the accumulating evidence regarding sex differences and lung biology[33]. Somewhat surprisingly, no specific protein expression differences were detected between female wild type and knock-out lungs. However, Hpgd, the major enzyme for degradation of prostaglandins, showed higher expression in all knock-out lungs compared to wild type, irrespective of sex. Given that prostaglandin signaling is abundant and important for lung and vascular function as well as angiogenesis[34], it could be speculated that prostaglandin signaling is associated with the emphysema phenotype, but that the *Pald1*$^{-/-}$ males are somehow protected. The lack of significant protein changes between female wild type and knock-out lungs, despite of the morphological differences and endothelial apoptosis observed at the time point analyzed, could be due to several reasons including sensitivity of the proteomics screen, use of complex tissue containing several cell types and/or due to time point of analysis. Even though we observe the greatest morphological changes at 4 weeks of age, the potential protein expression differences causing those changes might have occurred earlier.

Paladin was previously identified as a negative regulator of insulin signaling by *in vitro* screening for FOXO1A-driven reporter gene expression using a human cDNA library[5]. We detected a minor reduction in the ability to clear glucose from the blood stream in male mice as assessed by an intraperitoneal glucose tolerance test (Table S1). However, this is in contrast to the reported negative effect of *Pald1* on insulin receptor signaling in cells. Further studies will be needed to determine the significance of this finding.

It was reported that *Pald1* modulated the expression of key regulatory genes in neural crest development, and plasmid mediated over expression and morpholino-based knock-down of *Pald1* delayed neural crest migration in the chick embryo[4]. Even though we have noted a prominent expression of *Pald1* in migrating neural crest cells during embryonic development[3], we have not noted any differences in neural crest derived tissues such as cardiac outflow tract, melanocytes, cranial bones or myelination in adult *Pald1*$^{-/-}$ mice. However, a transient role of *Pald1* in neural crest migration during development has not been assessed.

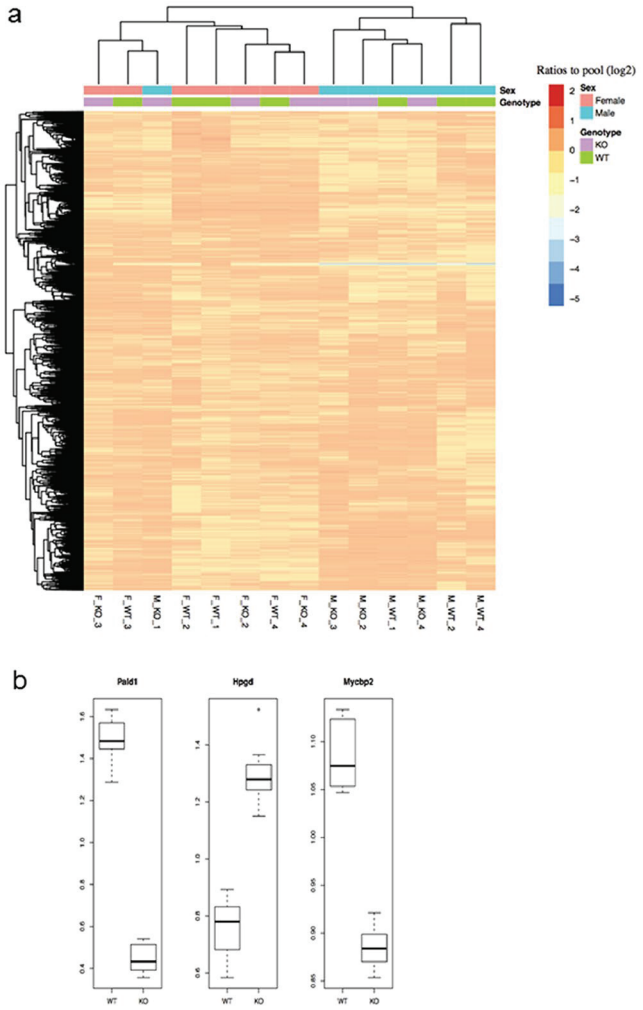

Figure 6. Proteomics data overview and significantly differentially expressed proteins. (**a**) Proteomics reveals sex-dependent protein expression differences in lung tissue. The heatmap shows proteome data overview of 8635 proteins with overlapping quantification in all 4 weeks of age lung samples using hierarchical clustering. Columns and rows represent lung samples and proteins, respectively. The samples are labels as sex_genotype_ID. The major factor for clustering is sex, and not genotype. (**b**) Boxplot of the three significantly differentially expressed proteins. The y-axis shows the ratios to the pool. For each gene, the ratios to the pool in the wild type group (WT) and knock-out group (KO) are plotted in the boxplot, respectively.

Taken together, our comprehensive description of the *Pald1*$^{-/-}$ mouse revealed that the putative phosphatase *Pald1* plays a role in the development and function of the lung, and specifically in female pulmonary endothelial cell survival and proliferation. Further studies are necessary to address how the lack of *Pald1* leads to endothelial cell apoptosis and proliferation, and how that is related to the emphysema phenotype in a sex-specific manner.

Materials and Methods

Paladin nomenclature and mouse model. Paladin is encoded by *Pald1* (phosphatase domain containing, paladin 1, also known as x99384 or *mKIAA1274*) in mice. C57BL/6 mice with constitutive deletion for *Pald1* (Exon 1–18 replaced by a LacZ reporter cassette) have been generated[3] and backcrossed for 10 generations. ROSA mT/mG × Tie2-Cre mice[35] were generated as previously described[25]. ROSA mT/mG mice (Jackson Stock 007576) were crossed to Sftpc-Cre[26] to generate ROSA mT/mG × Sftpc-Cre. All animal experiments were performed in accordance with the relevant laws and institutional guidelines and were approved by the Uppsala University board of animal experimentation. At the GMC mice were maintained in IVC cages with water and standard mouse chow according to the GMC housing conditions and German laws. All tests performed at the GMC were approved by the responsible authority of the district government of Upper Bavaria, Germany.

FACS and quantitative PCR. Isolation of single cells from ROSA mT/mG × Tie2-Cre and ROSA mT/mG × Sftpc-Cre lungs by FACS, mRNA extraction and quantitative PCR was done as previously described[25].

Western blot analysis. Snap frozen lungs from 2, 3 and 22-week old mice were lysed in 20 mM HEPES, 150 mM NaCl, 1% NP40, 1x protease inhibitor cocktail (Roche), homogenized with Tissue Tearor (BioSpec

Products) and sonicated six times for 5 sec at 200 W (Bioruptor, diagenode). Tissue lysates were incubated for one hour at 4 °C with rotation, and centrifuged at 21'100 g for 20 min at 4 °C. Protein concentration was measured with the BCA protein detection kit (Thermo Fisher Scientific). Lung lysates were denatured in sample buffer (Life Technologies) and proteins were separated on a 4–12% BisTris polyacrylamide gel (Novex by Life Technologies). Proteins were transferred to an Immobilon-P PVDF membrane (Millipore) using the XCell II™ Blot Module (Novex by LifeTechnologies). The membrane was blocked with 5% skimmed milk in TBS 0.1% Tween and incubated with rabbit anti-Pald1 (1:1000; Atlas Antibodies, HPA017343) or goat anti-actin (1:1000, Santa Cruz, sc-1615) antibodies overnight at 4 °C. Membranes were washed in TBS 0.1% Tween and incubated with horseradish peroxidase (HRP) conjugated secondary anti-rabbit (1:10'000, GE Healthcare) and anti-goat antibodies (1:10'000, Invitrogen), respectively. Membranes were washed in TBS 0.1% Tween and developed using ECL prime (GE Healthcare). Luminescence signal was detected by the ChemiDoc MP system (BioRad).

X-gal staining and immunohistochemistry of lung sections. Lungs were inflated and fixed intratracheally with 4% PFA. The trachea was tied under pressure, and the lung was fixed for 2 h in 4% PFA at 4 °C. For histochemical analysis, paraffin sections of fixed lungs were dehydrated gradually in a series of 70% ethanol to xylene and soaked in paraffin (for 6 h in total) prior to embedding. Paraffin sections (6 µm) were deparaffinized using xylene, rehydrated in graded alcohol series (99.6% to 70% ethanol) and rinsed in distilled water. For H&E staining, sections were immersed sequentially in hematoxylin and eosin solutions (Histolab). Stained sections were dehydrated (70% ethanol to 99.6% ethanol, xylene) and mounted in PERTEX mounting media (Histolab). Interalveolar septal wall distance was measured by the mean linear intercept (MLI). Images from H&E stained lung sections were acquired on a Nikon light microscope (Nikon Eclipse 80i, Nikon digital camera DXM 1200) at a 400x magnification. The MLI was obtained by dividing the length of a line drawn across the lung section by the total number of intercepts encountered in 10 lines per picture. Twenty-five images per section, and two sections per lung, were analyzed. One section was from the inferior lobe and another one from the superior lobe.

For frozen lung sections, lungs were collected and fixed as described. After overnight incubation in 30% sucrose in PBS, lung sections of 5–10 µm were cut, blocked (3% BSA, 0.1% Triton x-100, 5% Normal Donkey serum [Jackson Immunoresearch], 5% Normal Mouse serum [Invitrogen] in PBS) and stained with rabbit anti-ERG (1:100, Abcam, ab92513), mouse anti-ERG (1:100, Abcam, ab140520), mouse anti-αSMA (1:100, Sigma, C6198), rabbit anti-prosurfactant Protein C (1:100, Abcam, ab40879), mouse anti-cytokeratin (1:100, Sigma, P2871), rat anti-CD68 (1:100, AbD serotec, MCA1957), rabbit anti-cleaved caspase 3 Ab-5 (1:3000, Neomarkers, RB-1611-P1), and mouse anti-ki67 (1:100, Dako, M7240) in combination with appropriate fluorophore-coupled secondary antibodies. Images were obtained with the Zeiss LSM700 confocal microscope, 63x objective and analyzed by ImageJ. For x-gal staining, frozen lung sections were post-fixed in 0.2% PFA for 10 min on ice, rinsed in PBS with 2 mM $MgCl_2$ and permeabilized in detergent rinse (2 mM $MgCl_2$, 0.01% sodium deoxycholate, 0.02% Nonidet P-40, PBS) for 10 min on ice, prior to overnight staining at 37 °C with 1 mg/ml x-gal (Promega) diluted in staining solution (detergent rinse containing 5 mM potassium ferricyanide, 5 mM potassium ferrocyanide). Sections were washed twice for 10 min in detergent rinse, followed by PBS.

Statistical analysis of data sets of two groups was done by Student's t-test and of three or more groups by one-way ANOVA using GraphPad Prism6.

Lung function analysis. Lung function analysis were performed as previously reported[36]. Briefly, lung function was assessed by a forced maneuver system and a Fine-Pointe RC system (Buxco Research Systems; Wilmington, NC, USA).

Statistical analyses were performed using R-scripts (version 3.0.2, Foundation of Statistical Computing, Vienna, Austria) implemented in the database (MausDB). Differences between genotypes were evaluated by Wilcoxon test. Statistical significance was assumed at $p < 0.05$. Data are presented as median values ± interquartile range.

Proteome analysis. Mouse lung samples were lysed by SDS and prepared for mass spectrometry analysis using a modified version of the FASP protocol[29]. Peptides were labelled with TMT10plex reagent according to the manufacturer's protocol (Thermo Scientific) and separated by immobilized pH gradient - isoelectric focusing (IPG-IEF) on 3–10 strips as described previously[29]. Extracted peptide fractions from the IPG-IEF were separated using an online 3000 RSLCnano system coupled to a Thermo Scientific Q Exactive. MSGF + Percolator in the Galaxy platform was used to match MS spectra to the Ensembl 82 mouse protein database[37].

One of the samples in *Pald1* knock-out females was excluded from further analyses because it is highly likely that squamous epithelium could have contaminated the sample; protein expression pattern was completely different from others and some proteins specific to squamous epithelial cells had been detected. The remaining quantified proteomics data were processed in R software. To identify differentially expressed genes between different groups (knock-out group versus controls, male versus female), student's t test was used and multiple test correction was implemented using the false discovery rate method[38]. Heatmap analysis was performed using the pheatmap packages in R software. The genes were clustered using Pearson correlation distance and the samples were clustered using Euclidean distance. The average linkage cluster method was used to build the cluster dendrogram.

Data Availability. Mass spectrometry proteomics data is deposited to jPOSTrepo[39] with the dataset identifier JPST000225 & PXD005625.

All other data generated or analyzed during this study are included in this published article (and its Supplementary Information files).

References

1. Kalen, M. *et al*. Combination of reverse and chemical genetic screens reveals angiogenesis inhibitors and targets. *Chem Biol* **16**, 432–441, https://doi.org/10.1016/j.chembiol.2009.02.010 (2009).
2. Wallgard, E. *et al*. Identification of a core set of 58 gene transcripts with broad and specific expression in the microvasculature. *Arterioscler Thromb Vasc Biol* **28**, 1469–1476, https://doi.org/10.1161/ATVBAHA.108.165738 (2008).
3. Wallgard, E. *et al*. Paladin (X99384) is expressed in the vasculature and shifts from endothelial to vascular smooth muscle cells during mouse development. *Dev Dyn* **241**, 770–786, https://doi.org/10.1002/dvdy.23753 (2012).
4. Roffers-Agarwal, J., Hutt, K. J. & Gammill, L. S. Paladin is an antiphosphatase that regulates neural crest cell formation and migration. *Dev Biol* **371**, 180–190, https://doi.org/10.1016/j.ydbio.2012.08.007 (2012).
5. Huang, S. M., Hancock, M. K., Pitman, J. L., Orth, A. P. & Gekakis, N. Negative regulators of insulin signaling revealed in a genome-wide functional screen. *PloS one* **4**, e6871, https://doi.org/10.1371/journal.pone.0006871 (2009).
6. Reiterer, V., Eyers, P. A. & Farhan, H. Day of the dead: pseudokinases and pseudophosphatases in physiology and disease. *Trends in cell biology* **24**, 489–505, https://doi.org/10.1016/j.tcb.2014.03.008 (2014).
7. Roffers-Agarwal, J., Hutt, K. J. & Gammill, L. S. Paladin is an antiphosphatase that regulates neural crest cell formation and migration. *Dev Biol* **371**, 180–190, https://doi.org/10.1016/j.ydbio.2012.08.007 (2012).
8. Alonso, A. & Pulido, R. The extended human PTPome: a growing tyrosine phosphatase family. *FEBS J* **283**, 2197–2201, https://doi.org/10.1111/febs.13748 (2016).
9. Li, S., Wang, L., Berman, M., Kong, Y. Y. & Dorf, M. E. Mapping a dynamic innate immunity protein interaction network regulating type I interferon production. *Immunity* **35**, 426–440, https://doi.org/10.1016/j.immuni.2011.06.014 (2011).
10. Taraseviciene-Stewart, L. & Voelkel, N. F. Molecular pathogenesis of emphysema. *The Journal of clinical investigation* **118**, 394–402, https://doi.org/10.1172/JCI31811 (2008).
11. Lopez, A. D. & Murray, C. C. The global burden of disease, 1990–2020. *Nat Med* **4**, 1241–1243, https://doi.org/10.1038/3218 (1998).
12. Murray, C. J. & Lopez, A. D. Alternative projections of mortality and disability by cause 1990-2020: Global Burden of Disease Study. *Lancet* **349**, 1498–1504, https://doi.org/10.1016/S0140-6736(96)07492-2 (1997).
13. Kasahara, Y. *et al*. Endothelial cell death and decreased expression of vascular endothelial growth factor and vascular endothelial growth factor receptor 2 in emphysema. *American journal of respiratory and critical care medicine* **163**, 737–744, https://doi.org/10.1164/ajrccm.163.3.2002117 (2001).
14. Kasahara, Y. *et al*. Inhibition of VEGF receptors causes lung cell apoptosis and emphysema. *The Journal of clinical investigation* **106**, 1311–1319, https://doi.org/10.1172/JCI10259 (2000).
15. McGrath-Morrow, S. A. *et al*. Vascular endothelial growth factor receptor 2 blockade disrupts postnatal lung development. *American journal of respiratory cell and molecular biology* **32**, 420–427, https://doi.org/10.1165/rcmb.2004-0287OC (2005).
16. Tang, K., Rossiter, H. B., Wagner, P. D. & Breen, E. C. Lung-targeted VEGF inactivation leads to an emphysema phenotype in mice. *Journal of applied physiology* **97**, 1559–1566; discussion 1549, https://doi.org/10.1152/japplphysiol.00221.2004 (2004).
17. Hardin, M. *et al*. Sex-specific features of emphysema among current and former smokers with COPD. *Eur Respir J* **47**, 104–112, https://doi.org/10.1183/13993003.00996-2015 (2016).
18. March, T. H. *et al*. Modulators of cigarette smoke-induced pulmonary emphysema in A/J mice. *Toxicol Sci* **92**, 545–559, https://doi.org/10.1093/toxsci/kfl016 (2006).
19. Fuchs, H. *et al*. Mouse phenotyping. *Methods* **53**, 120–135, https://doi.org/10.1016/j.ymeth.2010.08.006 (2011).
20. Gailus-Durner, V. *et al*. Introducing the German Mouse Clinic: open access platform for standardized phenotyping. *Nat Methods* **2**, 403–404, https://doi.org/10.1038/nmeth0605-403 (2005).
21. Vanoirbeek, J. A. *et al*. Noninvasive and invasive pulmonary function in mouse models of obstructive and restrictive respiratory diseases. *American journal of respiratory cell and molecular biology* **42**, 96–104, https://doi.org/10.1165/rcmb.2008-0487OC (2010).
22. Du, Y., Guo, M., Whitsett, J. A. & Xu, Y. 'LungGENS': a web-based tool for mapping single-cell gene expression in the developing lung. *Thorax* **70**, 1092–1094, https://doi.org/10.1136/thoraxjnl-2015-207035 (2015).
23. Guo, M., Wang, H., Potter, S. S., Whitsett, J. A. & Xu, Y. SINCERA: A Pipeline for Single-Cell RNA-Seq Profiling Analysis. *PLoS Comput Biol* **11**, e1004575, https://doi.org/10.1371/journal.pcbi.1004575 (2015).
24. Pozarska, A. *et al*. Stereological monitoring of mouse lung alveolarization from the early postnatal period to adulthood. *American journal of physiology. Lung cellular and molecular physiology* **312**, L882–L895, https://doi.org/10.1152/ajplung.00492.2016 (2017).
25. Niaudet, C. *et al*. Gpr116 Receptor Regulates Distinctive Functions in Pneumocytes and Vascular Endothelium. *PloS one* **10**, e0137949, https://doi.org/10.1371/journal.pone.0137949 (2015).
26. Okubo, T., Knoepfler, P. S., Eisenman, R. N. & Hogan, B. L. Nmyc plays an essential role during lung development as a dosage-sensitive regulator of progenitor cell proliferation and differentiation. *Development* **132**, 1363–1374, https://doi.org/10.1242/dev.01678 (2005).
27. O'Donnell, D. E., Laveneziana, P., Webb, K. & Neder, J. A. Chronic obstructive pulmonary disease: clinical integrative physiology. *Clin Chest Med* **35**, 51–69, https://doi.org/10.1016/j.ccm.2013.09.008 (2014).
28. Ten Have-Opbroek, A. A. The development of the lung in mammals: an analysis of concepts and findings. *Am J Anat* **162**, 201–219, https://doi.org/10.1002/aja.1001620303 (1981).
29. Branca, R. M. *et al*. HiRIEF LC-MS enables deep proteome coverage and unbiased proteogenomics. *Nat Methods* **11**, 59–62, https://doi.org/10.1038/nmeth.2732 (2014).
30. Jokela, H. *et al*. Hydroxysteroid (17beta) dehydrogenase 7 activity is essential for fetal de novo cholesterol synthesis and for neuroectodermal survival and cardiovascular differentiation in early mouse embryos. *Endocrinology* **151**, 1884–1892, https://doi.org/10.1210/en.2009-0928 (2010).
31. Bhasin, M. *et al*. Bioinformatic identification and characterization of human endothelial cell-restricted genes. *BMC genomics* **11**, 342, https://doi.org/10.1186/1471-2164-11-342 (2010).
32. Giordano, R. J. *et al*. Targeted induction of lung endothelial cell apoptosis causes emphysema-like changes in the mouse. *J Biol Chem* **283**, 29447–29460, https://doi.org/10.1074/jbc.M804595200 (2008).
33. Carey, M. A. *et al*. It's all about sex: gender, lung development and lung disease. *Trends Endocrinol Metab* **18**, 308–313, https://doi.org/10.1016/j.tem.2007.08.003 (2007).
34. Nakanishi, M. *et al*. Prostaglandin E2 stimulates the production of vascular endothelial growth factor through the E-prostanoid-2 receptor in cultured human lung fibroblasts. *American journal of respiratory cell and molecular biology* **46**, 217–223, https://doi.org/10.1165/rcmb.2010-0115OC (2012).
35. Kisanuki, Y. Y. *et al*. Tie2-Cre transgenic mice: a new model for endothelial cell-lineage analysis *in vivo*. *Dev Biol* **230**, 230–242, https://doi.org/10.1006/dbio.2000.0106 (2001).
36. Sarker, R. S. *et al*. Coactivator-Associated Arginine Methyltransferase-1 Function in Alveolar Epithelial Senescence and Elastase-Induced Emphysema Susceptibility. *American journal of respiratory cell and molecular biology* **53**, 769–781, https://doi.org/10.1165/rcmb.2014-0216OC (2015).
37. Boekel, J. *et al*. Multi-omic data analysis using Galaxy. *Nat Biotechnol* **33**, 137–139, https://doi.org/10.1038/nbt.3134 (2015).
38. Hochberg, Y. B. A. Y. Controlling the False Discovery Rate: A Practical and Powerful Approach to Multiple Testing. *Journal of the Royal Statistical Society. Series B (Methodological)* **57**, 289–300 (1995).
39. Okuda, S. *et al*. jPOSTrepo: an international standard data repository for proteomes. *Nucleic Acids Research* **45** (D1):D1107–D1111 (2017).

Acknowledgements

This work was supported by the Swedish Cancer foundation, Beijer foundation, Åke Wiberg's foundation, Magnus Bergwall's foundation and Gustav Adolf Johansson foundation (IE, HK). In part this work has been funded by the German Federal Ministry of Education and Research to the GMC (Infrafrontier grant 01KX1012) and to the German Center for Vertigo and Balance Disorders (grant 01 EO 0901). We thank biostatistician Johan Westerberg Uppsala Clinical Research Center, Uppsala, Sweden, for advise regarding statistical methods. Dr Patrick Micke, pathologist at Akademiska University Hospital, Sweden, for blinded assessment of histological sections of *Pald1*$^{-/-}$ mice. We thank Hisamitsu Hayashi, Department of Surgical Sciences, Uppsala University, for help with cochleae dissections, and Ross Smith, Department of Immunology, Genetics and Pathology, Uppsala University, for help with setting-up the GMC screens. The SciLife Lab BioVis platform at Rudbeck laboratory, Uppsala University, Sweden was used for acquiring confocal images and sorting of cells. Mass spectrometry analysis was performed by the Clinical Proteomics Mass Spectrometry facility, Karolinska Institutet/ Karolinska University Hospital/ Science for Life Laboratory. We are grateful for support from Hillevi Andersson Sand & Jessie Thorslund from the facility.

Author Contributions

Experimental design and analysis of data: I.E., H.K., A.N., L.B., C.B.L., C.N., M.P., W.L., M.V., A.V., H.R.A., H.J.J., L.H., A.Ö.Y., G.M.C. Assembling manuscript figures: I.E., A.N., H.K. Supervision of project: H.F., V.G.D., T.K., A.Ö.Y., M.H.A., H.R.A., J.L., M.H. Manuscript writing: I.E., H.K., A.N., A.Ö.Y., M.H. All authors reviewed manuscript.

Additional Information

Supplementary information accompanies this paper at https://doi.org/10.1038/s41598-017-14894-9.

Competing Interests: The authors declare that they have no competing interests.

Publisher's note: Springer Nature remains neutral with regard to jurisdictional claims in published maps and institutional affiliations.

Consortia

German Mouse Clinic Consortium

Antonio Aguilar-Pimentel[2], Markus Ollert[13], Carsten Schmidt-Weber[14], Oana Amarie[2,15], Jochen Graw[15], Johannes Beckers[2,9,10], Lillian Garrett[2,15], Sabine M. Hölter[2,15], Annemarie Zimprich[2,15], Wolfgang Wurst[7,15,16,17], Kristin Moreth[2], Raffi Bekeredjian[18], Frauke Neff[2,19], Julia Calzada-Wack[2,19], Ildikó Rácz[2,20], Andreas Zimmer[20], Birgit Rathkolb[2,6,21], Eckhard Wolf[21], Jan Rozman[2,6], Martin Klingenspor[22,23], Tobias Stoeger[2,4], Oliver Eickelberg[4], Irina Treise[2], Dirk H. Busch[24], Manuela Östereicher[2], Ralph Steinkamp[2], Christoph Lengger[2], Holger Maier[2], Claudia Stoeger[2] & Stefanie Leuchtenberger[2]

[13]Department of Infection and Immunity, Luxembourg Institute of Health, Esch-sur-Alzette, Luxembourg, and Department of Dermatology and Allergy Center, Odense Research Center for Anaphylaxis, University of Southern Denmark, Odense, Denmark. [14]Center of Allergy & Environment (ZAUM), Technische Universität München, and Helmholtz Zentrum München, Ingolstädter Landstrasse, 85764, Neuherberg, Germany. [15]Institute of Developmental Genetics, Helmholtz Zentrum München, German Research Center for Environmental Health GmbH, Ingolstädter Landstrasse 1, 85764, Neuherberg, Germany. [16]Developmental Genetics, Center of Life and Food Sciences Weihenstephan, Technische Universität München, Ingolstädter Landstrasse 1, 85764, Neuherberg, Germany. [17]Munich Cluster for Systems Neurology (SyNergy), Adolf-Butenandt-Institut, Ludwig-Maximilians-Universität München, Schillerstrasse 44, 80336, Munich, Germany. [18]Department of Cardiology, University of Heidelberg, Im Neuenheimer Feld 410, 69120, Heidelberg, Germany. [19]Institute of Pathology, Helmholtz Zentrum München, German Research Center for Environmental Health GmbH, Ingolstädter Landstrasse 1, 85764, Neuherberg, Germany. [20]Institute of Molecular Psychiatry, University of Bonn, Sigmund-Freud-Strasse 25, 53127, Bonn, Germany. [21]Ludwig-Maximilians-Universität München, Gene Center, Institute of Molecular Animal Breeding and Biotechnology, Feodor-Lynen Strasse 25, 81377, Munich, Germany. [22]Molecular Nutritional Medicine, Technische Universität München, Else Kröner-Fresenius Center for Nutritional Medicine, 85350, Freising, Germany. [23]ZIEL – Center for Nutrition and Food Sciences, Technische Universität München, 85350, Freising, Germany. [24]Institute for Medical Microbiology, Immunology and Hygiene, Technical University of Munich, Trogerstrasse 30, 81675, Munich, Germany.

SUPPLEMENTARY INFORMATION

Female mice lacking *Pald1* exhibit endothelial cell apoptosis and emphysema

Isabel Egaña, Hiroshi Kaito, Anja Nitzsche, Lore Becker, Carolina Ballester-Lopez, Colin Niaudet, Milena Petkova, Wei Liu, Michael Vanlandewijck, Alexandra Vernaleken, Thomas Klopstock, Helmut Fuchs, Valerie Gailus-Durner, German Mouse Clinic Consortium, Martin Hrabe de Angelis, Helge Rask-Andersen, Henrik Johansson, Janne Lehtiö, Liqun He, Ali Ö. Yildirim, and Mats Hellström

SUPPLEMENTARY INFORMATION

SUPPLEMENTARY MATERIALS & METHODS

Auditory Brainstem response

Auditory Brainstem Response (ABR) measurements were performed using a RP2.1 workstation (Tucker-Davis Technologies, TDT, USA) as previously described[1]. In short, animals were anaesthetized and electrodes were placed on the vertex (reference) and ventrolateral to the ears (active and ground) of the animals. ABR potentials, as responses to broadband clicks or pure-tone frequencies, were recorded. Frequencies ranged from 6 to 30 kHz with a 6 kHz stepping, and sound pressure levels ranged from 0 to 85 dB with 5 dB steps. Hearing thresholds were determined for each frequency as the lowest SPL producing a measurable ABR pattern response.

Number of mice analyzed per genotype: at 12 weeks of age 7-8 male and 7 female mice, at 15 weeks of age 4-5 male and 5 female mice and at 18 weeks of age 10 male and 10 female mice. For statistical analysis, a Wilcoxon Rank Sum test is used to analyze the thresholds of the different auditory stimuli.

Genomic *cdh23* analysis

For genomic *cdh23* analysis a 547 bp area spanning exon7-intron7 boundary of *cdh23* was amplified (primers: TGTGTGTCTCCCAAGGATCA; AAAGCCTGCAGCATTAGGAA) using DNA isolated from *Pald1*$^{+/+}$ and *Pald1*$^{-/-}$ tail biopsies and sequenced by Sanger Sequencing at the Uppsala Genome Center (sequencing primers: CCTCTGTCTACATTGGCCAAC; ATGACTCAGCAACACGGATG.

Analysis of PDGFRα^{+} cells

Pald1$^{+/-}$ mice bred with PDGFRα^{EGFP} mice[2] to generate Pald1$^{+/}$+ : PDGFRα$^{EGFP/+}$ mice or Pald1$^{-/-}$:PDGFRα$^{EGFP/+}$ offspring. The number of EGFP+ cells was quantified in relation to the total number of Hoechst positive cells in mages that were obtained with the Zeiss LSM700 confocal microscope, 63x objective and analyzed by ImageJ.

Western blot analysis

Snap frozen lungs from 4-week old mice were lysed in 4% (w/v) SDS, 25 mM HEPES pH 7.6 and 1mM DTT in ultrapure water. Tissues were disrupted with Tissue Tearor Homogenizer (Biospec Products) and heated at 95 °C for 5 min on a pre-warmed block. They were centrifuged for 30 minutes at maximum speed at 4 °C after sonication with Bioruptor (Diagenode, Belgium) so that supernatant could be used for western blot analysis. Lung lysates were denatured in sample buffer (Life Technologies) and proteins were separated on a 4-12 % BisTris polyacrylamide gel (Novex by Life Technologies). Proteins were transferred to an Immobilon-P PVDF membrane (Millipore) using the XCell II™ Blot Module (Novex by LifeTechnologies). The membrane was blocked with 5 % skimmed milk in TBS 0.1 % Tween and incubated with rabbit anti-Hpgd (1:1000; abcam, EPR14332-19) or mouse anti-αTubulin (1:500, Sigma, T9026) antibodies overnight at 4°C. Membranes were washed in TBS 0.1 % Tween and incubated with horseradish peroxidase (HRP) conjugated secondary anti-rabbit (1:5,000, GE Healthcare) or anti-mouse antibodies (1:5,000, Invitrogen), respectively. Membranes were washed

in TBS 0.1 % Tween and developed using ECL prime (GE Healthcare). Luminescence signal was detected by the ChemiDoc MP system (BioRad).

4

SUPPLEMENTARY TABLES AND FIGURES

Table S1: Overview of tests performed by the German Mouse Clinic and summary of results.

Figure S1: Altered auditory responses in *Pald1* mutant mice is likely due to variations in *Cdh23*. (a-b) Auditory Brainstem response (ABR) indicates increased hearing sensitivity in *Pald1* mutant and pure background 129SvEv mice compared to $Pald1^{+/+}$ and pure background C57Bl/6 mice. Mean ABR thresholds SPL (Sound pressure level) for $Pald1^{+/+}$ and $Pald1^{-/-}$ mice at 12 (n = 14-15 mice per genotype), 15 (n = 9-10 mice per genotype; significantly decreased SPL for 12-30kHz) and 18 weeks (n = 20 mice per genotype; significantly decreased SPL for 24-30kHz) of age (a) or for 12-week old $Pald1^{+/+}$, $Pald1^{+/-}$ and $Pald1^{-/-}$ mice as well as pure background control C57Bl/6 and 129SvEv mice (b) is given for the indicated frequencies from 6 kHz to 30 kHz. Note overlapping ABR profiles between $Pald1^{+/+}$ and C57Bl/6, and between $Pald1^{+/-}$, $Pald1^{-/-}$ and 129SvEv mice. Error bars: IQR. ** $p \leq 0.01$, *** $p \leq 0.001$

(c) Genomic analysis of the *Cdh23* exon 7-intron boundary demonstrated the presence of $Cdh23^{753A}$ variant in $Pald1^{+/+}$ and pure background C57BL/6JBomTac mice. In contrast, a heterozygous or homozygous $Cdh23^{753G}$ allele was present in $Pald1^{-/-}$ mice, which were generated on the 129SvEv background, and in the pure background 129SvEv control mice. Sequencing was performed on both DNA strands, only forward strand is shown.

Expression of $Cdh23^{753A}$ leads to in-frame skipping of exon 7 and consequently results in reduced stability of cadherin 23 and hearing loss[3]. *Pald1* is within 0.6 Mb of *cdh23* on chromosome 10 and $Pald1^{-/-}$ mice still express the stable $Cdh23^{753G}$ derived from 129SvEv mouse strain. Therefore, it is likely that the differences in hearing sensitivity observed in *Pald1* mutant mice are due to different *Cdh23* variants and not related to the specific loss of paladin expression.

Figure S2: Paladin expression in male lungs. LacZ reporter activity (blue) is detected in male *Pald1*$^{LacZ/LacZ}$ mice 4 weeks and 19 weeks after birth. LacZ is broadly expressed in the lung tissue, except for the bronchial epithelium, which shows no reporter activity (arrow). Scale bar = 50 μm

Figure S3: Paladin is expressed both in the epithelial and mesenchymal compartment of the postnatal lung (P5 and 19 weeks of age). Combined X-gal and immunofluorescence staining of *Pald1*$^{LacZ/LacZ}$ mice at P5 and 19 weeks (a - e) show *Pald1* LacZ expression in the vasculature, i.e. endothelial cells in capillaries (a) but to a lesser extent in endothelial cells of larger blood vessels (b) as indicated by Erg staining (endothelial cell nuclei, green). In large blood vessels LacZ expression can be detected in vascular smooth muscle cells (c), α-smooth muscle actin, red). Paladin LacZ reporter is not active in pneumocytes type II at P5 but is active at 19 weeks (d, SPC, green), but is present in type I/II cells (e, cytokeratin, red). Scale bar = 20 μm.

Figure S4: PDGFRα positive cells in the lung (4 -10 weeks of age). Quantification of the relative proportion of PDGFRα-EGFP positive cells with (n=2 at 4 weeks and n=1 at 10 weeks) shows no differences between wild type and *Pald1* knock-out lungs as compared to total number of cells.

Figure S5: Examples of combined immunofluorescence staining for Erg and cleaved caspase-3 or Ki-67 in wild type female mice lung at P5. A small proportion of endothelial cells (Erg, red) are also positive for cleaved caspase-3 (green) or cell cycle marker Ki-67 (green). Scale bar = 20μm.

Figure S6: Hpgd protein levels in the lung. Western blot for Hpgd in both wild type and knock-out lungs was performed at 4 weeks after birth. a-Tubulin was used as a loading control. All samples were derived at the same time and divided into two parts for different secondary detection reagents.

Figure S7: Volcano plot of the statistics result of Pald1 proteomics data. The X-axis shows the log2 scaled fold change between the Pald1 knockout and control, and Y-axis shows the –log10 scaled p values of the two group comparison. Three proteins showed statistics significant (false discovery rate < 0.05): Pald1, Mycbp2 and Hpgd.

1. Ingham, N.J., Pearson, S. & Steel, K.P. Using the Auditory Brainstem Response (ABR) to Determine Sensitivity of Hearing in Mutant Mice. in *Current Protocols in Mouse Biology* (John Wiley & Sons, Inc., 2011).
2. Hamilton, T.G., Klinghoffer, R.A., Corrin, P.D. & Soriano, P. Evolutionary divergence of platelet-derived growth factor alpha receptor signaling mechanisms. *Mol Cell Biol* **23**, 4013-4025 (2003).
3. Noben-Trauth, K., Zheng, Q.Y. & Johnson, K.R. Association of cadherin 23 with polygenic inheritance and genetic modification of sensorineural hearing loss. *Nat Genet* **35**, 21-23 (2003).

Table S1

Overview of tests performed by the German Mouse Clinic and summary of results:

Screen	Tests	Phenotype summary *Pald1*$^{-/-}$ mice
Dysmorphology, Bone and Cartilage	Morphological observation, Clickbox test, DXA, X-Ray	None
Behavior	Pre-pulse Inhibition / Acoustic Startle Reflex	Increased Acoustic Startle Reflex in male mutant mice
	Open Field	Small increase in center entry latency in mutant mice
Neurology	Auditory Brainstem Response	Decreased sound pressure levels, related to Cdh23^{753G} genotype from 129SvEv mouse strain due to proximity to Pald1 locus (0,6 Mb) and not Pald1 genotype
	Grip Strength, Rotarod, Modified SHIRPA, Lactate	None
Eye Screen	Optical Coherence Tomography	Irregular/waved like pattern of the fundic blood vessels
	Eye size, Scheimpflug, Virtual Drum, Eye Morphology	None
Nociception	Hotplate	None
Metabolic Screen	Minispec and Indirect Calorimetry (TSE)	None
Clinical Chemistry and Hematology	Clinical Chemistry (ad lib. fed mice), Hematology, IpGTT	IpGTT: slightly increased blood glucose concentration 30-120 min after intraperitoneal glucose injection; small changes of unclear relevance in plasma composition in male mutant mice
Immunology Screen	Flow Cytometry	None
Allergy Screen	IgE levels	None
	Transepidermal water loss	None
Steroid Screen	Steroid levels	None
Cardiovascular Screen	Awake Echocardiography, Awake Electrocardiography	Shorter QT, QTc and ST interval duration mainly in male mutant mice
Lung Function Screen	Lung Function	Emphysema-like phenotype in female mutant mice
Pathology Screen	Macroscopy, Microscopy	Differences in heart weight of females of unclear relevance

Abbreviations: DXA - Dual-energy X-ray Absorptiometry; SHIRPA - SmithKline Beecham, Harwell, Imperial College, Royal London Hospital, phenotype assessment; IpGTT - Intraperitoneal Glucose Tolerance Test;

Egana et al. Figure S1

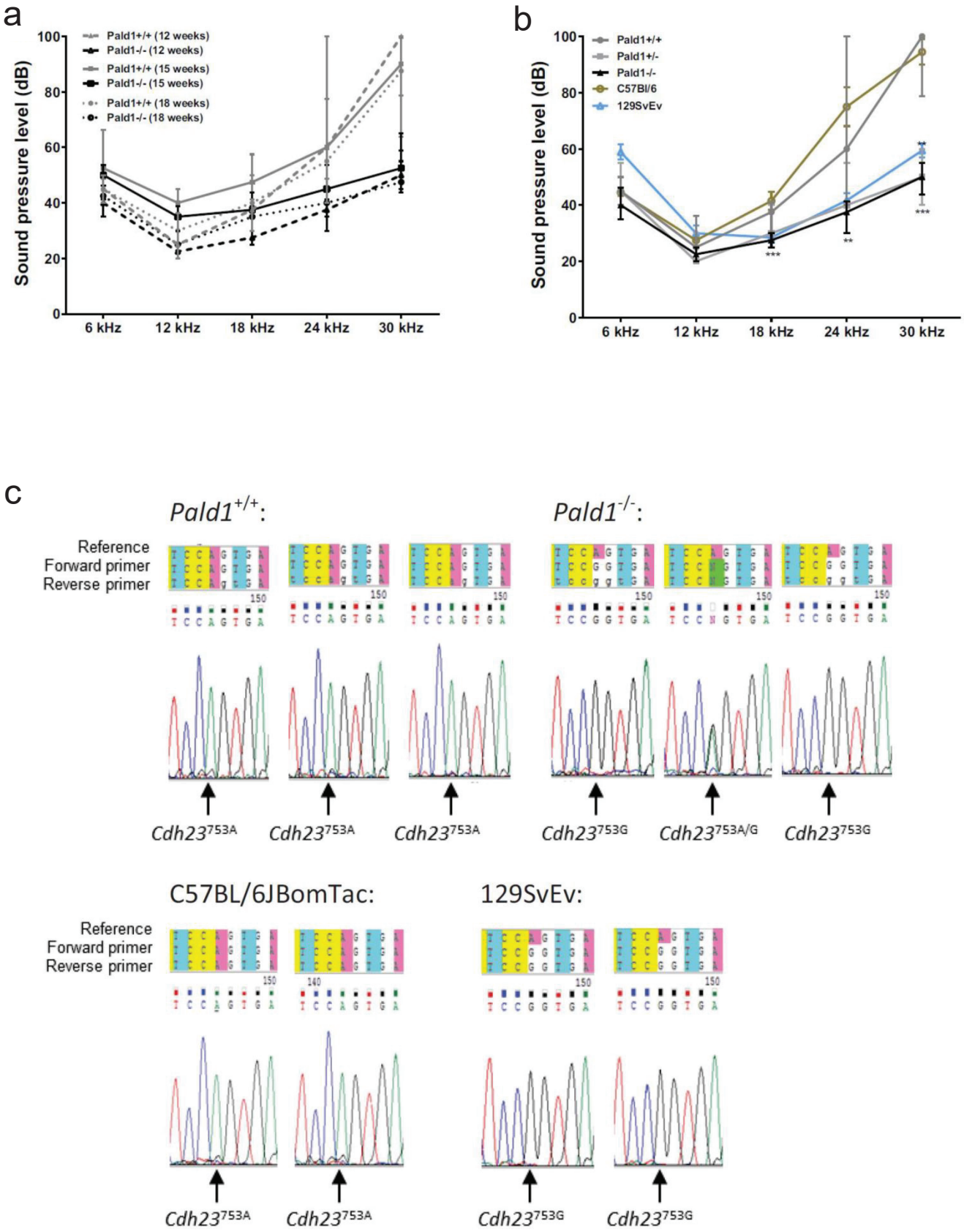

Egana et al. Figure S2

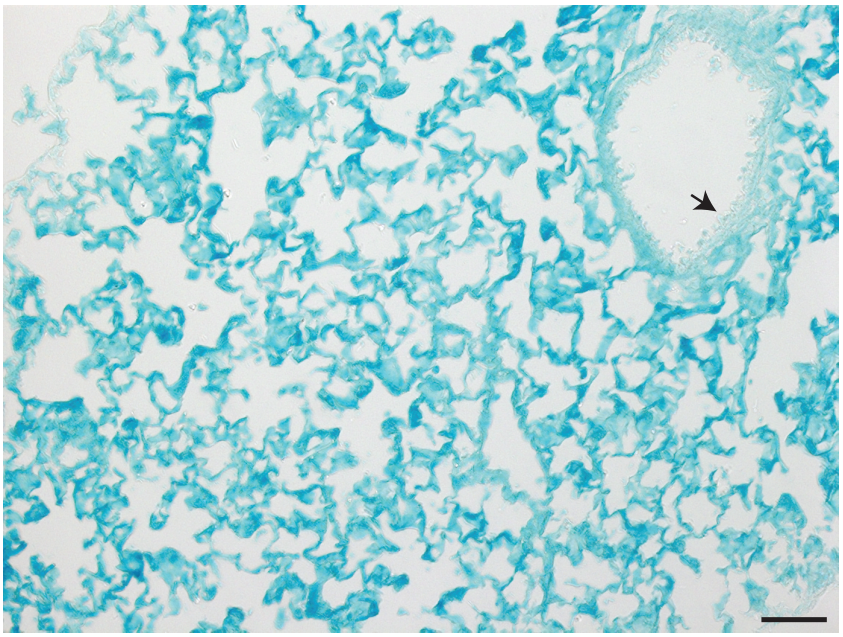

Egana et al. Figure S3

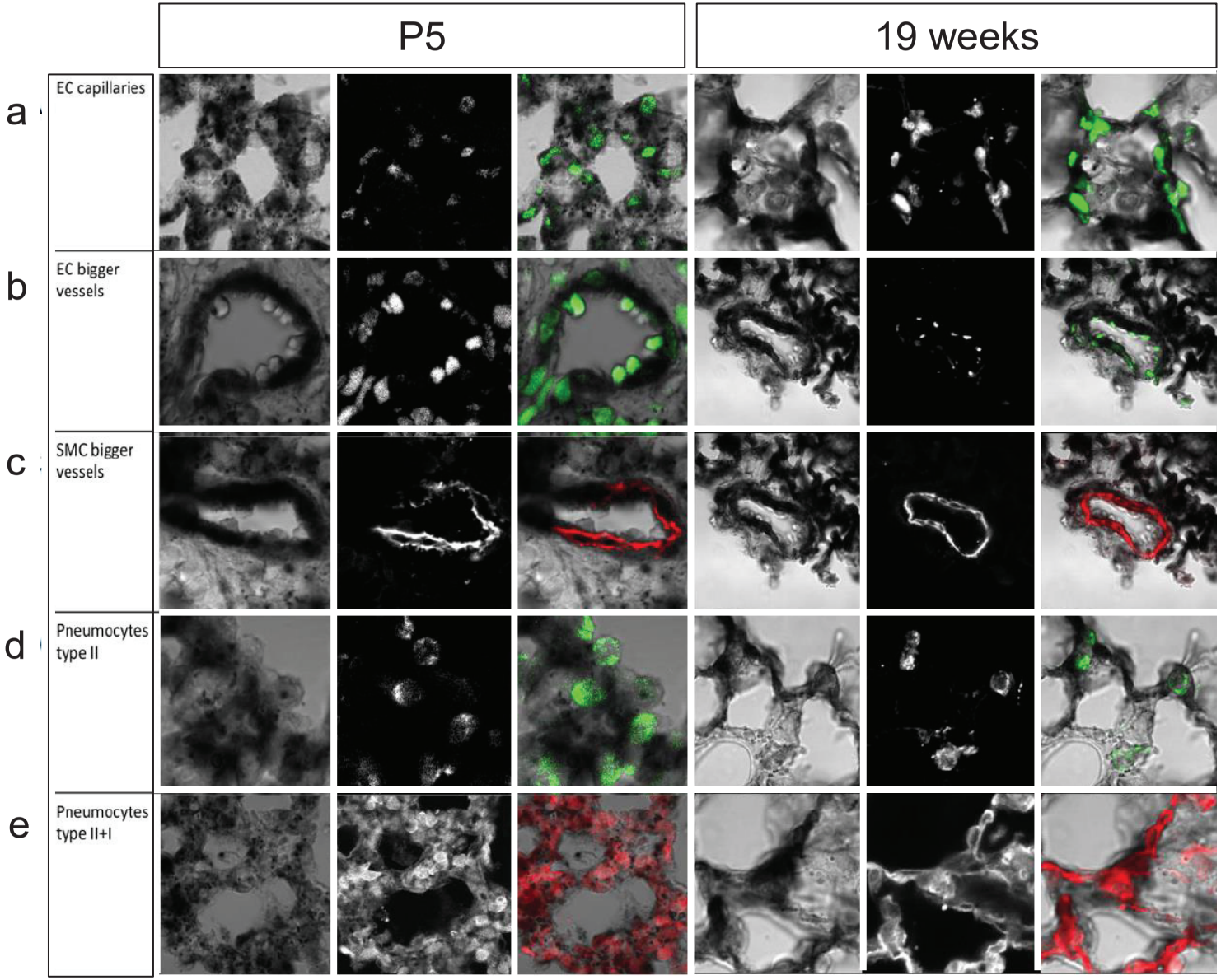

Egana et al. S4

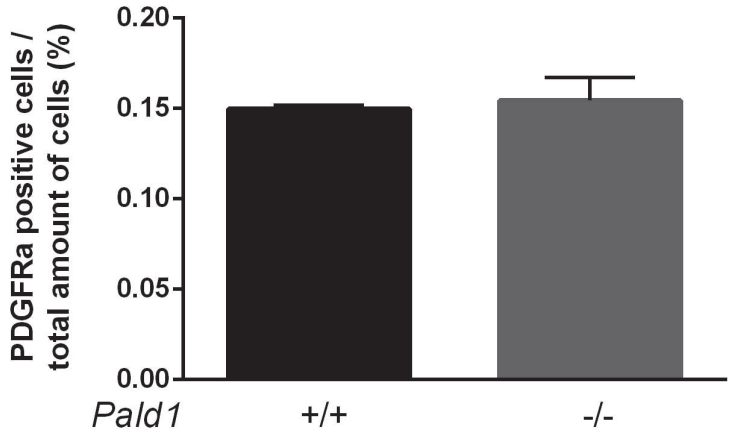

Egana et al. S5

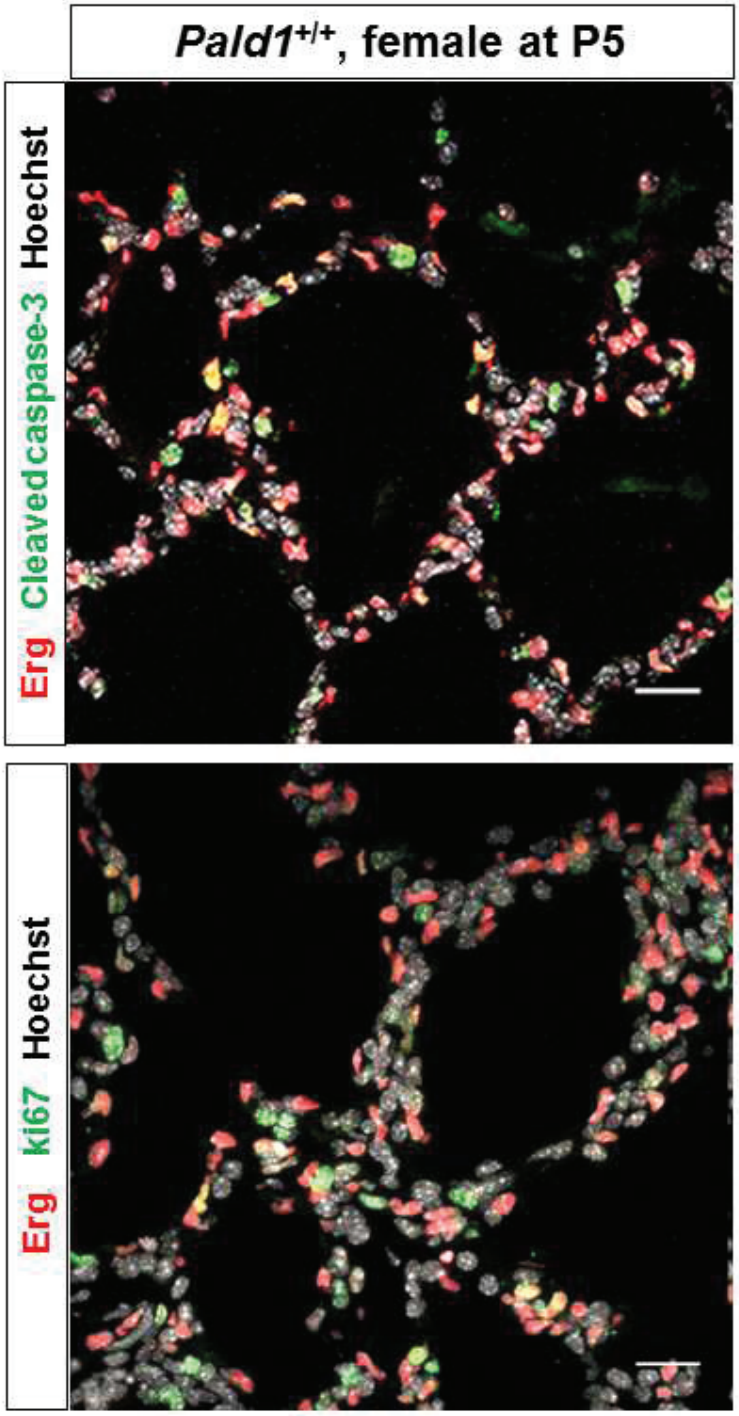

Egana et al. Figure S6

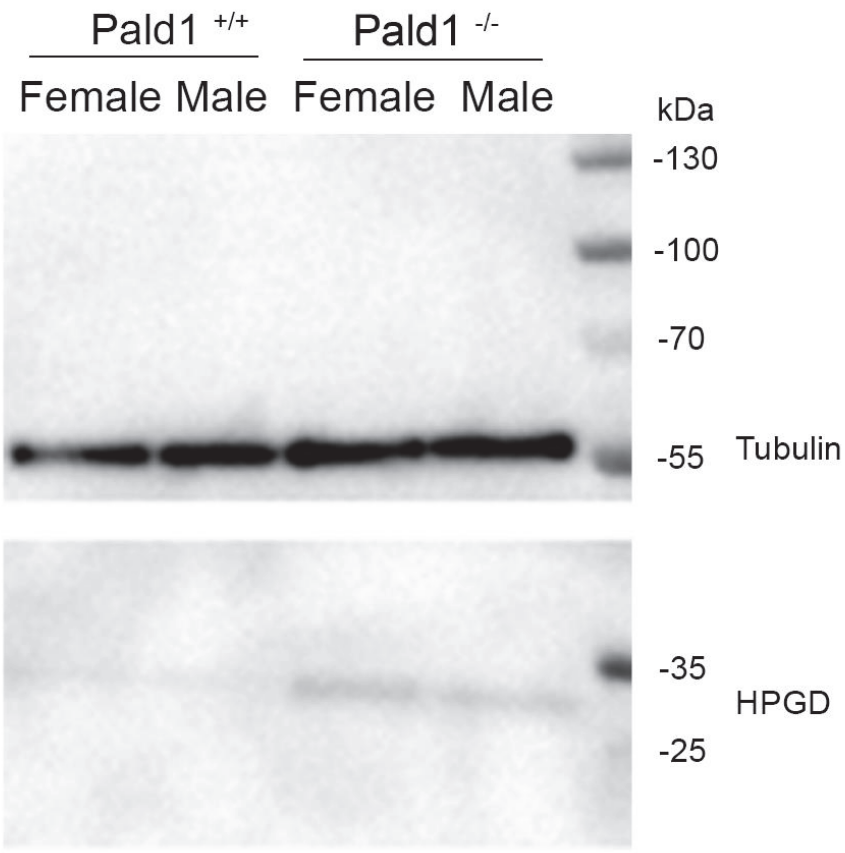

Egana et al. Figure S7

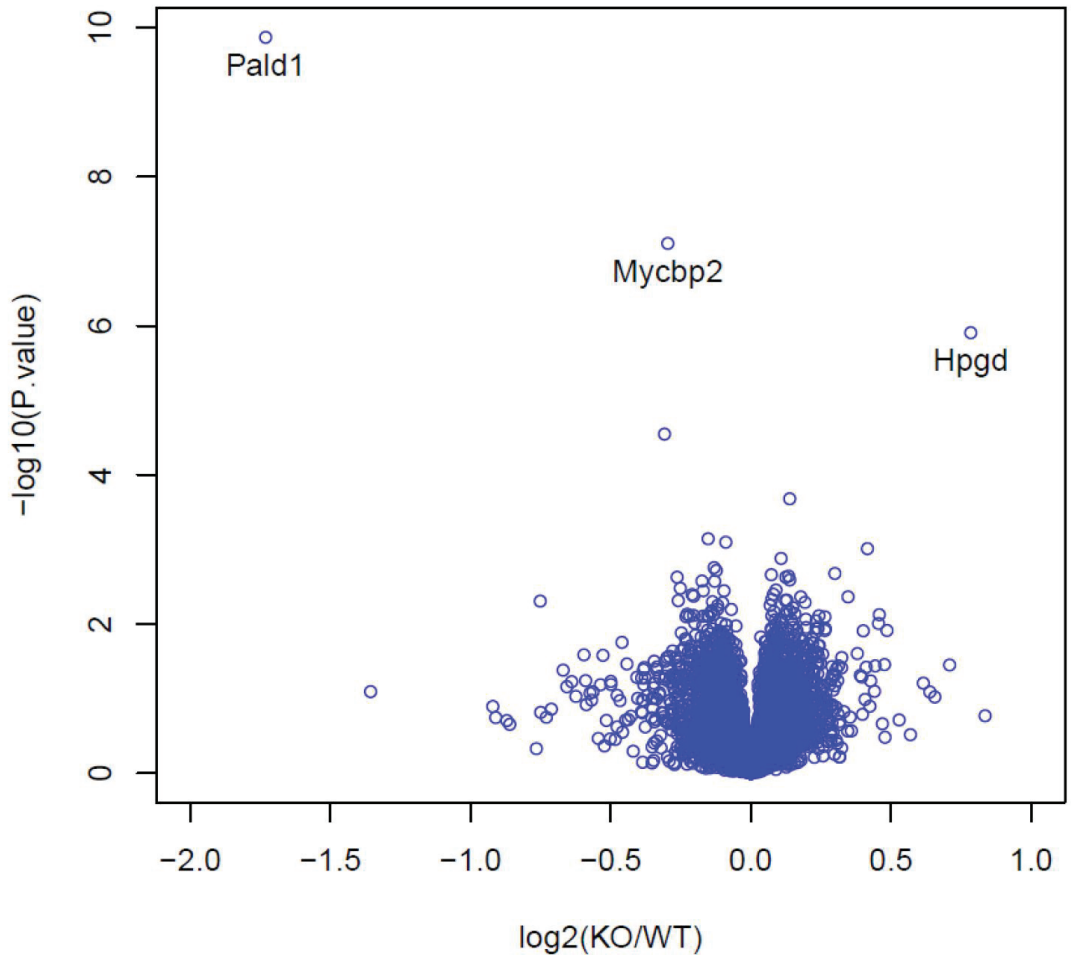

11. DISCUSSION: NOVEL PLAYERS IN COPD PATHOGENESIS

In 2017, more than 5% of the global population died from COPD, a number that keeps vertiginously increasing over recent years. Despite this there is no a curative treatment available today. Additionally, the complexity and heterogeneity of COPD pathogenesis makes difficult the investigation of new therapeutic strategies. Therefore, there is an unmet need in the treatment of COPD and exploration of novel targets is necessary. Here, we presented the first studies addressing the role of DNER and Paladin in COPD development, two novel proteins recently identified as potential players during disease pathogenesis.

11.1 DNER

Unfortunately there are few studies investigating the genes identified in GWAS, especially those about which little background information exists in the field of interest. Moreover, the fact that little overlap is found between microarray and GWAS studies leads to the debate of how relevant is the discoveries by GWAS. DNER was identified in a GWAS as a genetic risk factor for lung function decline independent of smoking effects. In our study, we have shown that *DNER* gene expression is increased in lungs from COPD patients and also in human monocyte derived macrophages after pro-inflammatory stimulus. Furthermore, immunostainings of COPD lung tissue showed that DNER was located in iNOS and Galectin3 double positive cells, corroborating that DNER is expressed in pro-inflammatory macrophages. Our human data not only support the findings by the GWAS, but also provide a new cell type for DNER expression.

Here, we demonstrate with the cigarette smoke (CS) induced COPD mouse model that indeed DNER would be a risk factor for COPD pathogenesis. We have observed that DNER deficient mice after 2 months of CS exposure did not present alveolar tissue destruction as in wild type (WT) mice. This was evidenced by stereological measurements and by lung function analysis, which showed improved performance in the case of CS exposed DNER deficient mice for the forced expiratory volume after 100ms in comparison to WT mice. Nevertheless, these data should be carefully interpreted. Even though we observed a phenotype after 2 months of CS exposure, this is not enough to fully induce the characteristic COPD pathological profile that we observe in human patients. After 2 months of CS, we observed mild emphysema development and chronic inflammation, but not the formation of tertiary lymphoid follicles and airway remodeling, which usually appears after 4 months of CS exposure. Therefore, further investigation is needed to completely understand the impact of DNER deficiency in the COPD phenotype. Nevertheless, the focus of this study was to understand DNER function in COPD pathogenesis, which we identified for the first time as expressing DNER in macrophages, in acute and chronic inflammation, which is discussed in the next section.

Taking together the GWAS and our study, it is clear that DNER has a role in COPD pathogenesis. On one side, GWAS suggests that people carrying a SNP in the *DNER* loci, have a higher predisposition

to develop COPD. On the other, we showed that COPD patients have increased *DNER* levels, and that inflammation triggers its expression. Therefore, we could conclude that COPD patients may have increased DNER expression because of the presence of the SNP but also due to the ongoing inflammation.

Furthermore, in this study, we showed that DNER regulates IFNγ expression in recruited macrophages during COPD pathogenesis. In the discussion section it is mentioned that excessive levels of IFNγ can lead to apoptosis of epithelial cells and therefore emphysema development, and interestingly we observed emphysema protection in 2 months CS exposed DNER deficient mice. How these two events are connected should be carefully interpreted since we do not have any evidence of a direct link yet. Indeed, it should not be forgotten that DNER is a transmembrane ligand able to bind to any Notch1-expressing cell, something abundant among the lung cell types, especially in a COPD context. This means that DNER-expressing macrophages could trigger non-canonical Notch signaling in any other signal-receiving cell. Understanding the non-canonical Notch pathway has been one of the most difficult challenges of this project. The main reason is the lack of consensus among experts on its molecular mechanism and the concomitant absence of cell markers to distinguish it from canonical signaling. Furthermore, most of the studies that analyze Notch activation focus on the molecular events that take place in the cytoplasmic fraction, but do not address which ligand is triggering the cellular response, especially in the lung field. Indeed, to our knowledge, this is the first study investigating the function of a non-canonical Notch ligand in the lung. Therefore, to justify that DNER is activating non-canonical Notch, we used the fact that DNER is classified as a non-canonical ligand due to the absence of the DSL domain, and that expression of canonical Notch target genes was not affected. Additionally, interaction between DNER and Notch1 in murine neuronal cells has been meticulously studied by Eiraku et al. [88], where they showed that DNER specifically bound to Notch1 by its first and second EGF-repeats instead of the DSL domain as happens in canonical ligands. Nevertheless, more detailed investigation is needed to completely discard that DNER affects canonical Notch activation.

This study not only identifies a novel player in COPD pathogenesis, but also provides a novel molecular mechanism to regulate IFNγ levels in macrophages and add new insights in the complexity of non-canonical Notch signalling.

11.2 PALD1

There is little knowledge about the regulation of angiogenesis during COPD progression. Paladin is a recently identified candidate to play a key role in endothelial cell survival and proliferation. In the present study, Paladin deficient female mice exhibited an emphysematous phenotype already present in the first stage of postnatal lung development (P5) and persisted until adult stage (4 and 19 weeks). Despite the fact that Paladin appeared to be expressed in a broad range of lung cell types,

quantification from histological staining showed that only endothelial cells are reduced in numbers in Paladin deficient female mice. Interestingly, these cells were showing significantly higher activation of apoptosis and proliferation. However, the reduction and cellular phenotype of endothelial cells in Paladin deficient female mice were only observed at 4 weeks of age, but not during postnatal development. Therefore, there is not enough evidence to directly link the endothelial cell death with the reduction in alveolar walls. Additionally, further investigation is needed to discriminate between the function of Paladin during lung development and during adult stages. Nevertheless, this study clearly shows that Paladin contributes to promote endothelial cell survival in female adult mice.

Another interesting aspect is the difference observed between the two genders. The lack of Paladin entails a significant susceptibility for emphysema development in females but not in male mice. Proteomics analysis showed dysregulated levels of hydroxyprostaglandin dehydrogenase (Hpdg) and Myc2 in both gender knock out mice. This suggests that the changes on the levels of these proteins could have a stronger impact in females than males regarding lung development and endothelial survival.

Here, in these studies we identified that Paladin is as another novel player in COPD pathogenesis and more interestingly, provide first evidences of a sex-specific mechanism in endothelium homeostasis. This discovery highlights once again the urgent need of aiming for personalized medicine as the future for COPD therapy.

12. CONCLUSIONS AND REMARKS

Both papers addressed the function of novel proteins in COPD development for the first time, not only contributing to improved understanding of COPD pathogenesis but also providing new insights to the immunology and cellular biology fields. On one hand, DNER appeared to localize to macrophages in the lung, where it regulates IFNγ release during chronic inflammation and COPD progression. On the other hand, Paladin is implicated in driving emphysema development in female mice and promoting survival of endothelial cells.

In this thesis we highlighted the importance of finding novel biomarkers and targets for future personalized and curative therapies. Despite the fact that further studies are needed to commend DNER and Paladin or its downstream signalling as targets, these two studies are the starting point to unravel the contribution of these novel proteins to the development and pathogenesis of COPD.

13. REFERENCES

1. Lopez-Campos, J.L., W. Tan, and J.B. Soriano, *Global burden of COPD.* Respirology, 2016. **21**(1): p. 14-23.
2. Allinson, J.P. and J.A. Wedzicha, *Update in Chronic Obstructive Pulmonary Disease 2016.* Am J Respir Crit Care Med, 2017. **196**(4): p. 414-424.
3. Disease, G.B.D., I. Injury, and C. Prevalence, *Global, regional, and national incidence, prevalence, and years lived with disability for 310 diseases and injuries, 1990-2015: a systematic analysis for the Global Burden of Disease Study 2015.* Lancet, 2016. **388**(10053): p. 1545-1602.
4. Adeloye, D., et al., *Global and regional estimates of COPD prevalence: Systematic review and meta-analysis.* J Glob Health, 2015. **5**(2): p. 020415.
5. Grigsby, M., et al., *Socioeconomic status and COPD among low- and middle-income countries.* Int J Chron Obstruct Pulmon Dis, 2016. **11**: p. 2497-2507.
6. Quaderi, S.A. and J.R. Hurst, *The unmet global burden of COPD.* Glob Health Epidemiol Genom, 2018. **3**: p. e4.
7. IHME, I., *GBD Compare Seattle, WA: IHME, University of Washington, 2013 [accessed July 16, 2015]*.
8. Make, B., et al., *Undertreatment of COPD: a retrospective analysis of US managed care and Medicare patients.* Int J Chron Obstruct Pulmon Dis, 2012. **7**: p. 1-9.
9. Rennard, S.I. and M.B. Drummond, *Early chronic obstructive pulmonary disease: definition, assessment, and prevention.* Lancet, 2015. **385**(9979): p. 1778-1788.
10. Soriano, J.B., J. Zielinski, and D. Price, *Screening for and early detection of chronic obstructive pulmonary disease.* Lancet, 2009. **374**(9691): p. 721-32.
11. Ehteshami-Afshar, S., et al., *The global economic burden of asthma and chronic obstructive pulmonary disease.* Int J Tuberc Lung Dis, 2016. **20**(1): p. 11-23.
12. Herse, F., T. Kiljander, and L. Lehtimaki, *Annual costs of chronic obstructive pulmonary disease in Finland during 1996-2006 and a prediction model for 2007-2030.* NPJ Prim Care Respir Med, 2015. **25**: p. 15015.
13. Chen, W., et al., *Excess economic burden of comorbidities in COPD: a 15-year population-based study.* Eur Respir J, 2017. **50**(1).
14. Organization, W.H., *Global status report on noncommunicable diseases 2010*. 2011: Geneva: World Health Organization.
15. Singh, D., et al., *Global Strategy for the Diagnosis, Management, and Prevention of Chronic Obstructive Lung Disease: The GOLD Science Committee Report 2019.* Eur Respir J, 2019.
16. Li, Y., M.H. Cho, and X. Zhou, *What do polymorphisms tell us about the mechanisms of COPD?* Clin Sci (Lond), 2017. **131**(24): p. 2847-2863.
17. Fishwick, D., et al., *Occupational chronic obstructive pulmonary disease: a standard of care.* Occup Med (Lond), 2015. **65**(4): p. 270-82.
18. Barnes, P.J., *Cellular and molecular mechanisms of asthma and COPD.* Clin Sci (Lond), 2017. **131**(13): p. 1541-1558.
19. Hazari, Y.M., et al., *Alpha-1-antitrypsin deficiency: Genetic variations, clinical manifestations and therapeutic interventions.* Mutat Res, 2017. **773**: p. 14-25.
20. Foreman, M.G., M. Campos, and J.C. Celedon, *Genes and chronic obstructive pulmonary disease.* Med Clin North Am, 2012. **96**(4): p. 699-711.
21. Barnes, P.J., et al., *Chronic obstructive pulmonary disease.* Nat Rev Dis Primers, 2015. **1**: p. 15076.
22. Rabe, K.F. and H. Watz, *Chronic obstructive pulmonary disease.* Lancet, 2017. **389**(10082): p. 1931-1940.
23. Abboud, R.T. and S. Vimalanathan, *Pathogenesis of COPD. Part I. The role of protease-antiprotease imbalance in emphysema.* Int J Tuberc Lung Dis, 2008. **12**(4): p. 361-7.
24. Brandsma, C.A., et al., *Lung ageing and COPD: is there a role for ageing in abnormal tissue repair?* Eur Respir Rev, 2017. **26**(146).

25. Boucherat, O., et al., *Bridging Lung Development with Chronic Obstructive Pulmonary Disease. Relevance of Developmental Pathways in Chronic Obstructive Pulmonary Disease Pathogenesis.* Am J Respir Crit Care Med, 2016. **193**(4): p. 362-75.
26. Baarsma, H.A. and M. Konigshoff, *'WNT-er is coming': WNT signalling in chronic lung diseases.* Thorax, 2017. **72**(8): p. 746-759.
27. John-Schuster, G., et al., *Inflammaging increases susceptibility to cigarette smoke-induced COPD.* Oncotarget, 2016. **7**(21): p. 30068-83.
28. Barnes, P.J., *Senescence in COPD and Its Comorbidities.* Annu Rev Physiol, 2017. **79**: p. 517-539.
29. Hardin, M., et al., *Sex-specific features of emphysema among current and former smokers with COPD.* Eur Respir J, 2016. **47**(1): p. 104-12.
30. Barnes, P.J., *Inflammatory mechanisms in patients with chronic obstructive pulmonary disease.* J Allergy Clin Immunol, 2016. **138**(1): p. 16-27.
31. Lappalainen, U., et al., *Interleukin-1beta causes pulmonary inflammation, emphysema, and airway remodeling in the adult murine lung.* Am J Respir Cell Mol Biol, 2005. **32**(4): p. 311-8.
32. Wang, Z., et al., *Interferon gamma induction of pulmonary emphysema in the adult murine lung.* J Exp Med, 2000. **192**(11): p. 1587-600.
33. Galban, C.J., et al., *Computed tomography-based biomarker provides unique signature for diagnosis of COPD phenotypes and disease progression.* Nat Med, 2012. **18**(11): p. 1711-5.
34. Ueno, M., et al., *Alendronate inhalation ameliorates elastase-induced pulmonary emphysema in mice by induction of apoptosis of alveolar macrophages.* Nat Commun, 2015. **6**: p. 6332.
35. Churg, A., S. Zhou, and J.L. Wright, *Series "matrix metalloproteinases in lung health and disease": Matrix metalloproteinases in COPD.* Eur Respir J, 2012. **39**(1): p. 197-209.
36. Xu, W.H., et al., *Peripheral Tc17 and Tc17/Interferon-gamma Cells are Increased and Associated with Lung Function in Patients with Chronic Obstructive Pulmonary Disease.* Chin Med J (Engl), 2016. **129**(8): p. 909-16.
37. Hogg, J.C., et al., *The nature of small-airway obstruction in chronic obstructive pulmonary disease.* N Engl J Med, 2004. **350**(26): p. 2645-53.
38. van der Strate, B.W., et al., *Cigarette smoke-induced emphysema: A role for the B cell?* Am J Respir Crit Care Med, 2006. **173**(7): p. 751-8.
39. Hwang, J.Y., T.D. Randall, and A. Silva-Sanchez, *Inducible Bronchus-Associated Lymphoid Tissue: Taming Inflammation in the Lung.* Front Immunol, 2016. **7**: p. 258.
40. John-Schuster, G., et al., *Cigarette smoke-induced iBALT mediates macrophage activation in a B cell-dependent manner in COPD.* Am J Physiol Lung Cell Mol Physiol, 2014. **307**(9): p. L692-706.
41. Mills, C.D., et al., *M-1/M-2 macrophages and the Th1/Th2 paradigm.* J Immunol, 2000. **164**(12): p. 6166-73.
42. Mills, C.D., *Anatomy of a discovery: m1 and m2 macrophages.* Front Immunol, 2015. **6**: p. 212.
43. Geissmann, F., et al., *Unravelling mononuclear phagocyte heterogeneity.* Nat Rev Immunol, 2010. **10**(6): p. 453-60.
44. Tan, S.Y. and M.A. Krasnow, *Developmental origin of lung macrophage diversity.* Development, 2016. **143**(8): p. 1318-27.
45. Yona, S., et al., *Fate mapping reveals origins and dynamics of monocytes and tissue macrophages under homeostasis.* Immunity, 2013. **38**(1): p. 79-91.
46. Yamasaki, K. and S.F.V. Eeden, *Lung Macrophage Phenotypes and Functional Responses: Role in the Pathogenesis of COPD.* Int J Mol Sci, 2018. **19**(2).
47. Franke-Ullmann, G., et al., *Characterization of murine lung interstitial macrophages in comparison with alveolar macrophages in vitro.* J Immunol, 1996. **157**(7): p. 3097-104.
48. Kapellos, T.S., et al., *Dysregulated Functions of Lung Macrophage Populations in COPD.* J Immunol Res, 2018. **2018**: p. 2349045.
49. Eapen, M.S., et al., *Abnormal M1/M2 macrophage phenotype profiles in the small airway wall and lumen in smokers and chronic obstructive pulmonary disease (COPD).* Sci Rep, 2017. **7**(1): p. 13392.

50. Wang, N., H. Liang, and K. Zen, *Molecular mechanisms that influence the macrophage m1-m2 polarization balance.* Front Immunol, 2014. **5**: p. 614.
51. Raggi, F., et al., *Regulation of Human Macrophage M1-M2 Polarization Balance by Hypoxia and the Triggering Receptor Expressed on Myeloid Cells-1.* Front Immunol, 2017. **8**: p. 1097.
52. Palaga, T., W. Wongchana, and P. Kueanjinda, *Notch Signaling in Macrophages in the Context of Cancer Immunity.* Front Immunol, 2018. **9**: p. 652.
53. Monsalve, E., et al., *Notch1 upregulates LPS-induced macrophage activation by increasing NF-kappaB activity.* Eur J Immunol, 2009. **39**(9): p. 2556-70.
54. Shin, H.M., et al., *Notch1 augments NF-kappaB activity by facilitating its nuclear retention.* EMBO J, 2006. **25**(1): p. 129-38.
55. Xu, H., et al., *Notch-RBP-J signaling regulates the transcription factor IRF8 to promote inflammatory macrophage polarization.* Nat Immunol, 2012. **13**(7): p. 642-50.
56. Barnes, P.J., *The cytokine network in asthma and chronic obstructive pulmonary disease.* The Journal of Clinical Investigation, 2008. **118**(11): p. 3546-3556.
57. Bogdan, C. and U. Schleicher, *Production of interferon-gamma by myeloid cells--fact or fancy?* Trends Immunol, 2006. **27**(6): p. 282-90.
58. Schroder, K., et al., *Interferon-gamma: an overview of signals, mechanisms and functions.* J Leukoc Biol, 2004. **75**(2): p. 163-89.
59. Bhat, P., et al., *Interferon-gamma derived from cytotoxic lymphocytes directly enhances their motility and cytotoxicity.* Cell Death Dis, 2017. **8**(6): p. e2836.
60. Gadgil, A. and S.R. Duncan, *Role of T-lymphocytes and pro-inflammatory mediators in the pathogenesis of chronic obstructive pulmonary disease.* Int J Chron Obstruct Pulmon Dis, 2008. **3**(4): p. 531-41.
61. Swanson, M.A., W.T. Lee, and V.M. Sanders, *IFN-gamma production by Th1 cells generated from naive CD4+ T cells exposed to norepinephrine.* J Immunol, 2001. **166**(1): p. 232-40.
62. Hu, X. and L.B. Ivashkiv, *Cross-regulation of signaling pathways by interferon-gamma: implications for immune responses and autoimmune diseases.* Immunity, 2009. **31**(4): p. 539-50.
63. Nakajima, Y., et al., *The role of tumor necrosis factor-alpha and interferon-gamma in regulating angiomotin-like protein 1 expression in lung microvascular endothelial cells.* Allergol Int, 2013. **62**(3): p. 309-22.
64. Zheng, T., et al., *Role of cathepsin S-dependent epithelial cell apoptosis in IFN-gamma-induced alveolar remodeling and pulmonary emphysema.* J Immunol, 2005. **174**(12): p. 8106-15.
65. Blanco, I., L. Piccari, and J.A. Barbera, *Pulmonary vasculature in COPD: The silent component.* Respirology, 2016. **21**(6): p. 984-94.
66. Kalen, M., et al., *Combination of reverse and chemical genetic screens reveals angiogenesis inhibitors and targets.* Chem Biol, 2009. **16**(4): p. 432-41.
67. Taraseviciene-Stewart, L. and N.F. Voelkel, *Molecular pathogenesis of emphysema.* J Clin Invest, 2008. **118**(2): p. 394-402.
68. Matarese, A. and G. Santulli, *Angiogenesis in chronic obstructive pulmonary disease: a translational appraisal.* Transl Med UniSa, 2012. **3**: p. 49-56.
69. Kasahara, Y., et al., *Inhibition of VEGF receptors causes lung cell apoptosis and emphysema.* J Clin Invest, 2000. **106**(11): p. 1311-9.
70. Tang, K., et al., *Lung-targeted VEGF inactivation leads to an emphysema phenotype in mice.* J Appl Physiol (1985), 2004. **97**(4): p. 1559-66; discussion 1549.
71. Franssen, F.M. and M.K. Han, *The ABC of GOLD ABCD*. 2013, Eur Respiratory Soc.
72. Cohen, J.S., et al., *Dual therapy strategies for COPD: the scientific rationale for LAMA + LABA.* Int J Chron Obstruct Pulmon Dis, 2016. **11**: p. 785-97.
73. Garth, J., J.W. Barnes, and S. Krick, *Targeting Cytokines as Evolving Treatment Strategies in Chronic Inflammatory Airway Diseases.* Int J Mol Sci, 2018. **19**(11).
74. van der Molen, T. and M. Cazzola, *Beyond lung function in COPD management: effectiveness of LABA/LAMA combination therapy on patient-centred outcomes.* Prim Care Respir J, 2012. **21**(1): p. 101-8.

75. Rabe, K.F., J.R. Hurst, and S. Suissa, *Cardiovascular disease and COPD: dangerous liaisons?* Eur Respir Rev, 2018. **27**(149).
76. Barnes, P.J., *Targeting cytokines to treat asthma and chronic obstructive pulmonary disease.* Nat Rev Immunol, 2018. **18**(7): p. 454-466.
77. Yi, G., et al., *A large lung gene expression study identifying IL1B as a novel player in airway inflammation in COPD airway epithelial cells.* Inflamm Res, 2018. **67**(6): p. 539-551.
78. Ruwanpura, S.M., et al., *Therapeutic Targeting of the IL-6 Trans-Signaling/Mechanistic Target of Rapamycin Complex 1 Axis in Pulmonary Emphysema.* Am J Respir Crit Care Med, 2016. **194**(12): p. 1494-1505.
79. Mannino, D.M., *Biomarkers in COPD: the search continues!* 2015, Eur Respiratory Soc.
80. Fermont, J.M., et al., *Biomarkers and clinical outcomes in COPD: a systematic review and meta-analysis.* Thorax, 2019: p. thoraxjnl-2018-211855.
81. Shakhnovich, V., *It's Time to Reverse our Thinking: The Reverse Translation Research Paradigm.* Clin Transl Sci, 2018. **11**(2): p. 98-99.
82. Wang, D.G., et al., *Large-scale identification, mapping, and genotyping of single-nucleotide polymorphisms in the human genome.* Science, 1998. **280**(5366): p. 1077-82.
83. Morrow, J.D., et al., *Functional interactors of three genome-wide association study genes are differentially expressed in severe chronic obstructive pulmonary disease lung tissue.* Sci Rep, 2017. **7**: p. 44232.
84. Hancock, D.B., et al., *Genome-wide joint meta-analysis of SNP and SNP-by-smoking interaction identifies novel loci for pulmonary function.* PLoS Genet, 2012. **8**(12): p. e1003098.
85. Liu, J.Z., et al., *Meta-analysis and imputation refines the association of 15q25 with smoking quantity.* Nat Genet, 2010. **42**(5): p. 436-40.
86. Wallgard, E., et al., *Identification of a core set of 58 gene transcripts with broad and specific expression in the microvasculature.* Arterioscler Thromb Vasc Biol, 2008. **28**(8): p. 1469-76.
87. Bhasin, M., et al., *Bioinformatic identification and characterization of human endothelial cell-restricted genes.* BMC Genomics, 2010. **11**: p. 342.
88. Eiraku, M., et al., *DNER acts as a neuron-specific Notch ligand during Bergmann glial development.* Nat Neurosci, 2005. **8**(7): p. 873-80.

14. ACKNOWLEDGMENT

As any PhD student would say at this stage, this was not an easy journey. However, difficult journeys are only possible when wonderful people accompany you. I am very grateful to Önder for giving me the opportunity to “have the fun” of doing a PhD in such a fantastic group. Although we had our challenging moments at times, I learned a lot thanks to him, not only scientifically but also personally.

I would also like to thank to my other supervisors that supported me with great input and advice along my PhD: Oliver, Ulla and Claudia. I am grateful to the CPC research school that has helped me to evolve as a scientist: Melanie, Hoeke and Claudia.

I also feel very lucky for the colleagues I got the chance to share my experience with, who became my friends and made the office/lab a place full of nice and fun memories: Jie, Gerrit, Julian, Christine, Tom, Gizem, Carmela, Aicha, Zeynep, Maxi, Hengshou, Sarah and Miriam. Jie, who was my senior PhD student during my first years and always found the patience to answer to my “Jie, do you have 5 min?” when it was never 5 min. Special thanks to Tom, from whom I learned a lot and was always there to help and guide me. Part of my PhD is also thanked to Christine, the best technician! Always there for you, even if you chase her 5 times per day. Gizem, Carmela and Aicha for listening to all my complaining and be supportive and helpful, I could not have survived without those coffee breaks. I am also grateful to my other CPC friends with whom I shared many good moments and were there for me: Aina, Rita, Flavia, Natalia, Raphael and Captain Morgan.

And of course, to all my friends and family who always supported and believed in me.